BMU
BAKI MÜHƏNDİSLİK UNİVERSİTETİ

Journal of Baku Engineering University

ISSN 2521-635X

MATHEMATICS AND COMPUTER SCIENCE

Volume 8
Number 1

2024

Journal is published twice a year
Number-1. June, Number-2. December

An International Journal

http://journal.beu.edu.az

CONTACT ADDRESS

Journal of Baku Engineering University
AZ0102, Khirdalan city, Hasan Aliyev str. 120, Absheron, Baku, Azerbaijan
Tel: 00 994 12 - 349 99 95 Fax: 00 994 12 349-99-90/91

e-mail: journal@beu.edu.az
web: http://journal.qu.edu.az
facebook: Journal Of Baku Engineering University

ISSN 2521-635X

ISSN 2521-635X

Journal of Baku Engineering University

MATHEMATICS AND COMPUTER SCIENCE

Baku - AZERBAIJAN

Journal of Baku Engineering University

MATHEMATICS AND COMPUTER SCIENCE

2024. Volume 8, Number 1

CONTENTS

UOT:519.6 (511)
DOİ: https://doi.org/10.30546/09090.2024.110.201

A NUMERICAL ANALYSIS OF A QUEUING-INVENTORY SYSTEM WITH CATASTROPHES

LAMAN POLADOVA[1*], GULNARA VALIJANOVA[2]

[1]institute of Control Systems[*]

[2]Institute of Control Systems, Odlar Yurdu University

lamanpoladova@gmail.com

gyulavelicanova@gmail.com

BAKU, AZERBAIJAN

ARTICLE INFO

Article history:
Received: 2024-07-17
Received in revised form: 2024-09-09
Accepted:2024-10-01
Available online

Keywords: queuing-inventory system, catastrophes, Markov chain, calculation

ABSTRACT

A mathematical model of a queuing-inventory system (QIS) with catastrophes is built. Incoming customers form a Poisson flow with rate λ. The customer servicing time in the considered QIS is zero. The (S, Q) replenishment policy is used to increase the inventory level in the system. Here, S is the maximum storage size of the QIS, and $Q = S - s$ indicates the fixed size of the proposed order, $(s < S/2)$. Analytical formulas for the calculation of steady-state probabilities and performance measures of the system are found. Key performance measures include average inventory levels, reorder rates, and customer loss probability. The results of numerical experiments are given. These experiments are used to study the behavior of performance measures of the system versus initial parameters of the considered hypothetical model.

1. INTRODUCTION

In classic queuing-inventory systems (QIS), it is assumed that the period to sell the inventory to consumers is zero and that system inventories never perish. There are also systems with perishable inventories. These systems fall under two classes: systems whose stocks perish within a certain time interval, and systems whose stocks are destroyed as a result of a catastrophe. Systems whose stocks perish within a certain time interval have been widely studied in [1-5]. Systems whose stocks are destroyed as a result of a catastrophe one by one are relatively understudied, see [6-8]. Systems whose entire stocks are instantly destroyed as a result of a catastrophe and whose servicing time is zero are studied in [9, 10]. In [9], using the "Up to S" replenishment policy is proposed. In the "Up to S" replenishment policy, when the inventory level reaches a certain level s, $0 \leq s < S$, an order is sent to increase inventory, and when new stocks arrive, the inventory level of the system reaches the full storage capacity. In this paper, the parameter S will also indicate the maximum size of the system storage. In [10], the random replenishment policy was used to increase the inventory level in the system. In this replenishment policy, when the inventory level drops to zero, an order is sent to increase inventory and the size of the proposed order is a random variable. In this paper, a similar model is studied using the (S, Q) replenishment policy, where $Q = S - s$ indicates the constant size of the proposed order.

2. DESCRIPTION OF THE MODEL AND PROBLEM STATEMENT

The maximum storage of the QIS under investigation is S and customers in it form a Poisson flow with rate λ. The order servicing time in the considered QIS is zero, i.e., it is a self-service system. Each customer receives a unit size inventory. If the inventory level is zero at the moment of arrival of a customer, it is lost with unity probability. Catastrophes may happen in the system storage. It is assumed that the flows of these catastrophes are also Poisson flows with rate κ. As a result of catastrophes, all stocks are instantly destroyed. If the inventory level of the system is zero, catastrophes do not affect the operation of the system.

The (s, Q) policy is used to increase the inventory level of the system. This policy is defined as follows: when the inventory level of the system reaches s, a new order is sent and the size of the order sent is S-s. The parameter of order lead time has exponential distribution with rate ν. The problem is to find the steady-state distribution of the system under consideration and its following performance measures: the average rate of orders sent to increase the inventory (Reorder Rate, RR), average inventory size, S_{av}, and the probability of loss of customers (P_l).

3. SOLUTION

One of the possible scenarios of changes in the system inventory level is shown in Fig. 2. Here, t_k, k=1,2,... are the instants when orders arrive in the system, ω_k, k=1,2,... are the instants when stocks enter the system, τ_k, k=1,2 indicates the instants when catastrophes occur.

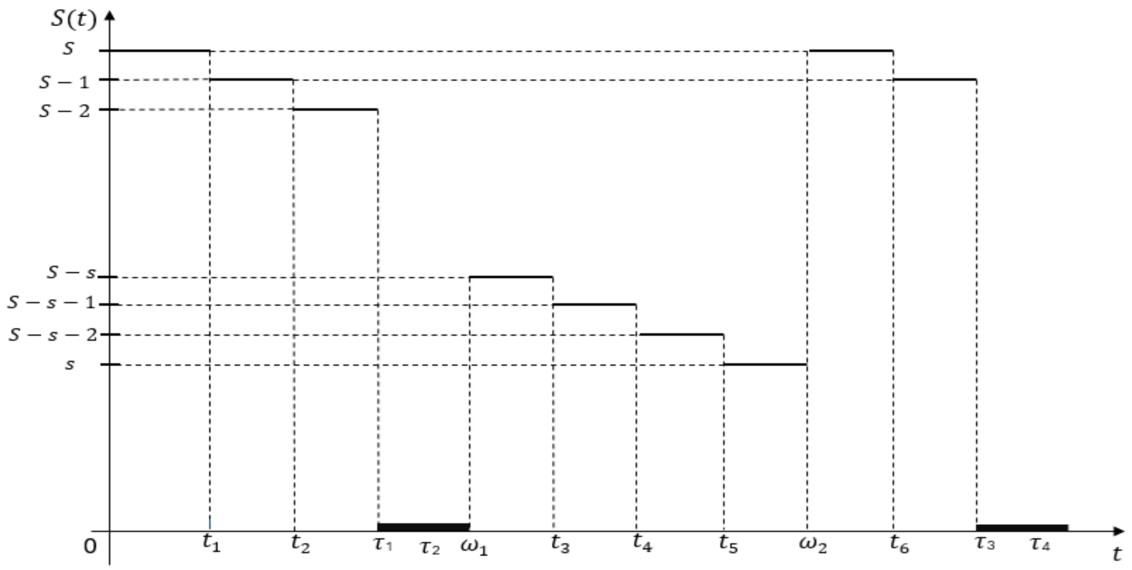

Fig. 1. A possible scenario of changes in the system inventory level

The state of the system at any time instant can be described by the inventory level. The inventory level of the system can take values $m = 0,1, \dots, S$, where S is the maximum size of the system storage. Since the flows (customers and catastrophes) entering the system are Poisson flows and the time required the stocks to enter the system obeys exponential distribution, we can say that the mathematical model of the system is a one-dimensional Markov chain. The state space of this chain is described by the set $E = \{0,1, \dots, S\}$.

The diagram of system states is shown in Fig. 2.

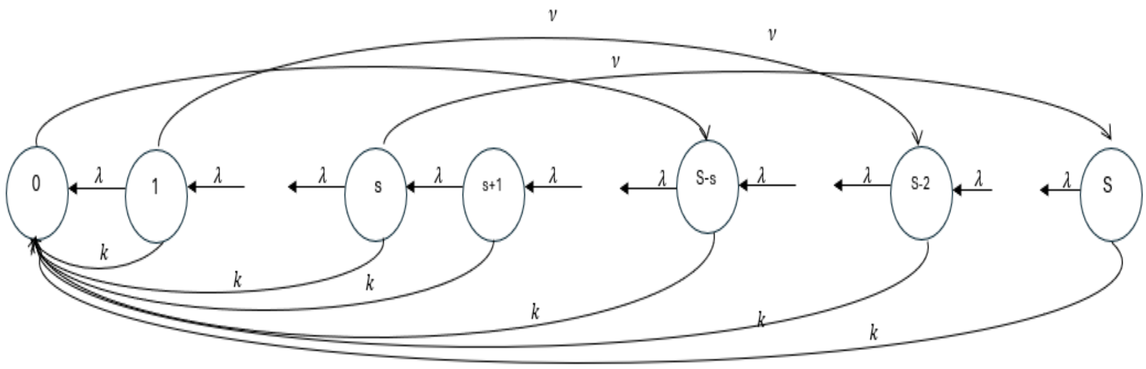

Fig 2. The diagram of system states

Denote the transition rate from a state m to a state m' by $q(m,m')$, $m,m' \in E$. Then the Markov chain generator is defined by the following formula:

$$q(m,m') = \begin{cases} \lambda \; if \; m > 1, m' = m-1 \\ \lambda + k \; if m = 1, m' = 0 \\ k \; if \; m > 1, m' = 0 \\ \nu \; if \; 0 \le m \le s, m' = m + S - s \end{cases} \qquad (1)$$

The finite Markov chain under investigation has a steady state, that is, it is irreducible. We denote the probability of the system being in a state $m \in E$ by $p(m)$. Then the equilibrium equations for steady-state probabilities according to formula (1) are written as follows:

$$-\nu p(0) + (\lambda + k)p(1) + k\big(p(2) + \cdots + p(S)\big) = 0 \qquad (2)$$

$$-(\nu + k + \lambda)p(m) + \lambda p(m+1) = 0, \quad 1 \le m \le s \qquad (3)$$

$$-(k + \lambda)p(m) + \lambda p(m+1) = 0, \quad s+1 \le m \le Q-1 \qquad (4)$$

$$\nu p(m-Q) - (\lambda + k)p(m) + \lambda p(m+1) = 0, \quad Q \le m \le S-1 \qquad (5)$$

$$\nu p(s) - (\lambda + k)p(S) = 0 \qquad (6)$$

The following normalizing condition (7) is added to equilibrium equations (2)-(6):

$$\sum_{m=0}^{S} p(m) = 1. \qquad (7)$$

According to equations (3)-(5), we can obtain the following formulas:

$$p(m+1) = a_{m+1}p(1), \quad a_{m+1} = (1 + \tfrac{(k+\nu)}{\lambda})^m, \quad 1 \le m \le s \qquad (8)$$

$$p(m+1) = a_{m+1}p(1), \quad a_{m+1} = (1 + \tfrac{k}{\lambda})^{m-s}, \quad s+1 \le m \le Q-1 \qquad (9)$$

$$p(m+1) = a_{m+1}p(1) - b_{m+1}p(0), \quad a_{m+1} = a_{s+1}\left(1 + \tfrac{k}{\lambda}\right)^{m-s} - \sum_{s=1}^{m-Q} a_s (1 + \tfrac{\nu}{\lambda})^{m-Q-s},$$

$$b_{m+1} = \tfrac{\nu}{\lambda}(1 + \tfrac{k}{\lambda})^{m-Q} \quad Q \le m \le S-1 \qquad (10)$$

Further, using equilibrium equation (2), we obtain the following formula for probabilities $p(0)$ and $p(1)$:

$$p(1) = p(0)\frac{k+\nu}{\lambda} - \frac{k}{\lambda} \qquad (11)$$

Using normalizing condition (7) and formulas (8)-(11), we obtain the following formula for probability $p(0)$:

$$p(0) + p(1) + p(1)(a_2 + \cdots + a_{s+1}) + p(1)(a_{s+2} + \cdots + a_s) - p(0)(b_{Q+1} + \cdots + b_S) = 1$$

$$p(0) = \frac{1+\frac{k}{\lambda}\sum_{m=1}^{S} a_m}{1+\frac{k+\nu}{\lambda}\sum_{m=1}^{S} a_m - \sum_{m=Q+1}^{S} b_m} \qquad (12)$$

After determining the steady-state probabilities, the performance measures of the system are calculated as follows.

- Average rate of orders sent to replenish the inventory (Reorder Rate, RR):

$$RR = \lambda p(s+1) + \kappa\left(1 - p(0)\right). \qquad (13)$$

- Average inventory size, S_{av}:

$$S_{av} = \sum_{m=1}^{S} mp(m) \qquad (14)$$

- If at the moment of arrival of customers, the inventory level is zero, customers leave the system without receiving stocks. For this reason, the probability of loss, P_l, of customers is determined as follows:

$$P_l = p(0) \qquad (15)$$

4. NUMERICAL RESULTS

Using obtained formulas (8)-(10), experiments were conducted to calculate the performance measures of the system. In the following, we consider the results of these numerical experiments. The purpose of these experiments was to study the relationship between the performance measures of the system and its input parameters. The maximum system storage size in all the experiments is assumed to be constant, i.e., $S = 50$.

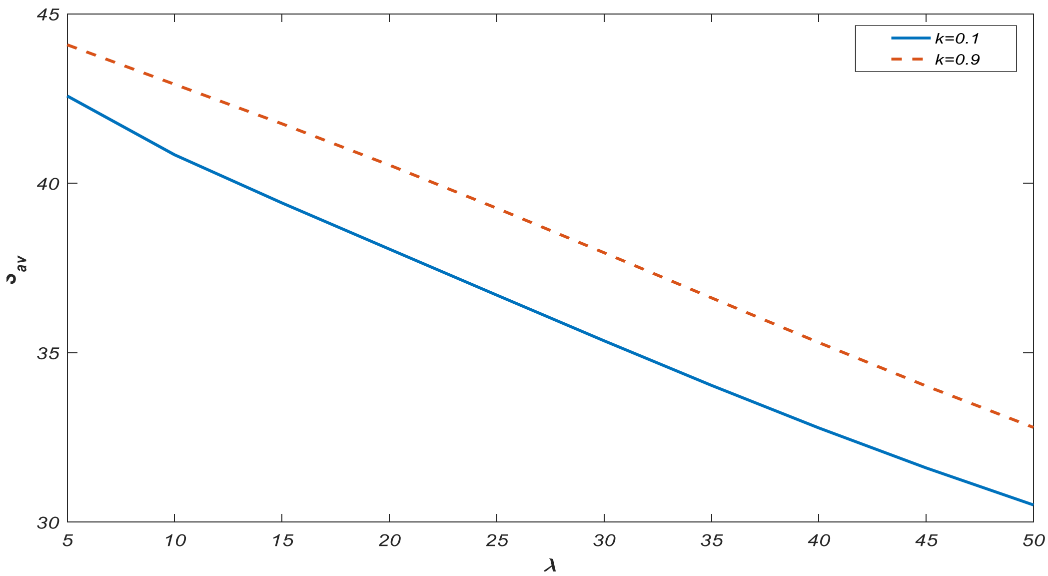

(a)

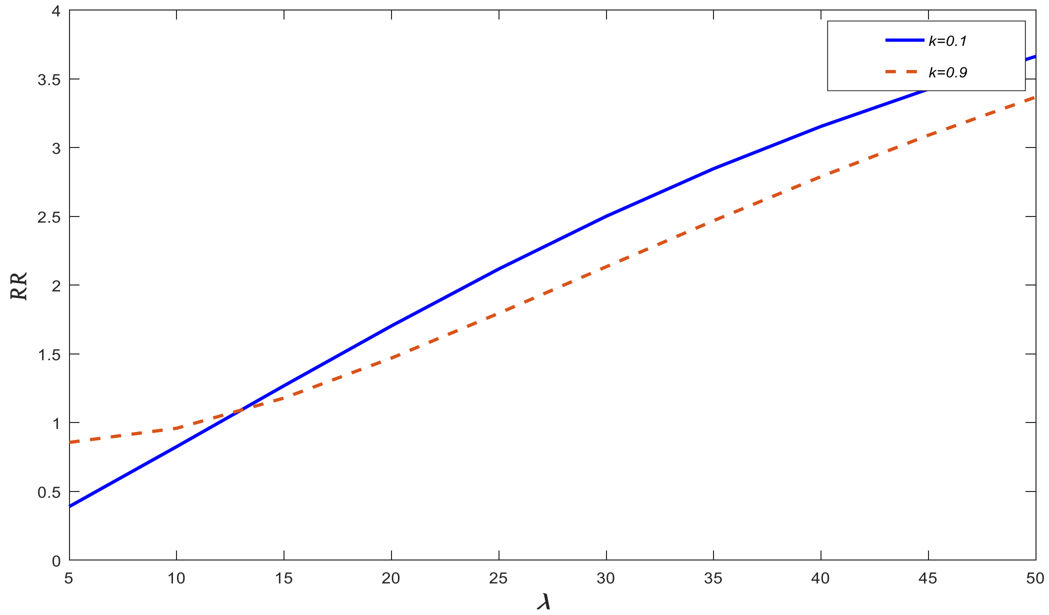

(b)

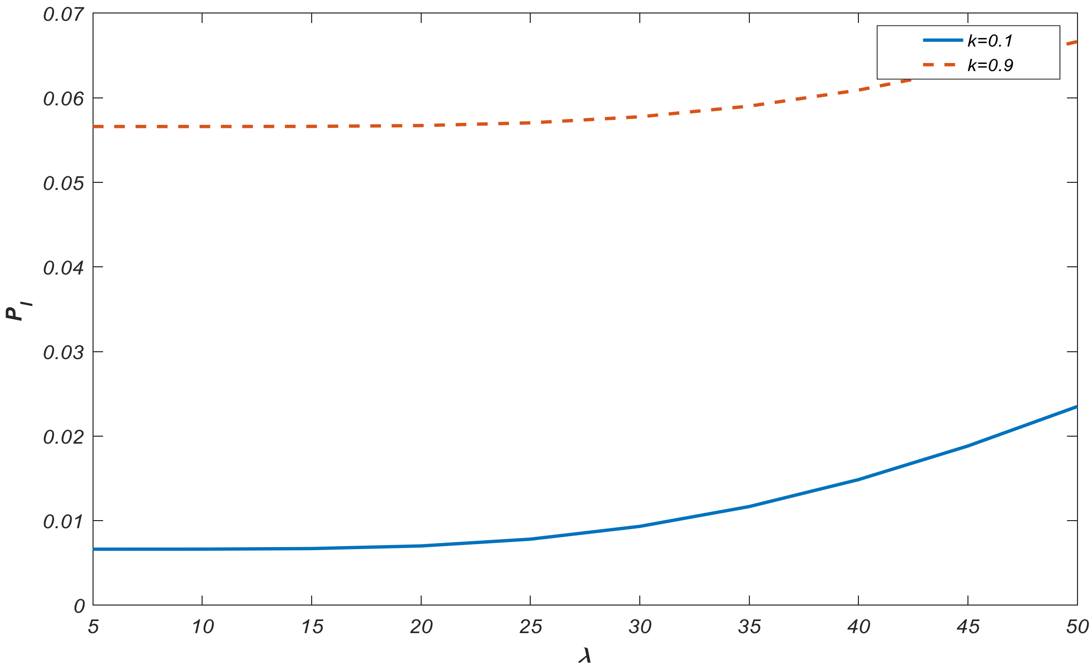

(c)

Fig.3. Performance measures vs λ;

Fig. 3 shows the graphs of the relationship between the performance measures of the system and the demand rate. As the demand rate increases, the average inventory level of the system decreases, see Fig. 3(a). Two different estimates of the catastrophe rate are examined in the graphs. The average inventory level of the system decreases relative to the change in the value of the catastrophe rate, see Fig. 3(a). When the value of the demand rate increases, the average rate of orders sent to replenish the system inventory (RR) increases; this is due to the fact that as the demand rate increases the inventory level rapidly drops to a critical level (s), see Fig. 3(b). Changes in the catastrophe rate have no significant effect on the average rate of replenishment orders sent, see Fig. 3(b). As the demand rate increases, the probability of order loss also increases, because the probability of the system inventory dropping to zero increases; as can be seen from the graph, as the catastrophe rate increases, the probability of order loss also increases, see Fig. 3(c).

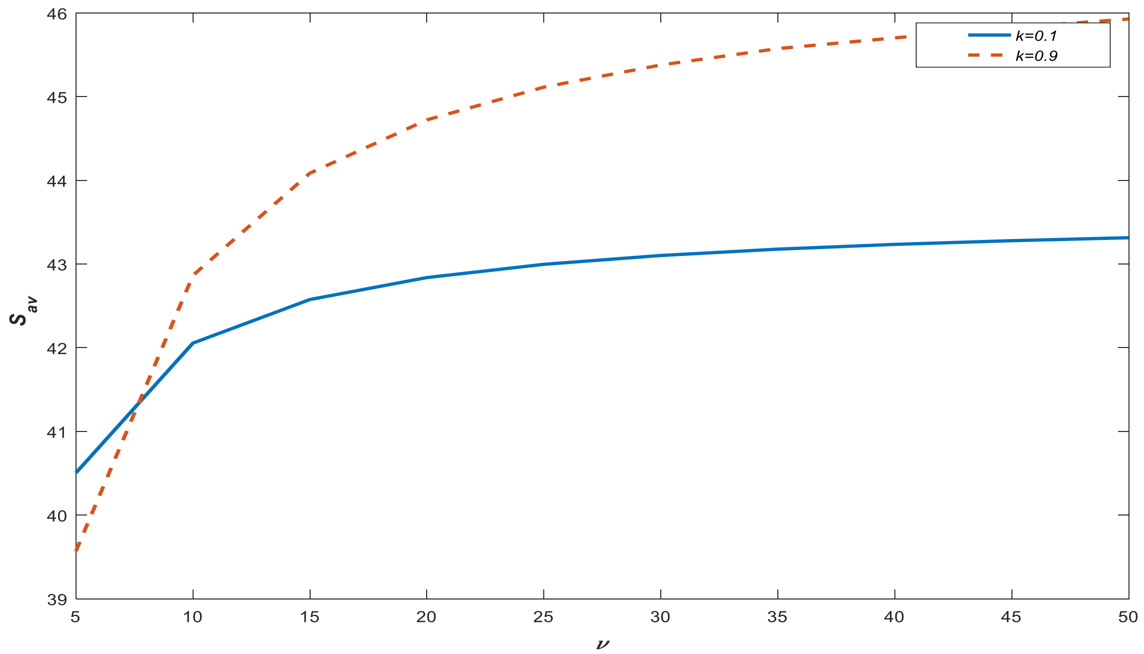

(a)

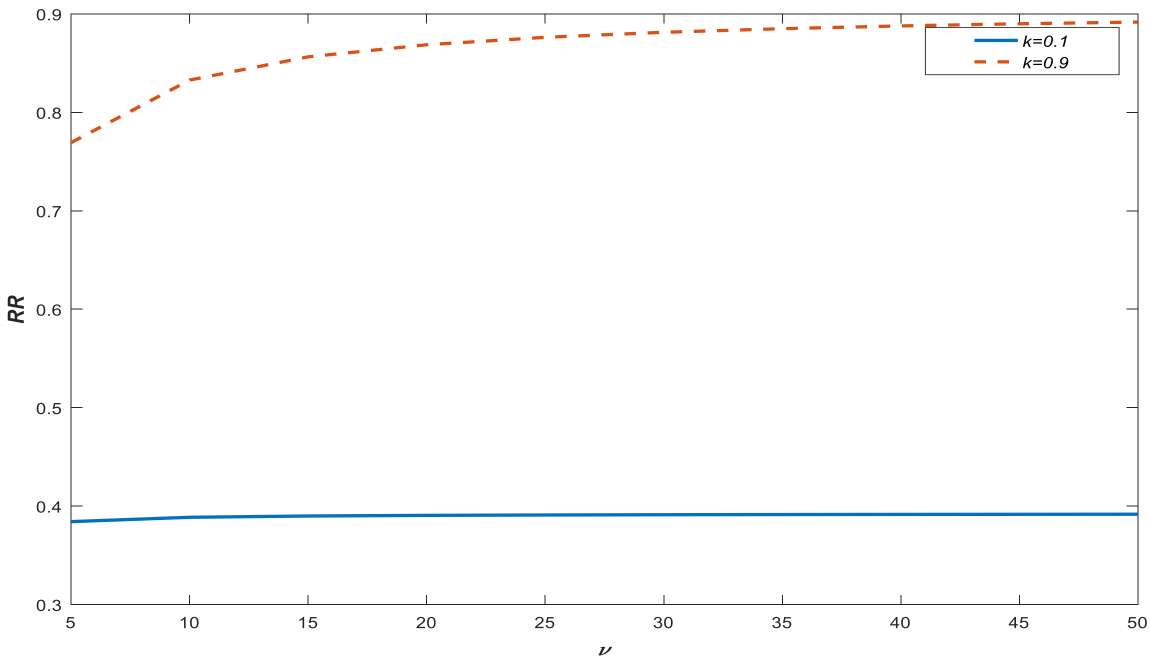

(b)

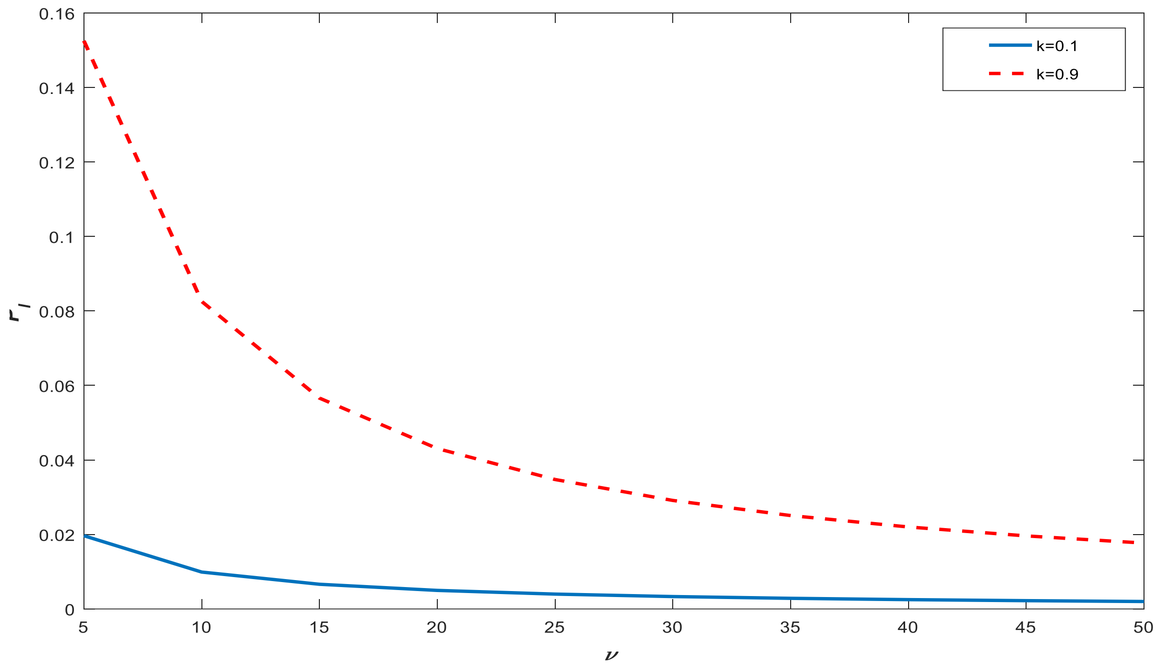

(c)

Fig.4. Performance measures vs ν;

Fig. 4 shows the relationship between the performance measures of the system and the inventory replenishment rate (ν). When the inventory replenishment rate increases, the average inventory level increases as well. At the same time, when the catastrophe rate increases, the probability of the system inventory dropping to zero increases, and because of this, the average inventory level decreases, see Fig. 4(a), for the selected initial values of the parameters, a twofold increase of the rate κ has no significant effect on the average level of such inventory. When the value of the inventory replenishment rate increases, the probability of the system inventory being non-zero increases, and because of this, the average reorder rate also increases, see formula (13). The average rate of orders sent to replenish the inventory increases relative to the variation of the catastrophe rate, and at small values of the parameter, changes in the catastrophe rate have no significant effect on the performance measure; however, at large values of the parameter, changes in the catastrophe rate have a significant effect on the performance measure, see Fig. 4(b). The decrease of the probability of customer loss is due to the fact that the probability of the system inventory dropping to zero decreases when the parameter increases; the performance measure increases relative to the variation of the catastrophe rate, which is particularly evident at small values of the parameter, see Fig. 4(c).

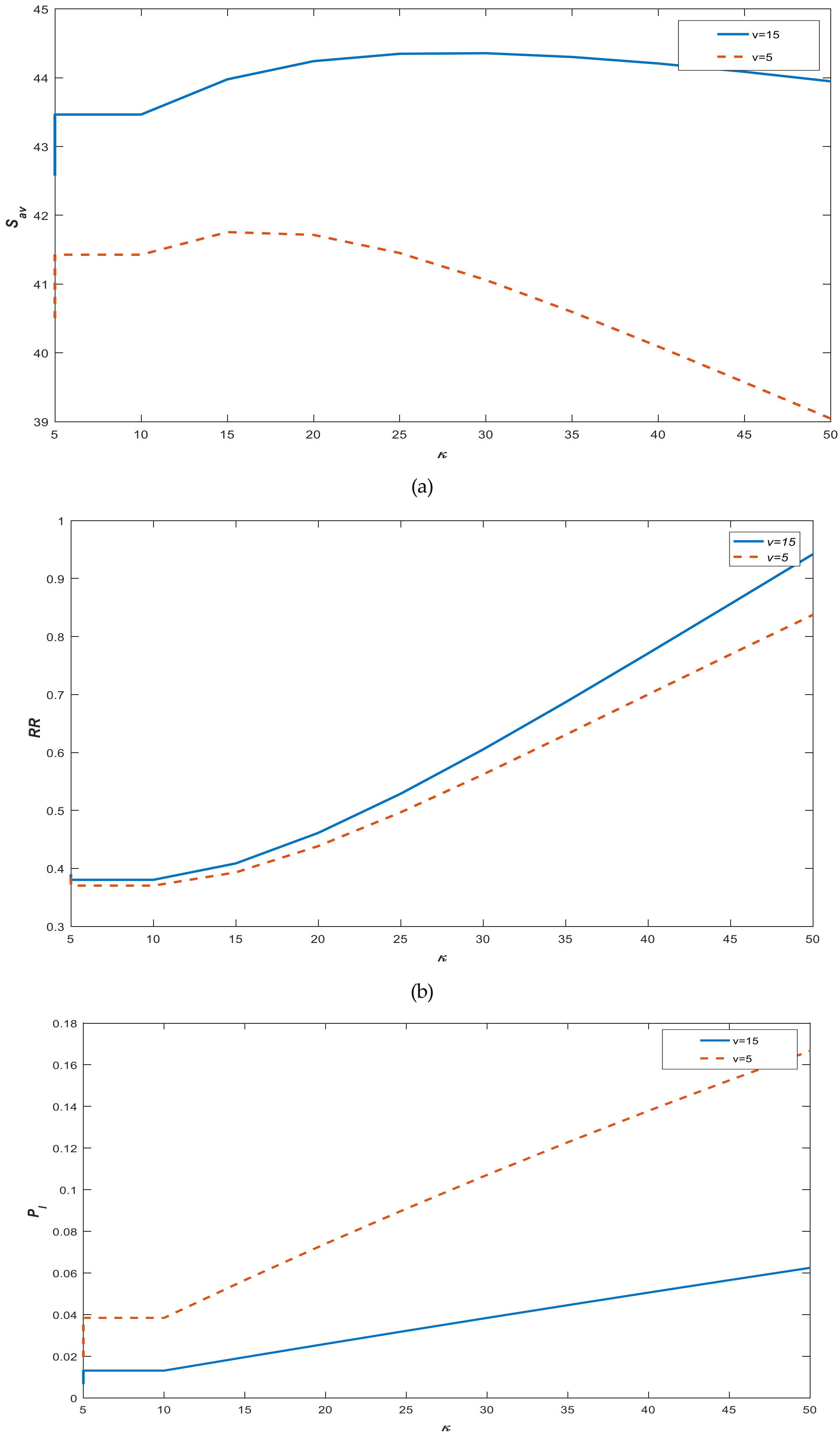

Fig.5. Performance measures vs κ;

Fig. 5(a) shows the relationship between the performance measures of the system and the catastrophe rate. As can be seen from the graphs, when the value of the parameter κ increases, the average inventory level of the system decreases. Different estimates of the inventory replenishment rate are examined in the graphs. For example, the average inventory level of the system increases relative to the inventory replenishment rate, see Fig. 5(a). When the value of the catastrophe rate increases, the inventory level of the system rapidly drops to zero, and for this reason, the average rate of orders sent to replenish the system inventory (see Fig. 5(b)) and the probability of customer loss (see Fig. 5(c)) increase. As can be seen from the graphs, changes in the inventory replenishment rate have a significant effect on the performance measures. Since at large values of the parameter κ the probability of the system inventory dropping to zero decreases, RR increases relative to the parameter, and P_l decreases; at large values of the parameter, changes in the inventory replenishment rate have a significant effect on the performance measures. See Fig. 5(a), Fig. 5(b).

REFERENCES

1. Hanukov, G.; Avinadav, T.; Chernonog, T.; Yechiali, U. (2019) Performance improvement of a service system via stocking perishable preliminary services. *Eur J Oper Res*, 274, 1000-1011.
2. Hanukov, G.; Avinadav, T.; Chernonog, T.; Yechiali, U. (2020) A service system with perishable products where customers are either fastidious or strategic. *Int. J. Prod. Economics*, 228, Article 107696.
3. Jose K.P.; Reshmi P.C. (2021). A production inventory model with deteriorating items and retrial demands. *OPSEARCH* 58(1), 71-82.
4. Ko, S.S. (2020) A Nonhomogeneous Quas-Birth Process Approach for an (s, S) Policy for a Perishable Inventory System with Retrial Demands. *J. Ind. & Manag. Opt.* 16, 1415-1433.
5. Melikov A., Krishnamoorthy A., Shahmaliyev M.O. (2019) Numerical Analysis and Long Run Total Cost Optimization of Perishable Queuing Inventory Systems with Delayed Feedback. *Queuing Models and Service Managements*. 2(1), 83-111.
6. Melikov A.Z. Mirzayev R.R. Nair S.S. (2022) Numerical Study of a Queuing-Inventory System with Two Supply Sources and Destructive Customers, J. Comput. Syst. Sci. Int. Vol.61. P.581–598.
7. Melikov A. Mirzayev R. Nair S.S. (2022) Double Sources Queuing-Inventory System with Hybrid Replenishment Policy. Mathematics, Vol. 10. 2423.
8. Melikov A. Mirzayev R. Sztrik J. (2023) Double-Sources Queuing-Inventory Systems with Finite Waiting Room and Destructible Stocks. Mathematics. Vol.11. 226.
9. Poladova L. (2022) On One Model of Inventory Management System with Catastrophes. Journal of Baku Engineering University, Mathematics and computer science, No.1. P.60-68.
10. Poladova L., Velicanova G. (2023) Model of queuing-inventory system with catastrophes and random replenishment policy. 2nd International Conference on Problems of Logistics, Management and Operation in The East-West Transport Corridor (PLMO 2023). DOI:10.54381/plmo2023.33.

2024. Volume 8, Number 1 Pages 12-20

UOT:002
DOİ: https://doi.org/10.30546/09090.2024.110.203

EVALUATING THE EFFECTIVENESS OF MICROSOFT INTUNE IN SECURING DEVICES: BALANCING SECURITY FEATURES AND USER EXPERIENCE IN ENTERPRISE ENVIRONMENTS

SAMUR AHMADOV

Azerbaijan Technical University

ARTICLE INFO

Article history:
Received: 2024-08-06
Received in revised form: 2024-09-12
Accepted: 2024-10-01
Available online

Keywords: Microsoft Intune;
Mobile device management;
Cloud security;
Enterprise mobility and security
JEL codes:
L86, O33, M15

ABSTRACT

Nearly every organization would like to adapt their environment to the cloud to increase productivity and decrease operational costs. By moving to the cloud, organizations are still struggling with enterprise mobile management systems. Managing devices can be challenging because of the complexity of the Microsoft ecosystem. However, Microsoft Intune is a service which was created to solve issues with managing devices and increase device security. This product can help to reduce potential security incidents within the organization and even during collaboration with other organizations.
The research employs a methodical approach where organizations utilize Microsoft Intune with its full capabilities and all available security configurations. This paper will examine Microsoft Intune's effectiveness in the matter of device management and security with different aspects.

1. Introduction

Users' device security is one of the significantly under-researched fields in Cloud Security. From the technical perspective, users can adapt to any changes within the organization. However, changes that were made previously need to provide a good user experience and not be overcomplicated. Consider a scenario where a device requires a BitLocker key, fingerprint, face recognition, and an additional password for sign-in. From a security perspective, it is a strongly secure way to have access to corporate devices and data. Users can find it frustrating and challenging to remember the BitLocker key and a strong password to type in every time users need to do their day-to-day tasks. This dichotomy between stringent security measures and user experience highlights a critical area for further investigation in device management.

More than 10 years ago, this topic was researched by Gustavo et al. [1], where researchers proposed a new security architecture for the mobile enterprise that uses network-based security and cloud computing. Other research was conducted in mobile device management by Song, X., & Yang, C.-H. [2]. They used the Android Open Source Project and SELinux to help enterprises manage and secure both corporate and bring-your-own-device (BYOD) mobile devices. The solution has options to track location, verify files, control permissions in real-time, and send informational push notifications. The system was developed using the Java programming language and tested on a customized Android 7.1.1 device.

Baltazar et al. [3] conducted research that underscores how Enterprise Information Systems (EIS) can be a key driver for improved and sustainable mobility. A case study was performed in one of the Portuguese companies for a carsharing platform. They also noted the significance of AI/ML for security.

Hasan et al. [4] presented a framework and guidelines for securing mobile enterprise applications. The framework includes a meta-model (UML diagram) that describes the framework components, a guidance model listing mobile security threats and countermeasures, and decision-making for logging security design decisions. The challenge of that framework could be with new threats and countermeasures and undefined or zero-day attacks. However, the proposed framework still supports enterprises in the decision-making process for mobile applications.

BYOD devices were discussed by Hina Batool [5], where the researcher discusses Mobile Device Management (MDM) systems for enterprises and partially for BYOD devices. The researcher identified major features of MDM such as profile management, location tracking, remote lock and wipe, malware detection, data backup and encryption, and URL blacklisting. The researcher reviewed MDM solutions such as AirWatch by VMware, IBM MaaS360, and Kaspersky Lab, and made a comparison. A comparison table was designed with Yes/No answers to security requirements. Almost all requirements were satisfied or partially satisfied by vendors. This research also doesn't cover the effectiveness of MDM in terms of security.

Another paper discussing the importance of developing strategies was written by Yucel [6]. The researcher used characterization of the mobile strategy based on different parameters such as objectives, users, mobile solution, mobile and backend platforms, benefits, drawbacks, risks and mitigation plans, strategies for distribution, launch, marketing, promotion and positioning, costs, etc. The generic model counts the rate of potential users and shows relationships between factors such as user adoption, benefits, economic utilities, and others. The idea of that research was increasing return on investment while receiving benefits from enterprise mobility.

Another field to study is mobile application management (MAM) for pushing applications through a centralized console. The MAM question was researched by Yamin, M. M., & Katt, B [7]. The research includes an introduction to MDM and its main functions, discussion of enabling protocols for MDM such as Smart Message, Open Mobile Alliance Device Management, and Over-The-Air Programming. MAM questions and challenges were also researched in different papers [8], [9].

Ana Maria Suduca and Mihai Bizoia [10] explored ways of integrating and pushing apps in the easiest way. Microsoft Intune was utilized to minimize application pushing effort. During the research, they pushed the videoconferencing application Zoom through Intune, which significantly reduced the amount of time required.

The majority of the researched articles use a similar research method – comparative analysis. In the modern world, comparing features is not sufficient for building a security fortress, especially for enterprises and government entities. Thus, this article will present a real test scenario with the proposed solution and highlight advantages for Security Operations Teams to quickly identify and address security issues.

2. Background

Microsoft Intune is Microsoft's cloud-based service that acts as an enterprise mobility management (EMM) and MDM solution. Microsoft Intune supports a diverse range of operating systems: Windows, macOS, Android, Linux, and iOS devices. There are several ways to accomplish the onboarding process for devices to Microsoft Intune: group-based, Autopilot, Apple Business Manager for iOS devices, and Android Enterprise for Android devices. Additionally, the user onboarding process can be performed automatically during the first sign-in with Windows credentials, or via the Company Portal application from the store for mobile devices. After the onboarding process, users will receive a set of policies that were configured in Microsoft's security portal and can receive new policy enforcements during subsequent policy update cycles. The high-level architecture of Microsoft Intune is given in the following figure.

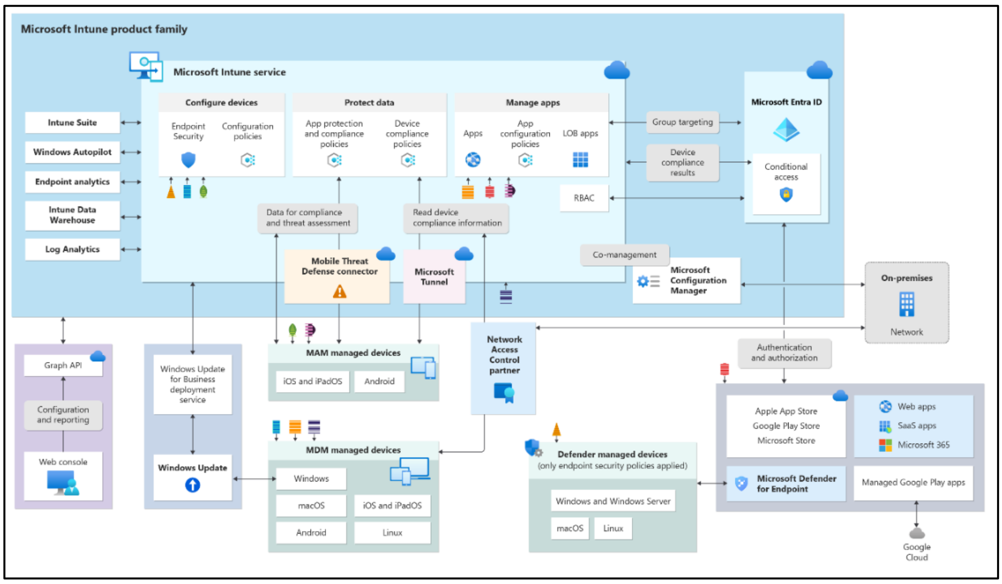

Fig. 1 High-level Microsoft Intune architecture

As shown in Fig. 1, the architecture consists of several components such as: Microsoft Intune service, Graph API, Windows Update for Business deployment service, MAM managed devices, Network Access Control partner, and Microsoft Configuration Manager for on-premises deployment. Moreover, the figure depicts Intune's integration with Microsoft Defender for Endpoint, a comprehensive security solution that functions as both an antivirus and endpoint detection and response suite. This integration underscores the security measures that can be implemented via Microsoft Defender for Endpoint within the Microsoft ecosystem.

3. Methodology

To evaluate the effectiveness of the solution, a structured approach is needed. The following figure shows the methodological steps.

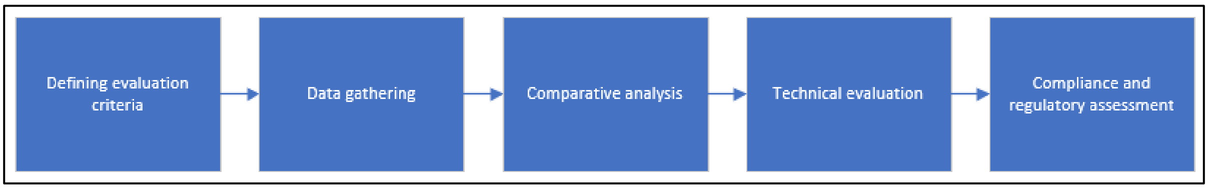

Fig. 2 Main steps to evaluate effectiveness of Microsoft Intune

These steps should be considered high-level steps that underscore the importance of Microsoft Intune and its capabilities across both Microsoft and non-Microsoft ecosystems

Defining evaluation criteria. This step includes several factors which should be evaluated during the usage of Microsoft Intune: device compliance rates, malware detection and prevention, remote wipe effectiveness, time to deploy security patches, time to update policies, app protection policy enforcement.

Microsoft Intune has compliance policies which can be defined in the portal. They are a set of rules and conditions that would be evaluated during the policy update timeframe. Malware detection and prevention criteria rely on Microsoft Defender for Endpoint system.

Data gathering. This step underscores the necessity of gathering important data for preventing attacks. For instance, an endpoint's IP address and agent status can be considered as data to understand the endpoint's current security status.

Comparative analysis. Microsoft Intune has many mechanisms in terms of configuration, policies, and integrations. Considering this, best practices will be used to build a secure ecosystem across the organization.

Technical evaluation. From a technical perspective, the solution should be scalable, adaptable for end users in terms of user experience, and easy to use for security administrators. This step will evaluate these parameters. The research was conducted in different environments that have varying compliance requirements and restriction levels.

Compliance and regulatory. Compliance ensures that this data is handled according to legal requirements and industry standards. There are global regulations, such as GDPR in the EU and HIPAA in US healthcare, as well as various industry-specific standards. Having compliance and regulation methods in place helps to quickly pass audits.

During this research, metrics will be used to calculate overall security posture and user experience. The following table contains information about metrics. Metrics were evaluated based on the security features, where 2 indicates the feature significantly affects user experience, 1 indicates the feature affects user experience, and 0 indicates the feature does not affect user experience.

Table 1
Parameters

Security features	User experience
Device encryption	Ease of enrollment
Multi-factor authentication	App accessibility
App protection policies	Performance impact
Conditional access	Privacy considerations
Data loss prevention	Self-service capabilities
Remote wipe capabilities	User interface intuitiveness
Compliance policies	Support and troubleshooting experience

4. Comparative Analysis of MDM Solutions

To provide context for Microsoft Intune's effectiveness, it's important to compare it with other major Mobile Device Management (MDM) solutions in the market. For this analysis, we'll compare Microsoft Intune with two other prominent solutions: VMware Workspace ONE (formerly AirWatch) and IBM MaaS360. Table 3 provides a high-level comparison of key features across the three MDM solutions:

Table 3
Feature Comparison of MDM Solutions

Feature	Microsoft Intune	VMware Workspace ONE	IBM MaaS360
Device enrollment	+	+	+
OS support	Windows, iOS, Android, macOS	Windows, iOS, Android, macOS, Linux	Windows, iOS, Android, macOS
App management	+	+	+
Device encryption	+	+	+
Remote wipe	+	+	+
Conditional access	+	+	+
Integration with identity managementt	Entra ID	VMware Identity Manager	IBM Cloud Identity
Threat defense integration	Microsoft Defender for Endpoint	VMware Carbon Black	IBM Trusteer
Unified endpoint management	+	+	+
Container-based separation	+	+	+

While Microsoft Intune, VMware Workspace ONE, and IBM MaaS360 all offer robust MDM capabilities, the choice between them often depends on an organization's existing IT infrastructure, specific security needs, and integration requirements.

5. Implementation and tests

Implementation and testing were performed in a test environment to ensure network isolation. To ensure data reliability, data were gathered from different types of organizations: financial institutions, accommodation businesses, hotels, and resorts.

Device encryption analysis. BitLocker provides full device encryption for Windows OS. Microsoft Intune allows creation of policies that ensure BitLocker is utilized across all devices. To perform encryption, security administrators can create a configuration profile in Intune. This setting can be implemented silently without user interaction, which significantly improves user experience.

Multi-factor authentication. The impact of multi-factor authentication (MFA) is significant in the modern world. MFA reduces almost 80% of attacks. Research conducted by Liu W. et al. [11] shows how MFA can be utilized not only in enterprises but also in the Internet of Things (IoT). While MFA reduces the risk of user credential theft, it adds an additional step during sign-in to the system. MFA can be performed in various ways: using push notifications, SMS, voice, or an authenticator app (code).

App protection policies. App protection policies (APP) are rules that ensure an organization's data remains safe or contained in managed apps. These policies protect company data at the app level. For instance, users can be required to enter a PIN to open an app in a work container, can have limited sharing options between apps, and cannot save company data in personal storage. These settings can reduce user-experience and require additional step for accessing company data.

Conditional access. Conditional access is a solution that works like an if-then statement. If the requirements are met, then access will be granted, blocked, or monitored. Microsoft Intune has an option called "device state". Device state can be compliant, non-compliant, or in a grace period, depending on the compliance policies. By using this parameter, entities can block access to high-level applications by requiring devices to be marked as compliant in the Intune portal. Conditional access policies have impact on the user-experience.

Data Loss Prevention. With profile isolation on mobile devices, Intune can use data loss prevention mechanisms. For example, with the help of mobile application management policies, users are unable to copy data from the work profile to personal profiles. It is also possible to enable redirection to company internal resources during searches in the Microsoft Edge web browser. These policies have impact on the user-experience.

Remote wipe capabilities. Wiping devices can be critically necessary when an employee is terminated or when a device is stolen. Based on the tests, remote wipe will take effect in less than one minute for Android devices and almost immediately for iOS devices. There are also different scenarios, such as when an organization buys corporate phones for workers and the devices need to be reassigned to other employees or departments. Other scenarios could include decommissioning old devices or providing access to contractors who will have only limited access to company applications to perform their jobs.

Compliance policies. Every organization has its own local policies and processes. Users should adhere to the principles and processes that were established previously and remain compliant while working with company data. Considering this, compliance policies have a significant impact on user experience.

During the research, all the mentioned parameters were evaluated. After testing on 650 devices, the statistical analysis mentioned earlier could be performed. Evaluating based on features alone is not enough; however, where security features and user experience have intersection points, statistical analysis can be performed. This analysis consists of all mentioned security features and user experience metrics. To gather information, a survey was conducted among users from different organizations. Based on the answers and the results of tests inside the laboratory environment, Table 3 was created.

The following table illustrates scoring based on different parameters across different organizations.

Table 3
Survey results

Security features	Ease of enrollment	App accessib ility	Perfor-mance	Privacy	Self-service capabilities	User interface intuitiveness	Sup port
Device encryption	1	0	1	0	0	1	1
Multi-factor authentication	1	1	2	2	2	2	1
App protection policies	0	1	1	1	0	1	1
Conditional access	2	1	2	1	0	1	1
Data loss prevention	1	1	2	2	0	1	1
Remote wipe capabilities	2	2	0	2	0	0	2
Compliance policies	2	2	1	2	0	1	2

This table could be used to evaluate the trade-offs between security features and user experience, helping to make informed decisions about which features to implement based on organizational priorities and the impact on various aspects of system use and management.

For each security feature, mean, median, and standard deviation were used. Considering that a number of coefficients are 7 and middle value could be used without averaging two middle numbers, median was used to determine standard deviation. Standard deviation helps quantify how consistently each security feature impacts different aspects of user experience. A low standard deviation indicates that a feature has a similar impact across various user experience factors, while a high standard deviation suggests the impact varies widely. The following formulas show the calculations for mean and standard deviation.

$$\mu = (\sum X)/n, \tag{1}$$

where μ – mean, x – each value in dataset, n – number of values

$$\sigma = \sqrt{[\sum(x-\mu)^2/N]} \tag{2}$$

where σ – standard deviation, μ – mean, x – each value in dataset, n – number of values

Table 4
Statistical Analysis of Survey Results

Security Feature	Mean	Median	Standard Deviation
Device encryption	0.57	1	0.53
MFA	1.57	2	0.53
APP	0.71	1	0.49
Conditional access	1.14	1	0.69
DLP	1.14	1	0.69
Remote wipe	1.14	2	1.07
Compliance policies	1.43	2	0.79

Statistical analysis of the survey results reveals interesting patterns in the impact of security features on user experience. Device encryption had the lowest mean impact (0.57), suggesting it's generally well-tolerated by users. In contrast, multi-factor authentication showed the highest mean impact (1.57), indicating it's perceived as more disruptive to the user experience. The following chart illustrates the mean, median, and standard deviation of the impact each security feature has on user experience. Higher values for mean and median indicate a greater impact on user experience, while higher standard deviation suggests more variability in how the feature affects different aspects of user experience

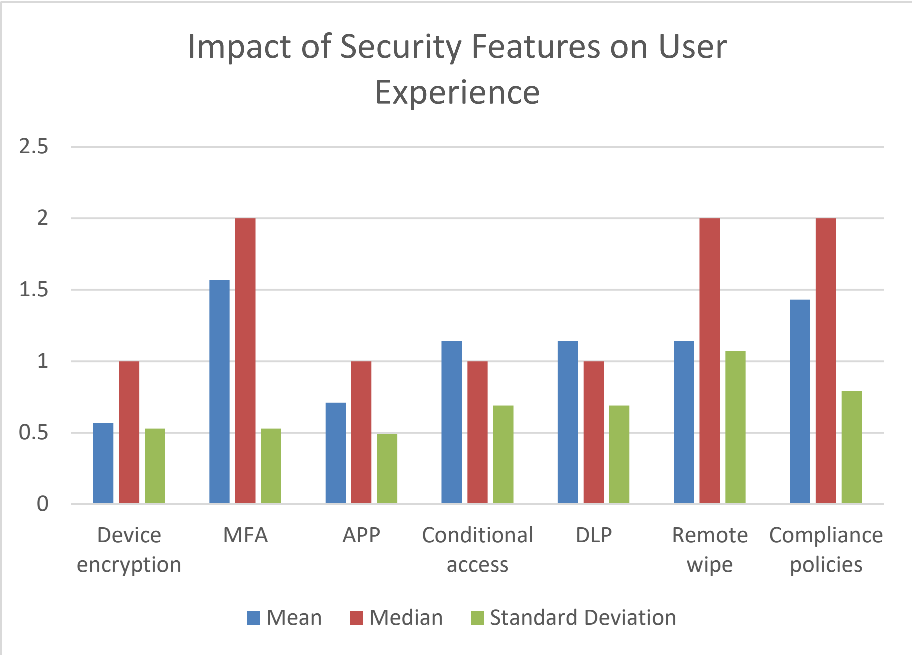

Fig. 3 Impact of Security Features on User Experience

The Fig.3 shows trade-off in a graphical way to easier to understand and compare security features and their impact on user experience. It helps identify features that might have extreme impacts in certain areas, which could be masked by looking at averages alone. Including standard deviation adds statistical rigor to your analysis, demonstrating a more thorough examination of the data beyond simple averages.

6. Conclusion

This research has conducted a comprehensive evaluation of Microsoft Intune's effectiveness in securing devices within enterprise environments, with a particular focus on the delicate balance between robust security features and user experience. Through a structured methodology of evaluation criteria definition, data gathering, comparative analysis, technical evaluation, and compliance considerations, valuable insights were obtained regarding Intune's capabilities.

The findings indicate that Microsoft Intune offers a set of features for device management, security, and integration between the two. To ensure device security, the following features were researched: device encryption, multi-factor authentication, app protection policies, conditional access, data loss prevention, remote wipe capabilities, and compliance policies. Each of these features contributes significantly to enhancing the organization's security posture.

The trade-off analysis between security features and user experience revealed that while some security measures like device encryption have minimal impact on usability, others such as multi-factor authentication and conditional access policies can significantly affect the user experience. This highlights the need for organizations to carefully balance security requirements with usability considerations when implementing Intune.

Research across different types of organizations, including financial institutions and hospitality businesses, demonstrated that Intune's effectiveness can vary depending on the specific needs and constraints of each sector. However, overall, Intune proved to be a versatile and powerful tool for managing and securing diverse device ecosystems.

While Intune demonstrates strong capabilities in device management and security, it is important to note that no single solution can address all security challenges. Organizations should view Intune as a critical component of a broader, layered security strategy that includes other measures such as regular security training for employees, network security solutions, and continuous monitoring and improvement of security practices.

In conclusion, Microsoft Intune proves to be an effective solution for securing devices in modern organizational environments. Its comprehensive feature set, coupled with its ability to balance security needs with user experience considerations, makes it a valuable tool for organizations seeking to enhance their mobile device management and security capabilities. However, successful implementation requires careful planning, ongoing management, and a clear understanding of the organization's specific security needs and user requirements.

Reference list

1. De los Reyes, G., Macwan, S., Chawla, D., & Serban, C. (2012). Securing the mobile enterprise with network-based security and cloud computing. 35th IEEE Sarnoff Symposium.
2. Song, X., & Yang, C.-H. (2017). Mobile Device Management System Based on AOSP and SELinux. IEEE Second International Conference on Data Science in Cyberspace (DSC).
3. Baltazar, S., Barreto, L., Amaral, A., & Pereira, T. (2020). Enterprise Information Systems (EIS) as a key driver towards improved mobility. 2020 IEEE International Conference on Engineering, Technology and Innovation (ICE/ITMC).
4. Hasan, B., Dmitriyev, V., Gomez, J. M., & Kurzhofer, J. (2014). A framework along with guidelines for designing secure mobile enterprise applications. 2014 International Carnahan Conference on Security Technology (ICCST).
5. Batool, H., & Masood, A. (2020). Enterprise Mobile Device Management Requirements and Features. IEEE INFOCOM 2020 - IEEE Conference on Computer Communications Workshops (INFOCOM WKSHPS).
6. Yucel, S. (2017). Evaluating Enterprise Mobility Strategy. 2017 International Conference on Computational Science and Computational Intelligence (CSCI).
7. Yamin, M. M., & Katt, B. (2019). Mobile device management (MDM) technologies, issues and challenges. Proceedings of the 3rd International Conference on Cryptography, Security and Privacy - ICCSP '19.
8. Raj Kumar Koneru, Pattabhi Rama Rao Dasari, Prajakt Deshpande, Vivek Iyer, Rajendra Komandur, Aravind Perumal, Sriram Ramanathan, Matthew Terry, Vamsi Krishna Vagvala, Sathyanarayana Vennapusala, et al. (2016). Mobile application management systems and methods thereof. US Patent 9,405,723.
9. Murali Krishna Medudula, Mahim Sagar, and Ravi Parkash Gandhi (2016). Mobile Device: Applications, Over the Top Services, Identity Protection and BYOD Policy. In Telecom Management in Emerging Economies. Springer, 207–227.
10. Ana Maria Suduca, Mihai Bizoia (2022). AI shapes the future of web conferencing platforms. 9th International Conference on Information Technology and Quantitative Management.
11. Liu, W., Wang, X., & Peng, W. (2019). Secure Remote Multi-Factor Authentication Scheme Based on Chaotic Map Zero-knowledge proof for Crowdsourcing Internet of Things. IEEE Access, 1–1.

2024. Volume 8, Number 1 Pages 21-31

UOT:519.6 (517.98)
DOİ: https://doi.org/10.30546/09090.2024.110.210

ON SOME HYPERSINGULAR INTEGRALS

CHINARA GADJIEVA

Baku Engineering University, Khirdalan city, Hasan Aliyev str., 120 az0101, Absheron, Azerbaijan

Department of Mathematics

Orcid: 0009-0003-6912-4271

chaciyeva@beu.edu.az

ARTICLE INFO	ABSTRACT
Article history: Received:2024-09-13 Received in revised form:2024-09-23 Accepted:2024-10-25 Available online *Key words: hypersingular integral,approximating operators,speed of convergence, Cauchy kernel.*	*The paper examines different types of hypersingular integrals with the Cauchy kernel on a segment and a unit circle and defines them using specific methods. It presents more general definitions for one-dimensional hypersingular integrals with the Cauchy kernel based on Hadamard's integral in the sense of a finite part. The paper also establishes the existence theorems of these hypersingular integrals and* ***formulas, which*** *demonstrates the accuracy of the resulting integrals that are applied in various applications and engineering problem-solving.* ***The proposed formulas are straightforward to calculate, making the new approximate method reliable and easy to apply and the obtained*** *numerical results demonstrate* ***the stability and efficiency of the approach.***

BƏZİ HİPERSİNQULYAR İNTEQRALLAR HAQQINDA

XÜLASƏ

İşdə parçada və vahid çevrədə müxtəlif növ Koşi nüvəli hipersinqulyar inteqrallar öyrənilir və onlar xüsusi üsulla təyin edilir, belə ki, bu birölçülü Koşi nüvəli hipersinqulyar inteqrallara J.Adamar mənada inteqral anlayışından istifadə edərək uyğun olaraq müxtəlif şəkildə təriflər verilir.İşdə həmçinin verilmiş hipersinqulyar inteqralların varlığı haqqında teoremlər isbat olunur və bu inteqrallar üçün mühəndislik məsələlərində və müxtəlif sahələrdə geniş tətbiq edilə bilən düsturlar verilir.

Açar sözlər: hipersinqulyar inteqral, approksimasiya operatorları, yığılma sürəti, Koşi nüvəsi.

О НЕКОТОРЫХ ГИПЕРСИНГУЛЯРНЫХ ИНТЕГРАЛАХ

АБСТРАКТ

В работе изучаются разные виды гиперсингулярных интегралов с ядром Коши на отрезке и на единичной окружности и определяются они специальным образом. Для одномерных гиперсингулярных интегралов с ядром Коши даются более общие, чем традиционные, определения, использующие идею Адамара о понятии интеграла в смысле конечной части. В работе также доказываются теоремы о существовании этих гиперсингулярных интегралов и показывается справедливость формул для интегралов, дающих более точные результаты в приложениях в разных областях и при решении различных инженерных задач.

Ключевые слова: Гиперсингулярный интеграл, аппроксимирующие операторы, скорости сходимости, ядро Коши.

1.Introduction

An active development of numerical methods for solving hypersingular integral equations is of considerable interest in modern numerical analysis. This is due to the fact that hypersingular integral equations have numerous applications in acoustics, aerodynamics, fluid mechanics, electrodynamics, elasticity, fracture mechanics, geophysics and etc. [8-12,13-21,27,29-30] Therefore the construction and justification of numerical schemes for approximate solutions of hypersingular integral equations is a topical issue and numerous works are devoted to their development.The development of constructive methods for solving hypersingular integral equations is impossible without studying the properties of hypersingular integral operators contained in these equations, and is associated with the approximation of such operators, which indicates the actuality of the subject of our mauscript. Hypersingular integrals were introduced by J. Hadamard for the solution of the Cauchy problem for a linear partial differential equations of a hyperbolic type. They also arise in solving Neumann problem for the Laplace equation, in solving integral equations of the linear theory of a bearing surface, in inverting generalized Riesz potentials, when presenting some classes of pseudo-differential operators and in other areas of mathematics and mechanics.

Present paper consist of introduction, two chapters and references list.

In the first chapter is investigated hypersingular integrals of the following forms

$$\int_a^b \frac{g(x)}{(x-x_0)^2}dx\,,\quad x_0\in(a,b)$$

$$\int_a^b \frac{g(x)}{(x-x_0)^m}dx\,,\quad m\geq 3,\quad m\in N\,,\quad x_0\in(a,b),$$

where the function $g(x)$ is Lebesgue integrable on the interval $[a,b]$.

In the second chapter are considered hypersingular integrals of the following forms

$$\int_{\gamma_0} \frac{\varphi(\tau)}{(\tau-t)^2}d\tau,\quad t\in\gamma_0$$

$$\int_{\gamma_0} \frac{\varphi(\tau)}{(\tau-t)^m}d\tau\quad,\; m\geq 3,\; m\in N\;,\; t\in\gamma_0\;,$$

where the function $\varphi(t)$ is Lebesgue integrable on the unit circle $\gamma_0=\{t\in C:|t|=1\}$.

In both chapters hypersingular integral is defined by the special way, using using the idea of Hadamard [28] finite part integral and are proved theorems about existence of given hypersingular integrals.

Note that, for the singular integral operators with Cauchy kernel and Hilbert kernel similar approximations and their applications to the singular integral equations are given in [1-5,22-26].

2. Cauchy hypersingular integrals on interval.

Consider the integral

$$\int_a^b \frac{g(x)}{(x-x_0)^2}dx\ , \quad x_0 \in (a,b), \tag{1}$$

where the function $g(x)$ is Lebesgue integrable on the interval $[a,b]$.

If we define this integral in a similar manner to the Cauchy integral, even $g \equiv 1$ we get the divergent integral:

$$\lim_{\varepsilon\to 0+}\left(\int_a^{x_0-\varepsilon} \frac{1}{(x-x_0)^2}dx + \int_{x_0+\varepsilon}^{b} \frac{1}{(x-x_0)^2}dx \right) = \lim_{\varepsilon\to 0+}\left(\frac{2}{\varepsilon} - \frac{1}{x_0-a} + \frac{1}{x_0-b} \right) = \infty\ .$$

Therefore, using the idea of Hadamard finite part integral [28], we will define the integral (1) as follows.

Definition 1. If a finite limit

$$\lim_{\varepsilon\to 0+}\left(\int_a^{x_0-\varepsilon} \frac{g(x)}{(x-x_0)^2}dx + \int_{x_0+\varepsilon}^{b} \frac{g(x)}{(x-x_0)^2}dx - \frac{2g(x_0)}{\varepsilon} \right),$$

exists, then the value of this limit is referred to as the hypersingular integral of the function $\frac{g(x)}{(x-x_0)^2}$ on $[a,b]$ and is denoted by $\int_a^b \frac{g(x)}{(x-x_0)^2}dx$.

The hypersingular integral (1) was studied in [7]. In [7] it is proved that, if $g(x) \in H_1(\alpha)$, i.e. $g(x)$ is differentiable on the interval $[a,b]$and $g'(x)$includes to the class of the Hölder continuous functions with exponent α , (i.e. the class of the functions that satisfy the following condition $\exists M_0 > 0 \quad \forall t_1, t_2 \in R: \ |g'(x_1) - g'(x_2)| \le M_0 \cdot |x_1 - x_2|^{\alpha}$) then (1) exists and the following equality holds:

$$\int_a^b \frac{g(x)}{(x-x_0)^2}dx = \frac{g(b)}{x_0-b} - \frac{g(a)}{x_0-a} - \int_a^b \frac{g'(x)}{x_0-x}dx\,, \tag{2}$$

where the integral standing on the right-hand side is understood in the sense of the Cauchy principal value.

Now consider the integral [6]

$$\int_a^b \frac{g(x)}{(x-x_0)^m}dx\ , \quad m \ge 3, \quad m \in N\,, \quad x_0 \in (a,b), \tag{3}$$

where the function $g(x)$ is Lebesgue integrable on $[a,b]$.

As in the case of the hypersingular integral (1) if we define the integral (3) in a similar manner to the Cauchy integral, even $g \equiv 1$ we get the divergent integral. Therefore, using the idea of Hadamard finite part integral [28], we will define the integral (3) as follows.

Definition 2. Let $m \geq 3$, $m \in N$, the function $g(x)$ is Lebesgue integrable on the interval $[a, b]$ and is differentiable $(m-2)$ times at the point $x_0 \in (a, b)$.

If a finite limit

$$\lim_{\varepsilon \to 0+} \left(\int_a^{x_0-\varepsilon} \frac{g(x)}{(x-x_0)^m} dx + \int_{x_0+\varepsilon}^{b} \frac{g(x)}{(x-x_0)^m} dx - 2 \sum_{k=0}^{p-1} \frac{g^{(2k)}(x_0)}{(2k)!(2p-2k-1)\varepsilon^{2p-2k-1}} \right)$$

when $m = 2p$, $p \in N$,

$$\lim_{\varepsilon \to 0+} \left(\int_a^{x_0-\varepsilon} \frac{g(x)}{(x-x_0)^m} dx + \int_{x_0+\varepsilon}^{b} \frac{g(x)}{(x-x_0)^m} dx - 2 \sum_{k=0}^{p-1} \frac{g^{(2k+1)}(x_0)}{(2k+1)!(2p-2k-1)\varepsilon^{2p-2k-1}} \right)$$

when $m = 2p+1$, $p \in N$,

exists, then the value of this limit is referred to as the hypersingular integral of the function $\frac{g(x)}{(x-x_0)^m}$ on $[a,b]$ and is denoted by $\int_a^b \frac{g(x)}{(x-x_0)^m} dx$.

From definitions 1 and 2 it follows that, if the function $g(x)$ is differentiable on $[a,b]$ and the integral $\int_a^b \frac{g'(x)}{(x-x_0)^{m-1}} dx$ exists, then (3) exists also, and the following formula by parts holds:

$$\int_a^b \frac{g(x)}{(x-x_0)^m} dx = \frac{1}{m-1} \left[\frac{g(a)}{(a-x_0)^{m-1}} - \frac{g(b)}{(b-x_0)^{m-1}} + \int_a^b \frac{g'(x)}{(x-x_0)^{m-1}} dx \right]. \qquad (4)$$

From (4) follows that, if the function $g(x)$ is differentiable $(m-2)$ times on $[a,b]$ and $(m-2)^{\text{th}}$ derivative of the function $g^{(m-2)}(x)$ absolutely continuous on $[a,b]$, then the integral (3) exists almost everywhere for all $x_0 \in (a,b)$ and the following equality is true:

$$\int_a^b \frac{g(x)}{(x-x_0)^m} dx = \sum_{k=0}^{m-2} \frac{(m-2-k)!}{(m-1)!} \left[\frac{g^{(k)}(a)}{(a-x_0)^{m-1-k}} - \frac{g^{(k)}(b)}{(b-x_0)^{m-1-k}} \right] + \frac{1}{(m-1)!} \int_a^b \frac{g^{(m-1)}(x)}{x-x_0} dx$$

If we apply formula (4) to the integral $\int_a^b \frac{u(x)v(x)}{(x-x_0)^{m+1}} dx$, we derive that, if the functions $u(x)$ and $v(x)$ have absolutely continuous $(m-2)^{\text{th}}$ derivatives on $[a,b]$, then the following relation holds almost everywhere for all $x_0 \in (a,b)$

$$\int_a^b \frac{u(x)v(x)}{(x-x_0)^{m+1}} dx = \frac{1}{m} \left[\frac{u(a)v(a)}{(a-x_0)^m} - \frac{u(b)v(b)}{(b-x_0)^m} + \int_a^b \frac{u'(x)v(x) + u(x)v'(x)}{(x-x_0)^m} dx \right].$$

As result we get the following integration by parts formula:

$$\int_a^b \frac{u(x)}{(x-x_0)^m}\,dv(x)=\left.\frac{u(x)v(x)}{(x-x_0)^m}\right|_a^b-\int_a^b v(x)d\left(\frac{u(x)}{(x-x_0)^m}\right)=$$

$$=\frac{u(b)v(b)}{(b-x_0)^m}-\frac{u(a)v(a)}{(a-x_0)^m}-\int_a^b\frac{u'(x)(x-x_0)-mu(x)}{(x-x_0)^{m+1}}v(x)dx. \qquad (5)$$

3. Cauchy hypersingular integrals on unit circle.

Let's consider the integral [3]

$$\int_{\gamma_0}\frac{\varphi(\tau)}{(\tau-t)^2}d\tau,\quad t\in\gamma_0\ , \qquad (6)$$

where the function $\varphi(t)$ is Lebesgue integrable on $\gamma_0=\{t\in C:|t|=1\}$.

Using definition1 for the hypersingular integral on interval, define the integral (6) in the following form

Definition 3. If a finite limit

$$\lim_{\varepsilon\to 0+}\left(\int_{\gamma_\varepsilon}\frac{\varphi(\tau)}{(\tau-t)^2}d\tau+\frac{2i\varphi(t)}{\varepsilon\cdot t}\right),$$

exists, then the value of this limit is called the hypersingular integral of the function $\frac{\varphi(\tau)}{(\tau-t)^2}$, and is denoted by $\int_{\gamma_0}\frac{\varphi(\tau)}{(\tau-t)^2}d\tau$, where $\gamma_\varepsilon=\{\tau\in\gamma_0:|\tau-t|>\varepsilon\}$.

From Definitions 1 and 3 we can deduce that, if $t=e^{ix_0}$, $x_0\in(-\pi,\pi)$, then

$$\int_{\gamma_0}\frac{\varphi(\tau)}{(\tau-t)^2}d\tau=\lim_{\varepsilon\to 0+}\left(\int_{\gamma_\varepsilon}\frac{\varphi(\tau)}{(\tau-t)^2}d\tau+\frac{2i\varphi(t)}{\varepsilon\cdot t}\right)=\lim_{\varepsilon\to 0+}\left(\int_{x_0+\delta(\varepsilon)}^{x_0+2\pi-\delta(\varepsilon)}\frac{\varphi\left(e^{ix}\right)\cdot ie^{ix}}{\left(e^{ix}-e^{ix_0}\right)^2}dx+\frac{2i\varphi\left(e^{ix_0}\right)}{\varepsilon\cdot e^{ix_0}}\right)=$$

$$=\lim_{\varepsilon\to 0+}\left(\int_{[-\pi,\pi]\setminus(x_0-\delta(\varepsilon),x_0+\delta(\varepsilon))}\frac{\varphi\left(e^{ix}\right)\cdot ie^{ix}}{(x-x_0)^2}\cdot\left(\frac{x-x_0}{e^{ix}-e^{ix_0}}\right)^2dx+\frac{2i\varphi\left(e^{ix_0}\right)}{\varepsilon\cdot e^{ix_0}}\right)=$$

$$=\int_{-\pi}^{\pi}\frac{\varphi\left(e^{ix}\right)\cdot ie^{ix}}{\left(e^{ix}-e^{ix_0}\right)^2}dx+\frac{2i\varphi\left(e^{ix_0}\right)}{e^{ix_0}}\cdot\lim_{\varepsilon\to 0+}\left(\frac{1}{\varepsilon}-\frac{1}{\delta(\varepsilon)}\right), \qquad (7)$$

where $\delta(\varepsilon)=2\arcsin\frac{\varepsilon}{2}$. Since

$$\lim_{\varepsilon\to 0+}\left(\frac{1}{\varepsilon}-\frac{1}{\delta(\varepsilon)}\right)=\lim_{\varepsilon\to 0+}\left(\frac{1}{\varepsilon}-\frac{1}{2\arcsin\frac{\varepsilon}{2}}\right)=0,$$

then from (7) it follows that,

$$\int_{\gamma_0}\frac{\varphi(\tau)}{(\tau-t)^2}d\tau=\int_{-\pi}^{\pi}\frac{\varphi\left(e^{ix}\right)\cdot ie^{ix}}{\left(e^{ix}-e^{ix_0}\right)^2}dx. \tag{8}$$

The formula (8) shows that, by means of the substitution $t=e^{ix}$ hypersingular integral (6) is reduced to the hypersingular integral on an interval.

Let's calculate the following integral

$$\int_{\gamma_0}\frac{d\tau}{(\tau-t)^2},\ t\in\gamma_0.$$

We get

$$\int_{\gamma_0}\frac{d\tau}{(\tau-t)^2}=\lim_{\varepsilon\to 0+}\left(\int_{\gamma_\varepsilon}\frac{d\tau}{(\tau-t)^2}+\frac{2i}{\varepsilon t}\right)=\lim_{\varepsilon\to 0+}\left(\frac{1}{t-t\cdot e^{-i\delta(\varepsilon)}}-\frac{1}{t-t\cdot e^{i\delta(\varepsilon)}}+\frac{2i}{\varepsilon\cdot t}\right)=$$

$$=\frac{1}{t}\lim_{\varepsilon\to 0+}\left(\frac{e^{i\delta(\varepsilon)}}{e^{i\delta(\varepsilon)}-1}-\frac{1}{1-e^{i\delta(\varepsilon)}}+\frac{2i}{\varepsilon}\right)=\lim_{\varepsilon\to 0+}\left(\frac{e^{i\delta(\varepsilon)}+1}{e^{i\delta(\varepsilon)}-1}+\frac{2i}{\varepsilon}\right), \tag{9}$$

where $\delta(\varepsilon)=2\arcsin\frac{\varepsilon}{2}\sim\varepsilon$ при $\varepsilon\to 0+$. Since

$$\lim_{\varepsilon\to 0+}\left(\frac{e^{i\delta(\varepsilon)}+1}{e^{i\delta(\varepsilon)}-1}+\frac{2i}{\varepsilon}\right)=\lim_{\varepsilon\to 0+}\left(\frac{2}{i\delta(\varepsilon)}+\frac{2i}{\varepsilon}\right)=2i\cdot\lim_{\varepsilon\to 0+}\left(\frac{1}{\varepsilon}-\frac{1}{\delta(\varepsilon)}\right)=0,$$

then from (9) it follows that,

$$\int_{\gamma_0}\frac{d\tau}{(\tau-t)^2}=0. \tag{10}$$

From (10) it follows that, existence of hypersingular integral $\int_{\gamma_0}\frac{\varphi(\tau)}{(\tau-t)^2}d\tau$ is equavivalent to existence of hypersingular integral $\int_{\gamma_0}\frac{\varphi(\tau)-\varphi(\tau)}{(\tau-t)^2}d\tau$ in the sense of the Cauchy principal value, then the following relation holds:

$$\int_{\gamma_0}\frac{\varphi(\tau)}{(\tau-t)^2}d\tau=\int_{\gamma_0}\frac{\varphi(\tau)-\varphi(\tau)}{(\tau-t)^2}d\tau,$$

where the integral standing on the right-hand side is understood in the sense of the Cauchy principal value.

According to (2) and (8), we get that, if $\varphi \in C^{1,\alpha}(\gamma_0)$, i.e. $\varphi(t)$ is differentiable on the unit circle γ_0 and $\varphi'(t)$ includes to the class of the Hölder continuous functions with exponent α , then (6) exists and the following equality holds:

$$\int\limits_{\gamma_0} \frac{\varphi(\tau)}{(\tau-t)^2} d\tau = \int\limits_{\gamma_0} \frac{\varphi'(\tau)}{\tau - t} d\tau \ , \tag{11}$$

where the integral standing on the right-hand side is understood in the sense of the Cauchy principal value.

State the next useful property of the hypersingular integral in the form (6).

Theorem 1. If the function φ absolutely continuous on γ_0 ,then the hypersingular integral (6) exists for almost all $t \in \gamma_0$,and (11) holds.

Proof: The existence of the derivative $\varphi'(\tau)$ of the function φ for almost all $t \in \gamma_0$ and Lebesgue integrablity of the function $\varphi'(\tau)$ on γ_0 ,follows from absolute continuity of the function φ on γ_0 .

For all points $t \in \gamma_0$, which the function $\varphi(t)$ is differentiable, the following equality is true:

$$\lim_{\varepsilon \to 0+} \left(\frac{\varphi\left(t \cdot e^{-i\delta(\varepsilon)}\right)}{t - t \cdot e^{-i\delta(\varepsilon)}} - \frac{\varphi\left(t \cdot e^{i\delta(\varepsilon)}\right)}{t - t \cdot e^{i\delta(\varepsilon)}} + \frac{2i\varphi(t)}{\varepsilon \cdot t} \right) =$$

$$= \lim_{\varepsilon \to 0+} \left[\frac{\varphi(t) + \varphi'(t) \cdot \left(t \cdot e^{-i\delta(\varepsilon)} - t\right) + o(\varepsilon)}{t - t \cdot e^{-i\delta(\varepsilon)}} - \frac{\varphi(t) + \varphi'(t) \cdot \left(t \cdot e^{i\delta(\varepsilon)} - t\right) + o(\varepsilon)}{t - t \cdot e^{i\delta(\varepsilon)}} + \frac{2i\varphi(t)}{\varepsilon \cdot t} \right] =$$

$$= \frac{\varphi(t)}{t} \lim_{\varepsilon \to 0+} \left(\frac{1}{1 - e^{-i\delta(\varepsilon)}} + \frac{1}{1 + e^{i\delta(\varepsilon)}} + \frac{2i}{\varepsilon} \right) = 0,$$

where $\delta(\varepsilon) = 2\arcsin\frac{\varepsilon}{2}$. If $t = e^{ix_0}$, then from the following relation

$$\int\limits_{\gamma_\varepsilon} \frac{\varphi(\tau)}{(\tau-t)^2} d\tau = \int\limits_{x_0+\delta(\varepsilon)}^{x_0+2\pi-\delta(\varepsilon)} \frac{\varphi\left(e^{ix}\right) \cdot ie^{ix}}{\left(e^{ix} - e^{ix_0}\right)^2} dx = -\int\limits_{x_0+\delta(\varepsilon)}^{x_0+2\pi-\delta(\varepsilon)} \varphi\left(e^{ix}\right) d\left(\frac{1}{e^{ix} - e^{ix_0}}\right) =$$

$$= \frac{\varphi\left(e^{i(x_0+2\pi-\delta(\varepsilon))}\right)}{e^{ix_0} - e^{i(x_0+2\pi-\delta(\varepsilon))}} - \frac{\varphi\left(e^{i(x_0+\delta(\varepsilon))}\right)}{e^{ix_0} - e^{i(x_0+\delta(\varepsilon))}} + \int\limits_{x_0+\delta(\varepsilon)}^{x_0+2\pi-\delta(\varepsilon)} \frac{1}{e^{ix} - e^{ix_0}} \cdot ie^{ix} \varphi'\left(e^{ix}\right) dx =$$

$$= \frac{\varphi\left(t \cdot e^{-i\delta(\varepsilon)}\right)}{t - t \cdot e^{-i\delta(\varepsilon)}} - \frac{\varphi\left(t \cdot e^{i\delta(\varepsilon)}\right)}{t - t \cdot e^{i\delta(\varepsilon)}} + \int\limits_{\gamma_\varepsilon} \frac{\varphi'(\tau)}{\tau - t} d\tau$$

it follows that, hypersingular integral (6) exists for almost all $t \in \gamma_0$,and (11) holds and this completes the proof of the theorem1.

As a result we can we can conclude that, even under weak restrictions on the function $\varphi(\tau)$, (11) holds.

Now consider the integrals of the following form:

$$\int\limits_{\gamma_0} \frac{\varphi(\tau)}{(\tau - t)^m} d\tau \quad , \ m \geq 3, \ m \in N \,, \ t \in \gamma_0 \ , \tag{12}$$

where the function $\varphi(t)$ is Lebesgue integrable on $\gamma_0 = \{t \in C : |t| = 1\}$.

Using definition 2 for hypersingular integral on interval, define the integral (12) as follows.

Definition 4. Let $m \geq 3$, $m \in N$, the function $\varphi(t)$ is Lebesgue integrable on the unit circle γ_0 and is differentiable $(m-2)$ times at the point $t \in \gamma_0$.

If a finite limit

$$\lim_{\varepsilon \to 0+} \left(\int\limits_{\gamma_\varepsilon} \frac{\varphi(\tau)}{(\tau - t)^m} d\tau - 2i \sum_{k=0}^{p-1} \frac{\left[\varphi\left(e^{ix}\right) e^{ix} \left(\dfrac{x - x_0}{e^{ix} - e^{ix_0}} \right)^m \right]^{(2k)} (x_0)}{(2k)!(2p - 2k - 1)[\delta(\varepsilon)]^{2p-2k-1}} \right)$$

when $m = 2p$, $p \in N$,

$$\lim_{\varepsilon \to 0+} \left(\int\limits_{\gamma_\varepsilon} \frac{\varphi(\tau)}{(\tau - t)^m} d\tau - 2i \sum_{k=0}^{p-1} \frac{\left[\varphi\left(e^{ix}\right) e^{ix} \left(\dfrac{x - x_0}{e^{ix} - e^{ix_0}} \right)^m \right]^{(2k+1)} (x_0)}{(2k)!(2p - 2k - 1)[\delta(\varepsilon)]^{2p-2k-1}} \right)$$

when $m = 2p+1$, $p \in N$,

where $\gamma_\varepsilon = \{\tau \in \gamma_0 : |\tau - t| > \varepsilon\}$, $t = e^{ix_0}$, $\delta(\varepsilon) = 2\arcsin\frac{\varepsilon}{2}$, then the value of this limit is referred to as the hypersingular integral of the function $\dfrac{\varphi(\tau)}{(\tau - t)^m}$ on the unit circle γ_0 and is denoted by $\int\limits_{\gamma_0} \dfrac{\varphi(\tau)}{(\tau - t)^m} d\tau$.

From definitions 2 and 4, and the following relation

$$\lim_{\varepsilon \to 0+} \left(\frac{1}{\varepsilon} - \frac{1}{\delta(\varepsilon)} \right) = 0 \,,$$

it follows,

$$\int\limits_{\gamma_0} \frac{\varphi(\tau)}{(\tau-t)^m} d\tau = \int\limits_{x_0-\pi}^{x_0+\pi} \frac{\varphi\left(e^{ix}\right) ie^{ix}}{\left(e^{ix}-e^{ix_0}\right)^m} dx, \tag{13}$$

where $t = e^{ix_0}$.

The formula (13) shows that, by means of the substitution $t = e^{ix}$ hypersingular integrals on the unit circle are reduced to the hypersingular integrals on an interval.

Theorem 2. If the function φ has absolutely continuous $(m-2)^{\text{th}}$ derivative on γ_0, then the hypersingular integral (12) exists for almost all $t \in \gamma_0$, and the following relation holds:

$$\int\limits_{\gamma_0} \frac{\varphi(\tau)}{(\tau-t)^m} d\tau = \frac{1}{m-1} \int\limits_{\gamma_0} \frac{\varphi'(\tau)}{(\tau-t)^{m-1}} d\tau. \tag{14}$$

Proof: The existence of the hypersingular integral (12) follows from (13). Let's prove equality (14). From (4), (5) and (13) it follows that,

$$\int\limits_{\gamma_0} \frac{\varphi(\tau)}{(\tau-t)^m} d\tau - \frac{1}{m-1} \int\limits_{\gamma_0} \frac{\varphi'(\tau)}{(\tau-t)^{m-1}} d\tau =$$

$$= \int\limits_{x_0-\pi}^{x_0+\pi} \frac{\varphi\left(e^{ix}\right) ie^{ix}}{\left(e^{ix}-e^{ix_0}\right)^m} dx - \frac{1}{m-1} \int\limits_{x_0-\pi}^{x_0+\pi} \frac{\varphi'\left(e^{ix}\right) ie^{ix}}{\left(e^{ix}-e^{ix_0}\right)^{m-1}} dx =$$

$$= \int\limits_{x_0-\pi}^{x_0+\pi} \frac{\varphi\left(e^{ix}\right) ie^{ix}}{\left(e^{ix}-e^{ix_0}\right)^m} dx - \frac{1}{m-1} \int\limits_{x_0-\pi}^{x_0+\pi} \frac{d\left(\varphi\left(e^{ix}\right)\right)}{\left(e^{ix}-e^{ix_0}\right)^{m-1}} =$$

$$= \int\limits_{x_0-\pi}^{x_0+\pi} \frac{\varphi\left(e^{ix}\right) ie^{ix}}{\left(e^{ix}-e^{ix_0}\right)^m} dx - \frac{1}{m-1} \left[\left. \frac{\varphi\left(e^{ix}\right)}{\left(e^{ix}-e^{ix_0}\right)^{m-1}} \right|_{x_0-\pi}^{x_0+\pi} - \int\limits_{x_0-\pi}^{x_0+\pi} \varphi\left(e^{ix}\right) d\left(\frac{1}{\left(e^{ix}-e^{ix_0}\right)^{m-1}} \right) \right] =$$

$$= \int\limits_{x_0-\pi}^{x_0+\pi} \frac{\varphi\left(e^{ix}\right) ie^{ix}}{\left(e^{ix}-e^{ix_0}\right)^m} dx - \frac{1}{m-1} \left[0 + (m-1) \int\limits_{x_0-\pi}^{x_0+\pi} \varphi\left(e^{ix}\right) \cdot \frac{ie^{ix}}{\left(e^{ix}-e^{ix_0}\right)^m} dx \right] = 0 \cdot$$

Theorem has been proved.

Corollary 1. If the function φ has absolutely continuous $(m-2)^{\text{th}}$ derivative on γ_0, then the the following relation holds:

$$\int_{\gamma_0} \frac{\varphi(\tau)}{(\tau-t)^m} d\tau = \frac{1}{(m-1)!} \int_{\gamma_0} \frac{\varphi^{(m-1)}(\tau)}{\tau - t} d\tau, \tag{15}$$

where the integral standing on the right-hand side is understood in the sense of the Cauchy principal value.

Corollary 2. If we take into consideration $\varphi(\tau) = \tau^k$, $k = \overline{0, m-2}$ in (15), then we get

$$\int_{\gamma_0} \frac{\tau^k}{(\tau-t)^m} d\tau = 0, \quad k = \overline{0, m-2}.$$

Corollary 3. If the function φ is differentiable $(m-1)$ times at the point t, then the following equality is true:

$$\int_{\gamma_0} \frac{\varphi(\tau)}{(\tau-t)^m} d\tau = \int_{\gamma_0} \frac{\varphi(\tau) - \sum_{k=0}^{m-2} \frac{\varphi^{(k)}(t)}{k!} (\tau - t)^k}{(\tau-t)^m} d\tau,$$

where the integral standing on the right-hand side is understood in the sense of the Cauchy principal value.

4. Conclusion

In this paper, we have introduced different methods in order to define for hypersingular integrals of types with optimal accuracy. The proposed formulas can be applied to solve real-world engineering problems and have various successful applications in numerical implementations.

REFERENCE LIST

[1] R. A. Aliev, A. F. Amrakhova, *A constructive method for the solution of integral equations with Hilbert kernel*, Tr. Inst. Mat. Mekh., 18:4 (2012), 14-25

[2] R.A.Aliev, *A new constructive method for solving singular integral equations*, Math. Notes, 79:(5-6) (2006), 749-770.

[3] R. A. Aliev, Ch. A. Gadjieva, *Approximation of Hilbert Transformation,* Tr. Inst. Mat. Mekh., **25:2** (2019), 31-41

[4] R. A. Aliev, Ch. A. Gadjieva, *Approximation of hypersingular integral operators with Cauchy kernel*, Numer. Funct. Anal. Optim., 37:9 (2016), 1055-1065.

[5] R. A. Aliev, Ch. A. Gadjieva, *Approximate solution of hipersingulyar integral equations with Cauchy kernel*, Trans. Natl. Acad. Sci. Azerb. Ser. Phys.-Tech. Math. Sci., 37:1 (2017), 20-29.

[6] A. F. Amrakhova, Ch. A. Gadjieva, *Approximation of a hypersingular integral operator on the circle,* News BU Ph. Math. Sc. Ser.,4 (2015), 43-50.

[7] A. Yu. Anfinogenov, I. K. Lifanov, P. I. Lifanov, *On certain one and two dimensional hypersingular integral equations*, Sb. Math. 192:8 (2001), 1089-1131.

[8] W. T. Ang, *Hypersingular Integral Equations in Fracture Analysis*, Woodhead Publishing, Cambridge, (2013).

[9] V. Babenko, O. Kovalenko, N. Parfinovych , *On approximation of hypersingular integral operators by bounded ones*, J. Math. Anal. Appl.,513 (2022) 126-215

[10] I. V. Boikov, M. A. Syomov, *On a Method of Calculation of Hypersingular Integrals*, Russian Math. (Iz. VUZ), 60:3 (2016), 1–13.

[11] I.V. Boykov, *Approximate Methods for Evaluation of Singular and Hypersingular Integrals,* Part 1, Singular Integrals; Penza State University Press: Penza, Russia (2005).

[12] I.V. Boykov, A. I. Boykova, E. S. Ventsel, *Fundamental solutions for thick sandwich plates*, Eng. Anal. Bound. Elem., 28 (2004),1437–1444.

[13] I.V. Boykov, *Numerical methods of computation of singular and hypersingular integrals*, Int. J. Math. Math. Sci.,28:3 (2001),127–179.

[14] I.V. Boykov, E.S. Ventsel, A.I. Boykova, *An approximate method for evaluating hypersingular integrals*, Eng. Anal. Bound. Elem.,30 (2006),799–807.

[15] H. T. Cai, *A fast solver for a hypersingular boundary integral equation*, Appl. Numer. Math., 59:8 (2009),1960-1969.

[16] Z. Chen, Y. F.Zhou, *A new method for solving hypersingular integral equations of the first kind*, Appl. Math. Lett.,24 (2011), 636-641.

[17] M. C. De Bonis, V. Sagaria, *Numerical method for hypersingular integrals of highly oscillatory functions on the positive semiaxis*, Dolomites Res. Notes Approx.,15 (2022),49-64

[18] T. Diogo, P. Lima, D. Occorsio, *A numerical method for finite-part integrals*, Dolomites Res. Notes Approx.,13 (2020),1-11

[19] Q.K. Du, *Evaluations of certain hypersingular integrals on interval*, Internat. J. Numer. Methods Engrg., 51 (2001),1195-1210.

[20] V. J. Ervin, E. P.Stephan, *Collocation with Chebyshev polynomials for a hypersingular integral equation on an interval*, J. Comput. Appl. Math., 43 (1992), 221-229.

[21] H. Feng, X. Zhang, J.Li, *Numerical solution of a certain hypersingular integral equation of the first kind*, BIT, 51:3 (2011),609-630.

[22] Ch. A. Gadjieva, *A new approximate method for hypersingular integral operator with Hilbert kernel*, JCAM, 13:1(2023), 99-110.

[23] Ch. A. Gadjieva, *A new approximate method for solving hypersingular integral equations with Hilbert kernel*, Proc. Inst. Math. Mech. Natl. Acad. Sci. Azerb, 43:2 (2017),316-329

[24] Ch. A. Gadjieva, *A new constructive method for solving of bisingular integral equations with Cauchy kernel*, Proc. Inst. Math. Mech. Natl. Acad. Sci. Azerb., 42:1 (2016), 50-66.

[25] Ch. A. Gadjieva, *Approximation of a hypersingular integral operator with Cauchy kernel*, News BU Ph. Math. Sc. Ser.,1 (2017),76-87.

[26] Ch. A. Gadjieva, *Approximation of hypersingular integral operators on Hölder spaces*, CJAMEE, 5:2 (2017), 96-105.

[27] M. Gülsu, Y. Öztürk, *Numerical approach for the solution of hypersingular integro-differential equations*, Appl. Math. Comput.,230 (2014), 701–710.

[28] J. Hadamard, *Lectures on Cauchy's problem in linear partial differential equations,* Dover publication, New-York, (2003).

[29] J. Huang, Z. Wang, R. Zhu, *Asymptotic error expansions for hypersingular integrals,* Adv. Comput. Math.,38:2 (2013), 257-279.

[30] Cha. Hu, T. Lü, *Approximations of hypersingular integrals for negative fractional exponent*, J. Comput. Math.,36:5 (2018) 627–643.

JOURNAL OF BAKU ENGINEERING UNIVERSITY- MATHEMATICS AND COMPUTER SCIENCE
2024. Volume 8, Number 1 *Pages 32-35*

UOT: 002.6:025.3/.4

DOİ: ***https://doi.org/10.30546/09090.2024.110.216***

MANAGİNG THE MOVEMENT OF A HEXACOPTER İN THE EVENT OF ENGİNE FAİLURE

GULUSH NABADOVA

Baku Engineering University, Baku, Azerbaijan

gnabadova@beu.edu.az

ARTICLE INFO

Article history:

Received:2024-09-17

Received in revised form:2024-09-24

Accepted:2024-10-30

Available online

Keywords: Hexacopter, route, control parameters, failed motor, quaternion, spatial orientation, unmanned aerial vehicle.

ABSTRACT

In this article, the issue of controlling the movement of a hexacopter-type unmanned aerial vehicle (UAV) along a route is investigated. The movement of the hexacopter is modeled as the movement of a rigid body, and in this process, the forces of gravity and aerodynamic resistance are taken into account. The spatial orientation of the hexacopter is expressed using quaternions. The movement route is considered as a broken line consisting of straight segments, and the parameters controlling its flight are determined when one of the hexacopter's motors is not working. Mathematical justification is provided for how the operational motors are controlled to continue the hexacopter's movement in its previous manner when one motor fails.

Introduction

In recent years, due to the widespread use of multi-engine drones and depending on their purpose and the requirements placed on them, various types have become particularly popular [1, 2, 3]. Unlike single-engine drones, the failure of engines in multi-rotor devices can lead to safety-related problems. Many published articles propose solving this problem by redesigning the control law and adjusting the control force [4, 5]. However, this approach is difficult to implement, as it often requires the addition of extra devices to change the control force in this way.

Quadrotor-type unmanned aerial vehicles (UAVs), equipped with four rotors, have garnered significant attention from researchers due to their ability to maintain stationary flight and stable hovering by balancing the forces generated by the rotors. Recently, UAVs with more than four rotors, such as hexacopters and octocopters, have also become a focal point of interest. To evaluate flight characteristics and achieve robust control of UAVs, computer simulations are frequently employed. Various types of UAVs have been developed in Azerbaijan. In this study, the development of a simulation system is presented to experiment with the flight of the hexacopter-type UAV known as Əqrəb 5.0.

Most previous studies have focused only on quadcopters with one engine failure. The second approach is based on quaternion theory, but there is not enough material on how a hexacopter can be controlled using these methods when one engine fails.

This article studies the control of a hexacopter when one of its engines fails, particularly when there are power limitations on the remaining engines. The proposed system can assist in managing flight when an engine malfunctions and increases the chances of a successful emergency landing.

Problem statement. When there are no limitations on the power of the hexacopter's engines (referred to as the normal case below), it can be observed (Figure 1) that even if two symmetrically placed engines of the hexacopter fail, it can still be normally controlled along a straight trajectory. The failure of one of the hexacopter's engines refers to a situation where one of its six engines is not functioning. In such cases, typically, the engine symmetrically placed relative to the center of the hexacopter is turned off. It is clear that when the number of engines decreases from six to four, their power needs to be increased. However, a question arises: if there is a limitation on the power of the engines in the hexacopter, can the work of one engine be compensated by the remaining five? This article investigates this issue. Below, the mathematical formalization and solution of the problem are provided.

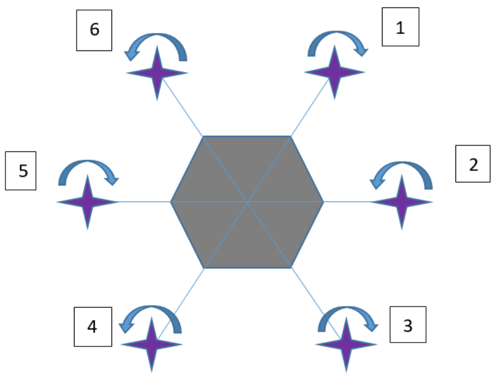

Figure 1. The direction of rotation of the propellers of hexacopter

Coordinate systems. The mathematical model of the hexacopter is expressed through the relationship between quantities calculated in local and global coordinate systems. Let's introduce the coordinate systems used, as shown in the diagram below (Figure 2).

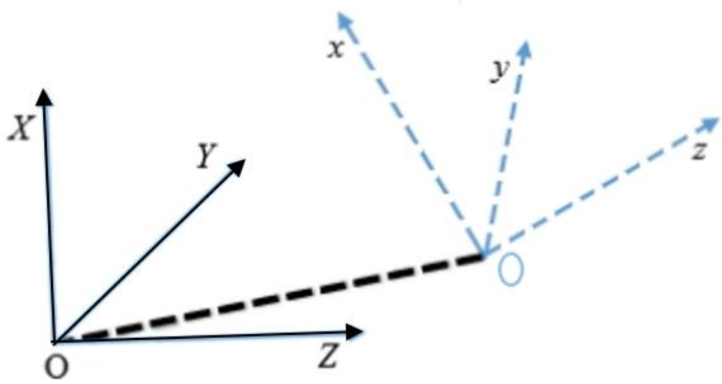

Figure 2. Lokal (body fixed) ($oxyz$) and global ($OXYZ$) coordinate systems

The $OXYZ$ coordinate system is an inertial frame attached to a fixed point on the Earth's surface, while the $oxyz$ system is a local coordinate system related to the hexacopter, with its origin at the center of gravity, used to determine the hexacopter's orientation in space.

Thus, for the hexacopter to fly in a straight line, it first needs to be oriented correctly by adjusting the rotational speeds of the propellers, achieving the necessary pitch. After that, it is controlled along the desired trajectory using the engines operating at the appropriate rotational speeds. (Note that the calculation of propeller rotational speeds for changing the UAV's orientation is not discussed in this article).

Controlling hexacopter with engine failure. The optimal control of straight-line flight, when all motors are functioning normally, is ensured by the propellers rotating at the same frequency. Let's assume that one of the hexacopter's motors has malfunctioned. Without loss of generality, we can assume that the malfunctioning motor is the 6th motor. In the absence of restrictions on the rotation frequencies of the motors, the control of the hexacopter's movement has been examined in [6], and it was shown that when $\omega_3 = 0$, straight-line trajectory control is possible. In this case a question arises: if the power of the motors is limited and they cannot maintain their rotation frequencies, is it possible to control the hexacopter in the previous mode with only 5 motors?

This problem, from a mathematical perspective, is a constrained extremum problem. Various approaches can be applied to solve this problem [7]. During the research, the Kuhn-Tucker method was used [8]. If there is a solution to this problem, then its solution must satisfy all the minimums obtained when each individual additional condition is addressed.

It is clear that a similar result is obtained when one of the 2nd, 3rd, or 5th motors malfunctions. For clarity, if we consider the case where the 1st motor fails instead of the 6th, by solving the system in a similar manner, it is again concluded that the hexacopter cannot be controlled with 5 motors when there is a power limitation on the motors. Naturally, the results are analogous if the 4th motor fails. Thus, this means that under the given constraints, the hexacopter cannot be controlled along a straight-line trajectory with only 5 motors.

Conclusion

Thus, the studies showed that when one engine of the hexacopter fails, its movement along the previous trajectory can be maintained by the other engines, excluding the engine symmetrically positioned relative to the failed one. In this case, when there are no technical limitations on engine power, it is necessary to increase the rotation speed of the propellers to maintain the previous speed of movement.

However, if there are limitations on engine power, continuing the flight along the trajectory can be achieved by reducing the flight speed. It was also mathematically justified that under such limitations, the power deficit across four engines cannot be compensated by the fifth engine to maintain the previous flight speed along a straight trajectory.

REFERENCES

1. Alderete, T.S. 1995. "Simulator aero model implementation." NASA Ames Research Center, Moffett Field, California.
2. Bekir, E. 2007. Introduction to modern navigation systems. World Scientific. ISBN not provided.
3. Cefalo, M., and J.M. Mirats-Tur. 2011. "A comprehensive dynamic model for class-1 tensegrity systems based on quaternions." International Journal of Solids and Structures 48 (5): 785-802.
4. Aoki, Y., Y. Asano, A. Honda, N. Motooka, K. Hoshino, and T. Ohtsuka. 2021. "Nonlinear model predictive control for hexacopter with failed rotors based on quaternions—simulations and hardware experiments—." Mechanical Engineering Journal 8 (5): 21-00204.
5. Wen, F.H., F.Y. Hsiao, and J.K. Shiau. 2021. "Analysis and management of motor failures of hexacopter in hover." In Actuators, Vol. 10, No. 3, p. 48. MDPI.
6. AOKI Y, ASANO Y, HONDA A, MOTOOKA N, HOSHINO K, OHTSUKA T. Nonlinear model predictive control for hexacopter with failed rotors based on quaternions—simulations and hardware experiments—. Mechanical Engineering Journal. 2021;8(5):21-00204.
7. Bertsekas, D.P. 1996. Constrained Optimization and Lagrange Multipliers Methods. Athena Scientific. ISBN 1-886529--04-3.
8. LMS SSEU. „§ 2.4. Методы исключения переменных из системы линейных уравнений". Accessed: 30.08.2024. Available at: https://lms2.sseu.ru/courses/eresmat/metod/met2/parmet2_4.htm
9. Cheng, G., L. Xu, and L. Jiang. 2006. "A sequential approximate programming strategy for reliability-based structural optimization." Computers & Structures 84 (21): 1353-1367.

2024. Volume 8, Number 1 Pages 36-44

UOT: 517.938
DOİ: https://doi.org/10.30546/09090.2024.110.219

MULTIPLICITY OF EIGENVALUES OF THE DIFFUSION OPERATOR WITH A SPECTRAL PARAMETER QUADRATICALLY CONTAINED IN THE BOUNDARY CONDITION

G.S.MAMMEDZADEH

Azerbaijan State University of Economics

guldane.mammedzadeh@mail.ru

ARTICLE INFO	ABSTRACT
Article history: Received:2024-10-08 Received in revised form:2024-10-08 Accepted:2024-11-19 Available online *Keywords: diffusion operator; nonseparated boundary conditions; eigenvalues; spectral parameter.*	*The paper considers a boundary value problem generated by a differential diffusion equation and nonseparated boundary conditions. One of the boundary conditions contains a quadratic function of the spectral parameter. The multiplicity of eigenvalues of the boundary value problem under consideration is investigated. A criterion for the multiplicity of eigenvalues and zeros of the characteristic function of a boundary value problem is obtained.The found necessary and sufficient conditions are expressed through the values of the fundamental solutions of the diffusion equation and the coefficients of the boundary conditions. Note that the results obtained can be used in the study of direct and inverse problems of spectral analysis for various differential operators. These results also play an important role in studying the structure of the spectrum, in establishing the order of arrangement of eigenvalues of boundary value problems, and in finding sufficient conditions for the reconstruction of the corresponding problems.*

Let's consider a boundary value problem defined on an interval $[0,\pi]$ by the diffusion differential equation

$$y'' + [\lambda^2 - 2\lambda p(x) - q(x)]y = 0 \tag{1}$$

and boundary conditions of the form

$$\begin{aligned} &(m\lambda^2 + \alpha\lambda + \beta)y(0) + y'(0) + \omega y(\pi) = 0, \\ &-\overline{\omega}y(0) + \gamma y(\pi) + y'(\pi) = 0, \end{aligned} \tag{2}$$

where $p(x) \in W_2^1[0,\pi]$, $q(x) \in L_2[0,\pi]$ are real functions, λ is the spectral parameter, ω is complex, $\overline{\omega}$ is the conjugate to ω, and m, α, β, γ are real numbers.

Using $W_2^n[0,\pi]$, we denote the Sobolev space of functions $f(x)$, $x \in [0,\pi]$, such that functions $f^{(m)}(x)$, $m = 0,1,2,\ldots,n-1$, are absolutely continuous and $f^{(n)}(x) \in L_2[0,\pi]$. We will denote problem (1)-(2) by P.

Definition. The values of the parameter λ for which the boundary value problem P has nontrivial solutions are called eigenvalues, and the corresponding nontrivial solutions are called eigenfunctions of problem P. The set of eigenvalues is called the spectrum of P. The number of linearly independent solutions of problem P for a given eigenvalue λ_0 is called the multiplicity of the eigenvalue λ_0.

The spectral properties of Sturm-Liouville and diffusion operators with separated boundary conditions (i.e., at $\omega = 0$) are well studied (see works [1-4] and the bibliography within them). It has been proven that, in this case, the eigenvalues of boundary value problems are simple (i.e., each eigenvalue corresponds to a unique eigenfunction, up to a constant multiplier). In [5-18], direct and inverse spectral problems for the equation (1) (under conditions $p(x) \equiv 0$ and $p(x) \not\equiv 0$) with various types of non-separated boundary conditions have been investigated, including periodic, anti-periodic, quasi-periodic, and generalized periodic boundary conditions.In the article [19], a criterion for multiplicity was obtained, and the order of the eigenvalue distribution of the quadratic pencil of Sturm-Liouville operators was established in the case of non-separated boundary conditions without a spectral parameter. The multiplicity of the eigenvalues of diffusion and Dirac operators under non-separated boundary conditions containing a linear function of the spectral parameter has been studied in [20-21].

In this work, necessary and sufficient conditions are found for the multiplicity of eigenvalues (as well as for the multiplicity of the zero of the characteristic function) of the boundary value problem P.

Further, we will assume that $m > 0$ and that, for all functions $y(x) \in W_2^2[0,\pi]$, $y(x) \not\equiv 0$ satisfying conditions (2), the inequality

$$\gamma |y(\pi)|^2 - 2\operatorname{Re}\left[\omega \overline{y(0)} y(\pi)\right] - \beta |y(0)|^2 + \int_0^\pi \left\{ |y'(x)|^2 + q(x)|y(x)|^2 \right\} dx > 0$$

holds.

Under this condition, the eigenvalues of the boundary value problem P are real and non-zero, and this problem has no associated functions corresponding to the eigenfunctions. Furthermore, if $y(x)$ is an eigenfunction of problem P corresponding to the eigenvalue λ, then

$$2\int_0^\pi [\lambda - p(x)] |y(x)|^2 dx + (2m\lambda + \alpha)|y(0)|^2 \neq 0. \tag{3}$$

(see [15]).

Let's introduce the fundamental system of solutions $c(x,\lambda)$, $s(x,\lambda)$ of equation (1), defined by the initial conditions

$$c(0,\lambda) = s'(0,\lambda) = 1,\ c'(0,\lambda) = s(0,\lambda) = 0. \tag{4}$$

The Wronskian of these solutions is identically equal to one:

$$\begin{vmatrix} c(x,\lambda) & s(x,\lambda) \\ c'(x,\lambda) & s'(x,\lambda) \end{vmatrix} = c(x,\lambda)s'(x,\lambda) - s(x,\lambda)c'(x,\lambda) = 1 \tag{5}$$

Let us denote

$$a(\lambda)=m\lambda^2+\alpha\lambda+\beta. \tag{6}$$

It is clear that the eigenvalues of boundary value problem P coincide with the zeros of the function

$$\Delta(\lambda)=\begin{vmatrix} a(\lambda)+\omega c(\pi,\lambda) & 1+\omega s(\pi,\lambda) \\ -\overline{\omega}+\gamma c(\pi,\lambda)+c'(\pi,\lambda) & \gamma s(\pi,\lambda)+s'(\pi,\lambda) \end{vmatrix}.$$

This function is called the characteristic function of problem P. Expanding this determinant and taking into account identity (5), we have

$$\Delta(\lambda)=2\operatorname{Re}\omega-\eta(\lambda)+|\omega|^2 s(\pi,\lambda)+a(\lambda)\sigma(\lambda), \tag{7}$$

where

$$\eta(\lambda)=c'(\pi,\lambda)+\gamma\, c(\pi,\lambda),\ \ \sigma(\lambda)=s'(\pi,\lambda)+\gamma\, s(\pi,\lambda)\ . \tag{8}$$

Theorem 1. *Eigenvalue λ_0 of boundary value problem P will be multiple if and only if the number is real and nonzero and the following equalities are satisfied:*

$$a(\lambda_0)+\omega c(\pi,\lambda_0)=\sigma(\lambda_0)=0\,. \tag{9}$$

The proof of this theorem is similar to the proof of Theorem 2.1 in [19].

The eigenvalue λ_0 can be a multiple of zero of the characteristic function $\Delta(\lambda)$ of boundary value problem P.

Theorem 2. *In order for the zero λ_0 of the characteristic function $\Delta(\lambda)$ of the boundary value problem P to be multiple, it is necessary and sufficient that the conditions for the multiplicity of the eigenvalue λ_0 be satisfied, i.e. the number ω is real and nonzero and equalities (9) are valid.*

Proof. *Necessity.* Hereafter, we will denote the derivative with respect to parameter λ by a dot over the function. First, we prove that if $\Delta(\lambda_0)=0$ and $\sigma(\lambda_0)\neq 0$, then $\dot{\Delta}(\lambda_0)\neq 0$. According to (1) and (4), we have

$$\dot{c}''(x,\lambda)+[\lambda^2-2\lambda p(x)-q(x)]\dot{c}'(x,\lambda)=2[p(x)-\lambda]c(x,\lambda)$$
$$\dot{c}(0,\lambda)=\dot{c}'(0,\lambda)=0$$

As in [19] we find

$$\dot{c}(x,\lambda)=\int_0^x h(x,t,\lambda)c(t,\lambda)dt\,,\ \ \dot{s}(x,\lambda)=\int_0^x h(x,t,\lambda)s(t,\lambda)dt\ , \tag{10}$$

$$\dot{c}'(x,\lambda)=\int_0^x h'_x(x,t,\lambda)c(t,\lambda)dt\,,\ \dot{s}'(x,\lambda)=\int_0^x h'_x(x,t,\lambda)s(t,\lambda)dt\ , \tag{11}$$

where

$$h(x,t,\lambda) = 2\big(c(x,\lambda)s(t,\lambda) - s(x,\lambda)c(t,\lambda)\big)\cdot\big(\lambda - p(t)\big), \tag{12}$$

$$h'_x(x,t,\lambda) = 2\big(c'(x,\lambda)s(t,\lambda) - s'(x,\lambda)c(t,\lambda)\big)\cdot\big(\lambda - p(t)\big). \tag{13}$$

To simplify the notation, in the future we will often write $c, c', s, s'.$ instead of $c(\pi,\lambda), c'(\pi,\lambda), s(\pi,\lambda), s'(\pi,\lambda)$.

Let's find the derivative of function (7) with respect to λ:

$$\dot{\Delta}(\lambda) = |\omega|^2 \dot{s} + (2m\lambda + \alpha)\sigma(\lambda) + a(\lambda)\dot{\sigma}(\lambda) - \dot{\eta}(\lambda). \tag{14}$$

Taking into account (6), (10) and (11) in the last equality, we obtain

$$\dot{\Delta}(\lambda) = \int_0^\pi |\omega|^2 h(\pi,t,\lambda)s(t,\lambda)dt + a(\lambda)\cdot\left[\int_0^\pi h'_x(\pi,t,\lambda)s(t,\lambda)dt + \int_0^\pi \gamma h(\pi,t,\lambda)s(t,\lambda)dt\right] -$$

$$-\int_0^\pi \gamma h(\pi,t,\lambda)c(t,\lambda)dt - \int_0^\pi h'_x(\pi,t,\lambda)c(t,\lambda)dt + (2m\lambda+\alpha)\sigma(\lambda).$$

From here, by virtue of (8), (12) and (13), it follows

$$\dot{\Delta}(\lambda) = 2\int_0^\pi \Big[\sigma(\lambda)c^2(\lambda,t) - \big(\eta(\lambda) + |\omega|^2 s + a(\lambda)\sigma(\lambda)\big)c(\lambda,t)s(\lambda,t) +$$

$$+\big(|\omega|^2 c + a(\lambda)\eta(\lambda)\big)s^2(\lambda,t)\Big]\big(\lambda - p(t)\big)dt + (2m\lambda+\alpha)\sigma(\lambda). \tag{15}$$

Since $\Delta(\lambda_0) = 0$, then λ_0 is an eigenvalue of problem P. Let $f_0(x)$ be the corresponding eigenfunction. It is easy to verify that

$$f_0(x) = f_0(0)c(x,\lambda_0) + f'_0(0)s(x,\lambda_0). \tag{16}$$

By virtue of this equality we obtain

$$|f_0(x)|^2 = f_0(x)\overline{f_0(x)} = |f_0(0)|^2 c^2(\lambda_0,x) + |f'_0(0)|^2 s^2(\lambda_0,x) +$$

$$+\Big[f_0(0)\overline{f'_0(0)} + \overline{f_0(0)}f'_0(0)\Big]c(\lambda_0,x)s(\lambda_0,x). \tag{17}$$

From (16) we obtain

$$f'_0(\pi) = f_0(0)c'(\pi,\lambda_0) + f'_0(0)s'(\pi,\lambda_0).$$

According to the second of the boundary conditions (2) (taking into account (17)) we have

$$-\overline{\omega}f_0(0) + \gamma f_0(0)c(\pi,\lambda_0) + \gamma f'_0(0)s(\pi,\lambda_0) + f_0(0)c'(\pi,\lambda_0) + f'_0(0)s'(\pi,\lambda_0) = 0$$

or

$$f_0(0)(-\overline{\omega} + \eta(\lambda_0)) + f'_0(0)\sigma(\lambda_0) = 0$$

From here

$$f_0'(0) = \frac{\overline{\omega} - \eta(\lambda_0)}{\sigma(\lambda_0)}\, f_0(0). \tag{18}$$

It is obvious that

$$|\, f_0'(0)|^2 = f_0'(0)\,\overline{f_0'(0)} = \frac{\overline{\omega} - \eta(\lambda_0)}{\sigma(\lambda_0)} \cdot \frac{\omega - \eta(\lambda_0)}{\sigma(\lambda_0)} |\, f_0(0)|^2 =$$

$$= \frac{|\omega|^2 - \overline{\omega}\eta(\lambda_0) - \omega\eta(\lambda_0) + \eta^2(\lambda_0)}{\sigma^2(\lambda_0)} |\, f_0(0)|^2 =$$

$$= \frac{|\omega|^2 - \eta(\lambda_0)(2\operatorname{Re}\omega - \eta(\lambda_0))}{\sigma^2(\lambda_0)} |\, f_0(0)|^2 .$$

Hence,

$$|\, f_0'(0)|^2 = \frac{|\omega|^2 + \eta(\lambda_0)\left[a(\lambda_0)\sigma(\lambda_0) + |\omega|^2 s)\right]}{\sigma^2(\lambda_0)} |\, f_0(0)|^2 . \tag{19}$$

Using identity (5) and relations (18) and (19), we have

$$|\, f_0'(0)|^2 = \frac{|\omega|^2 + (c' + \gamma c)\left[a(\lambda_0)\sigma(\lambda_0) + |\omega|^2 s\right]}{\sigma^2(\lambda_0)} |\, f_0(0)|^2 =$$

$$= \frac{|\omega|^2 + a(\lambda_0)\sigma(\lambda_0)c' + |\omega|^2 (cs' - 1) + a(\lambda_0)\gamma cs' + a(\lambda_0)\gamma^2 cs + \gamma|\omega|^2 cs}{\sigma^2(\lambda_0)} |\, f_0(0)|^2 =$$

$$= \frac{a(\lambda_0)\sigma(\lambda_0)c' + |\omega|^2 c\sigma(\lambda_0) + a(\lambda_0)\sigma(\lambda_0)\gamma c}{\sigma^2(\lambda_0)} |\, f_0(0)|^2 =$$

$$= \frac{a(\lambda_0)\eta(\lambda_0) + |\omega|^2 c}{\sigma(\lambda_0)} |\, f_0(0)|^2 ,$$

$$f_0(0)\overline{f_0'(0)} + \overline{f_0(0)} f_0'(0) = \frac{\omega - \eta(\lambda_0)}{\sigma(\lambda_0)}\, \overline{f_0(0)} f_0(0) + \frac{\overline{\omega} - \eta(\lambda_0)}{\sigma(\lambda_0)}\, \overline{f_0(0)} f_0(0) =$$

$$= \frac{2\operatorname{Re}\omega - 2\eta(\lambda_0)}{\sigma(\lambda_0)} |\, f_0(0)|^2 .$$

According to the ratio

$$\Delta(\lambda_0) = 2\operatorname{Re}\omega + |\omega|^2 s + a(\lambda_0)\sigma(\lambda_0) - \eta(\lambda_0) = 0 \tag{20}$$

we have

$$\frac{2\operatorname{Re}\omega - 2\eta(\lambda_0)}{\sigma(\lambda_0)} |\, f_0(0)|^2 = -\frac{|\omega|^2 s + a(\lambda_0)\sigma(\lambda_0) + \eta(\lambda_0)}{\sigma(\lambda_0)} |\, f_0(0)|^2$$

Therefore, from (17) we obtain that

$$|f_0(x)|^2 = |f_0(0)|^2 c^2(\lambda_0, x) + \frac{a(\lambda_0)c' + |\omega|^2 c + a(\lambda_0)\gamma c}{\sigma(\lambda_0)} s^2(\lambda_0, x)|f_0(0)|^2 +$$

$$+ \frac{-c' - \gamma c - |\omega|^2 s - a(\lambda_0)\gamma s - a(\lambda_0)s'}{\sigma(\lambda_0)} s(\lambda_0, x)c(\lambda_0, x)|f_0(0)|^2 =$$

$$= \left[\frac{\left[|\omega|^2 c + a(\lambda_0)\eta(\lambda_0)\right]s^2(\lambda_0, x) + \left[-|\omega|^2 s - a(\lambda_0)\sigma(\lambda_0) - \eta(\lambda_0)\right]s(\lambda_0, x)c(\lambda_0, x)}{\sigma(\lambda_0)} + \right.$$

$$\left. + \frac{\sigma(\lambda_0)c^2(\lambda_0, x)}{\sigma(\lambda_0)} \right] |f_0(0)|^2 .$$

Multiplying both sides of this equality by $\lambda_0 - p(x)$, then integrating within $[0, \pi]$ and taking into account (15) and (17), we get

$$2\int_0^\pi [\lambda_0 - p(x)]\, |f_0(x)|^2 = \frac{|f_0(0)|^2}{\sigma(\lambda_0)} \left[\dot{\Delta}(\lambda_0) - (2m\lambda_0 + \alpha)\sigma(\lambda_0)\right].$$

Thus,

$$2\int_0^\pi [\lambda_0 - p(x)]\, |f_0(x)|^2 + (2m\lambda_0 + \alpha)|f_0(0)|^2 = \frac{|f_0(0)|^2}{\sigma(\lambda_0)} \dot{\Delta}(\lambda_0).$$

From here, by virtue of (3), we have $\dot{\Delta}(\lambda_0) \neq 0$.

Let us assume that $\Delta(\lambda_0) = \dot{\Delta}(\lambda_0) = 0$. If $\sigma(\lambda_0) \neq 0$, then, according to what was proved above, $\dot{\Delta}(\lambda_0) \neq 0$ takes place, which contradicts our condition. Hence $\sigma(\lambda_0) = 0$. Then, by virtue of identity

$$c(\pi, \lambda_0)\sigma(\lambda_0) - s(\pi, \lambda_0)\eta(\lambda_0) = 1 \tag{21}$$

we obtain

$$s(\pi, \lambda_0)\eta(\lambda_0) = -1. \tag{22}$$

From $\Delta(\lambda_0) = 0$ according to (7) we have

$$2\operatorname{Re}\omega + |\omega|^2 s(\pi, \lambda_0) + \frac{1}{s(\pi, \lambda_0)} = 0. \tag{23}$$

From here, taking into account the relation

$$|\omega|^2 = \operatorname{Re}^2 \omega + \operatorname{Im}^2 \omega,$$

we obtain

$$1 + 2s(\pi, \lambda_0)\operatorname{Re}\omega + s^2(\pi, \lambda_0)\operatorname{Re}^2 \omega + s^2(\pi, \lambda_0)\operatorname{Im}^2 \omega = 0,$$
$$(1 + s(\pi, \lambda_0)\operatorname{Re}\omega)^2 + (s(\pi, \lambda_0)\operatorname{Im}\omega)^2 = 0,$$

i.e.

$$1+s(\pi,\lambda_0)\operatorname{Re}\omega = s(\pi,\lambda_0)\operatorname{Im}\omega = 0. \tag{24}$$

By virtue of (22) we have $s(\pi,\lambda_0)\neq 0$. Then from (24) it follows that

$$\operatorname{Im}\omega = 0,\ \omega\neq 0,\quad 1+\omega s(\pi,\lambda_0)=0.$$

It remains to prove that the equality

$$a(\lambda_0)+\omega c(\pi,\lambda_0)=0$$

also holds.

Since ω is real, then $\operatorname{Re}\omega=\omega,\ |\omega|^2=\omega^2$. Then from (23)

$$-2\omega-\omega^2 s(\pi,\lambda_0)+\eta(\lambda_0)=0.$$

Since $\omega s(\pi,\lambda_0)=-1$, then

$$2\omega^2 s(\pi,\lambda_0)-\omega^2 s(\pi,\lambda_0)+\eta(\lambda_0)=0,$$

or

$$\omega^2 s(\pi,\lambda_0)+\eta(\lambda_0)=0. \tag{25}$$

Therefore, from formula (15) it follows that

$$\left[\omega^2 c+a(\lambda_0)\eta(\lambda_0)\right]\int_0^{\pi}\left[\lambda_0-p(t)\right]s^2(t,\lambda_0)dt=0. \tag{26}$$

Since $1+\omega s(\pi.\lambda_0)=\sigma(\lambda_0)=0$ and $\operatorname{Im}\omega=0$, then

$$a(\lambda_0)s(0,\lambda_0)+s'(0,\lambda_0)+\omega s(\pi,\lambda_0)=0,$$

$$-\omega s(0,\lambda_0)+\gamma s(\pi,\lambda_0)+s'(\pi,\lambda_0)=0.$$

This means that function $s(x,\lambda_0)$ satisfies the boundary conditions (2). Then $s(x,\lambda_0)$ is an eigenfunction of the boundary value problem P. Therefore, according to (3)

$$\int_0^{\pi}\left[\lambda_0-p(t)\right]s^2(t,\lambda_0)dt+(2m\lambda_0+\alpha)|s(0,\lambda_0)|^2\neq 0.$$

From (26) it follows that

$$\omega^2 c(\pi,\lambda_0)+a(\lambda_0)\eta(\lambda_0)=0. \tag{27}$$

Next, by virtue of equality $\omega s(\pi,\lambda_0)=-1$, we sequentially find

$$\eta(\lambda_0)+\omega^2 s(\pi,\lambda_0)=0,\ \eta(\lambda_0)+\omega\cdot\omega s(\pi,\lambda_0)=0,\ \eta(\lambda_0)-\omega=0,\ \eta(\lambda_0)=\omega.$$

Then from (27) we find that $\omega^2 c(\pi,\lambda_0)+a(\lambda_0)\omega=0$. Hence $a(\lambda_0)+\omega c(\pi,\lambda_0)=0$.

Sufficiency. Let $\Delta(\lambda_0)=0$, $\operatorname{Im}\omega=0$, $\omega\neq 0$ and the equalities (9) hold.

According to (20) and (21)

$$\Delta(\lambda_0)=2\omega-\eta(\lambda_0)+\omega^2 s(\pi,\lambda_0)=2\omega+\frac{1}{s(\pi,\lambda_0)}+\omega^2 s(\pi,\lambda_0)=0$$

From here

$$2\omega s(\pi,\lambda_0)+1+\omega^2 s^2(\pi,\lambda_0)=0,$$

$$[\omega s(\pi,\lambda_0)+1]^2=0, \text{ т.е. } \omega s(\pi,\lambda_0)=-1.$$

Then

$$\Delta(\lambda_0)=2\omega-\eta(\lambda_0)-\omega=\omega-\eta(\lambda_0)=0,$$

i.e. $\omega=\eta(\lambda_0)$. By the condition $a(\lambda_0)+\omega c(\pi,\lambda_0)=0$. Then

$$\omega^2 c(\pi,\lambda_0)+a(\lambda_0)\omega=\omega^2 c(\pi,\lambda_0)+a(\lambda_0)\eta(\lambda_0)=0.$$

Using this equality and taking into account the relations

$$\sigma(\lambda_0)=\eta(\lambda_0)+\omega^2 s(\pi,\lambda_0)+a\sigma(\lambda_0)=0$$

from (15) we obtain that $\dot{\Delta}(\lambda_0)=0$, i.e. λ_0 is a multiple zero of the function $\Delta(\lambda)$.

The theorem is proven.

REFERENCE LIST

1. Marchenko V.A. Sturm-Liouville Operators and Their Applications. Kyiv: Naukova Dumka, 1977, 332 p.
2. Akhtyamov A.M. Theory of Identification of Boundary Conditions and Its Applications. Moscow: Fizmatlit, 2009, 272 p.
3. Gasyumov M.G., Guseynov G.Sh. Determination of the Diffusion Operator by Spectral Data // Dokl. AN Azerb. SSR, 1981, vol. 37, no. 2, pp. 19-23.
4. Ala V., Mamedov Kh.R. On a Discontinuous Sturm-Liouville Problem with Eigenvalue Parameter in the Boundary Conditions // Dynamic Systems and Applications. 2020. Vol. 29. P. 182-191.
5. Gasyumov M.G., Guseynov I.M., Nabiev I.M. Inverse Problem for the Sturm-Liouville Operator with Non-separated Self-adjoint Boundary Conditions // Sib. Math. J., 1990, vol. 31, no. 6, pp. 46-54.
6. Guseynov I.M., Nabiev I.M. Solution of a Class of Inverse Boundary Problems for Sturm-Liouville Operators // Math. Sbornik, 1995, vol. 186, no. 5, pp. 35-48.
7. Guseynov I.M., Nabiev I.M. On a Class of Inverse Problems for a Quadratic Pencil of Sturm-Liouville Operators // Differ. Equations, 2000, vol. 36, no. 3, pp. 418-420.
8. Binding P.A., Volkmer H. Inverse Oscillation Theory for Sturm-Liouville Problems with Non-separated Boundary Conditions // Inverse Problems, 2007, vol. 23, no. 1, pp. 343-355.
9. Guseynov I.M., Nabiev I.M. Inverse Spectral Problem for Bundles of Differential Operators // Math. Sbornik, 2007, vol. 198, no. 11, pp. 47-66.
10. Sadovnichiy V.A., Sultanaev Ya.T., Akhtyamov A.M. Inverse Problem for a Bundle of Operators with Non-decaying Boundary Conditions // Dokl. RAN, 2009, vol. 425, no. 1, pp. 31-33.
11. Nabiev I.M. Determination of the Diffusion Operator on an Interval // Colloquium Mathematicum, 2014, vol. 134, no. 2, pp. 165-178.
12. Freiling G., Yurko V. Recovering Nonselfadjoint Differential Pencils with Non-separated Boundary Conditions // Applicable Analysis, 2015, vol. 94, no. 8, pp. 1649-1661.
13. Yurko V.A. Inverse Spectral Problems for Differential Operators with Non-separated Boundary Conditions // Journal of Inverse and Ill-posed Problems, 2020, vol. 28, no. 4, pp. 567-616.

14. Mammadova L.I., Nabiev I.M., Rzayeva Ch.H. Uniqueness of the Solution of the Inverse Problem for Differential Operators with Semi-separated Boundary Conditions // Baku Mathematical Journal, 2022, vol. 1, no. 1, pp. 47-52.
15. Mammedzadeh G.S. On a Boundary Value Problem with Spectral Parameter Quadratically Contained in the Boundary Condition // Trans. Natl. Acad. Sci. Azerb. Ser. Phys.-Tech. Math. Sci. Mathematics, 2022, vol. 42, no. 1, pp. 141-150.
16. Nabiev I.M. Reconstruction of the Differential Operator with Spectral Parameter in the Boundary Condition // Mediterr. J. Math., 2022, vol. 19, no. 3, pp. 1–14.
17. Nabiev I.M., Mammadova L.I., Mammedzadeh G.S. Algorithms for Recovery of Diffusion and Sturm-Liouville Operators with Semi-separated Boundary Conditions // Proc. of Institute of Math. and Mech. of National Academy of Sci. of Azerbaijan, 2023, vol. 49, no. 2, pp. 219-227.
18. Mammadova L.I., Nabiev I.M. Solvability of the Inverse Spectral Problem for the Sturm-Liouville Operator with Spectral Parameter in the Boundary Condition // Baku Mathematical Journal, 2024, vol. 3, no. 1.
19. Nabiev I.M. Multiplicity and Mutual Arrangement of Eigenvalues of the Quadratic Pencil of Sturm-Liouville Operators // Math. Notes, 2000, vol. 67, no. 3, pp. 369-381.
20. Ibadzade Ch.G. Multiplicity of Eigenvalues of the Diffusion Operator with a Spectral Parameter in the Boundary Condition // J. of Qafqaz University - Mathematics and Computer Science, 2015, vol. 3, no. 2, pp. 188-195.
21. Farzullazadeh A.Q. On the Multiplicity of Eigenvalues of the Dirac Operator // Journal of Baku Engineering University, Mathematics and Computer Science, 2020, vol. 4, no. 2, pp. 111-119.

2024. Volume 8, Number 1 *Pages 45-54*

UOT:002.6:025.3/.4
DOİ: ***https://doi.org/10.30546/09090.2024.110.209***

IMPLICATIONS OF ARTIFICIAL INTELLIGENCE DRIVEN DRONE SYSTEMS FOR RECOGNITION OF ENVIRONMENTAL HAZARDS

FAIG SAFIYEV
Landau School, G. Aliyev, 9, Baku, Azerbaijan
famak9386@gmail.com

ARTICLE INFO

Article history:
Received:2024-09-12
Received in revised form:2024-09-16
Accepted:2024-12-09
Available online

Keywords: environmental impact, machine learning, artificial intelligence, ethical concerns, remote sense technology, drone systems, noise pollution

ABSTRACT

Artificial intelligence driven drone systems offer promising solutions for early detection and response to environmental hazards like wildfires and oil leaks. However, their widespread adoption raises significant ethical and environmental implications, including privacy infringements, algorithmic bias, data security, noise pollution, and greenhouse gas emissions. This study addresses these issues through literature reviews, surveys of affected populations, and prototype testing of AI models for disaster identification, in order to mitigate ethical issues. A specific metric was developed to rate drone components and identify the most sustainable options, minimizing the environmental impact. By promoting these solutions, this research aims to ensure the sustainable and responsible integration of artificial intelligence systems in environmental monitoring, protecting ecosystems and communities effectively.

1. INTRODUCTION

Modern technologies allow us to achieve things we never imagined would be real. One of them is artificial intelligence systems, currently experiencing the peak of their hype. They enable us, humans, to leverage them for our own benefit, using them everywhere including private houses, offices, applications, websites, cars, and recently, drones. They help us with everything, starting from writing emails and essays, and ending with driving cars and delivery of items. However, specifically, this paper will discuss implementations of artificial intelligence in drone systems for recognition of environmental hazards and the implications of this approach.

Such drones are divided into two main groups. The first group is used after a disaster to provide high-resolution images, and real-time visual and audio access, assisting in mapping the extent of destruction, identifying safe routes for ground teams, monitoring flood levels, locating missing individuals and aiding in rescue operations. These drones are typically deployed after fires, earthquakes, hurricanes, tsunamis, similar events. The second group is used to locate disasters, identify them as soon as they occur, and inform the admin panel, which can then verify and call the nearest emergency services, such as in detecting wildfires and oil leaks.

Examples of the usage of the first group of drones, also known as unmanned aerial vehicles (UAVs), are numerous: the Nepal earthquakes in 2015, Hurricane Harvey in 2017, the California wildfires in 2018, the floods in Indian states from 2018 to 2022, wildfires in Türkiye in 2020 and many more. In all of these catastrophes, without the opportunities drones provide it would have been much more difficult to rescue people and manage the situation. The efficiency of drones comes from their compact size, enabling them to navigate through small holes and areas filled with smoke and fire, while capturing real-time data. Importantly, their relatively low cost makes drones a preferred choice for most organizations and agencies over human-led missions.

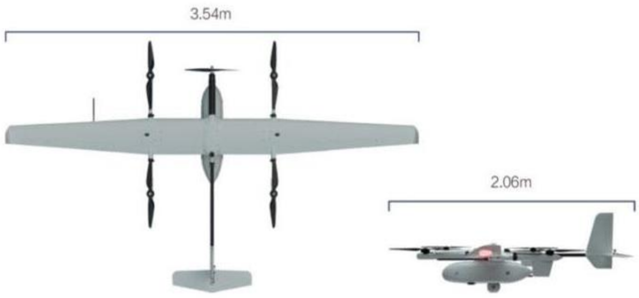

Fig. 1. Dimensions of the CW-15D drone

In comparison, the usage of drones from the second group is not as widespread. One example is the CW-15D drone flying over forests in high risk areas of Sichuan province, China. As can be seen in Fig. 1, although the drones might appear large, they are actually considered relatively small, with a wingspan of 3.54 meters and a length of 2.06 meters. They are equipped with visible and infrared cameras, capturing videos from low and medium altitudes and monitoring the key forest areas. However, the biggest drawback of this scheme is that the videos and photos are analyzed and processed by humans, sitting in their offices, behind monitors. While decisions made by humans are typically accurate, there are inherent limitations. One person can only monitor a limited number of drones, making it very expensive and challenging to implement such systems in bigger areas, as well as slowing down the process. And that is where artificial intelligence comes in. Instead of paying hundreds of thousands dollars to humans to monitor the areas, and still be limited to a certain number, it is more rational to create a specific program with a built in artificial intelligence and implement it into the drone's system, allowing it to recognize natural disasters autonomously and quite accurately.

One of the first, successful AI-driven drones was launched during Carmel Forest fire in Israel, 2020, and the Dixie fires in California, 2022. The drones identified and located fire, and were used to map the fire's perimeter, identify hot spots, and assess the damage. This information helped CAL FIRE (California Department of Forestry and Fire Protection) and the Israeli fire service to come in time, make better decisions about where to deploy firefighters. Once again, the valuable resources, time, and most importantly, human lives were saved due to the existence of artificial intelligence. The rescue team already knew their route and quickly executed the operation, spending much less time in the fires and smoke than they would have if they had to search for people without a particular plan or path, saving both their own lives and the lives of people they were looking for. The efficient data processing by the artificial intelligence system in these cases was due to extensive training done beforehand, using huge databases and data sets, full of information and media regarding fires.

While having significant potential and as of current offering substantial benefits to society, this method also comes with its own set of implications. Despite numerous studies on the technical capabilities of artificial intelligence driven drones, there is limited research on the ethical and environmental implications of their deployment. Furthermore, existing metrics to evaluate drone components often fail to consider and overlook sustainability factors. Thus, this study addresses those gaps and issues. Among these concerns are privacy questions, wildlife disturbance, noise pollution and greenhouse gas emission. The study further extends to offer potential solutions and strategies to mitigate or at least minimize these concerns, ensuring that the integration of artificial intelligence into drones is responsible, ethical and sustainable.

2. RELATED WORK

Latest studies have shown that the rate of the growth of systems with artificial intelligence is increasing on a daily basis, as do the capabilities of such systems.

Recent research from MIT has introduced a significant advancement in the implementation of artificial intelligence for drone navigation through the use of liquid neural networks. These networks are designed to mimic the adaptability of biological brains, allowing drones to navigate and perform tasks in unfamiliar environments with greater precision and resilience. Unlike traditional neural networks, liquid neural networks can continuously alter their parameters over time, enabling them to handle unexpected or noisy data more effectively. This adaptability is crucial for drones that must operate in diverse and changing conditions, such as moving from a forest to an urban environment. The MIT team trained their liquid neural networks using data collected by human pilots, which allowed the drones to learn from expert navigation and then generalize these skills to new and drastically different environments. In tests, these drones outperformed other state-of-the-art navigation systems, successfully handling tasks like tracking moving targets and navigating through occluded and rotated objects in various settings. The researchers believe that this technology could significantly improve the efficiency and reliability of autonomous drones for applications such as search and rescue, environmental monitoring, and delivery services. The ability to adapt to new environments without additional training makes liquid neural networks a promising solution for the challenges faced by current AI-driven drone systems.

Another significant development is the usage of deep learning algorithms and edge computing to enhance real-time object detection capabilities in UAVs. This approach uses GPU-based edge computing platforms, systems and lightweight convolutional layers to optimize performance on resource-limited devices, making them highly effective for emergency rescue and precision agriculture applications. These extensive studies examined various real-time object detection networks across multiple domains, providing insights into the efficiency and accuracy of different detection architectures, such as anchor-based and transformer-based models. The papers have also explored the impact of variables like image size and confidence thresholds on the detection performance. A comprehensive survey focused on deep learning methods for object detection and tracking using UAV data addressed challenges such as scale diversity, small object detection, and direction diversity. Advanced techniques like multi-scale feature maps and deformable convolution kernels were highlighted for their ability to enhance detection capabilities in varied and complex environments. This review provided a detailed understanding of data processing and algorithmic strategies needed for effective UAV-based object detection. These studies underscore the progress in integrating AI with drone technology, improving the detection, monitoring of natural disasters. By leveraging deep learning and edge computing, these systems are becoming more efficient and reliable, paving the way for better disaster response and management.

3. METHODOLOGY

A script has been designed to build and train a convolutional neural network (CNN) using the Keras library for image classification tasks. The script begins by importing necessary libraries and defining constants such as image dimensions, directory paths for training and validation data, and the number of samples for each set. The build_model() function creates a sequential CNN model with convolutional, activation, pooling, flattening, and dense layers. It compiles the model using binary cross-entropy loss, and the RMSprop optimizer. The train_model () function prepares image data generators for both training and validation sets with specified augmentation techniques and rescaling. It then generates batches of augmented data and fits the model using the training data while validating it on the validation data. The main () function initializes the model, trains it, and saves the trained model to a file. In conclusion, the program automates the process of building, training, and saving a CNN model for image classification tasks. Then, another code sets up a web application using Flask, enabling uploading images and receiving predictions from the machine learning model that distinguishes between "Oil Spills" and "Wildfires". Key constants such as labels for the two classes, paths to sample images, the upload folder, allowed file extensions, and the model filename are defined at the beginning. The application includes functions to load the model and handle file uploads securely. The main route renders an HTML page where users can upload an image, which is then saved to the server if it is of an allowed type. Upon upload, the image is processed and fed into the model to generate a prediction, which is then displayed back to the user. The application configuration is set with necessary parameters, including secret keys and session management, and the Flask server is run with these settings. Successfully identified images are then stored in the system for further training and usage for comparison.

3.1 Methodology for ethical concerns

A quick survey effective for identifying the main concerns of the population regarding the AI driven drone system has been conducted among 100 people. The question set was designed in such a way that the responses would reflect both the issues people have encountered with AI-driven drone systems and the issues they would prefer to avoid in the future. The questions are following:

1. How familiar are you with the AI driven drones?
2. What ethical concerns might you have if AI-driven drones were used in your area?
3. How important is it to you that AI-driven drones operate with strong privacy protections?
4. To what extent are you concerned about the potential misuse of AI-driven drones for unauthorized surveillance?
5. How confident are you that current regulations adequately address the ethical implications of AI-driven drones?
6. How do you believe the ethical use of AI-driven drones can be improved?
7. Would you support the deployment of AI-driven drones if ethical concerns were adequately addressed?

This set of survey questions was chosen because they comprehensively address the ethical side of the implications, which is a critical aspect for understanding public concerns. These questions will help identify key areas such as privacy invasion, data security, bias in AI decision making. By gathering detailed feedback on these specific issues, this study points on the main ethical concerns and develops targeted solutions to address them. The artificial intelligence model created earlier will be adjusted based on the received feedback to mitigate the ethical concerns of the public.

3.2 Methodology for environmental concerns

To address the environmental concerns, the methodology involves a detailed and systematic approach focusing on noise pollution, carbon emissions, and wildlife disturbances. Numerous studies highlight the issues with drones being too noisy and emitting significant amounts of carbon, which can impact both human populations and wildlife. To eliminate, a comprehensive literature review will be undertaken to identify various drone components and designs that are quieter and environmentally friendly. Then, through experiment and analysis, a specific metric, Environmental Impact and Efficiency Metric (EIEM), which includes factors like noise pollution level, energy efficiency and carbon emissions, will be calculated and evaluated to compare the noise levels and carbon emissions of different drone models. The Environmental Impact and Efficiency Metric (EIEM) will be calculated using the following formula:

$$EIEM = (W_n \times (N_m \div N_t)) + (W_c \times (C_m \div C_t)) + (W_e \times (E_m \div E_t))$$

Where N_m is the noise level in decibels (dB), N_t is the maximum acceptable noise level in decibels (dB), C_m is the carbon emissions of the drone (in kg CO2 per hour of operation), C_t is the maximum acceptable carbon emissions (in kg CO2 per hour of operation), E_m is the energy efficiency of the drone (in watt-hours per km), E_t is the baseline energy efficiency for comparison (in watt-hours per km), W_n and W_c and W_e are the weights assigned to noise, carbon emissions, and energy efficiency, respectively, summing to 1. The weightings represent how important and crucial it is to reduce the particular measurement, with a lower magnitude of EIEM indicating a better result. Using this metric, a detailed table will be created that lists various drones along with their environmental impact scores. This table will serve as a comparative tool to identify the most suitable drones for our purposes. The data collected will assist in selecting the components and designs that produce the least noise and emissions, ensuring that the drone system is both quiet and sustainable.

4. EXPERIMENTS AND ANALYSIS

Initially, the developed artificial intelligence model was trained and tested for errors using a dataset, compiled from public repositories and simulated scenarios, of several hundred images, which included wildfires, oil leaks, both, or none. Out of 325 images processed, 318 were correctly determined, making the accuracy approximately 98% which means it is a quite precise model for our purpose. All of the 100 images were saved in the system for additional training, to further increase the accuracy and precision.

4.1 Analysis of the survey

The survey was conducted among nearly 100 people of diverse backgrounds and classes to ensure and maximize accuracy and minimize bias, as mentioned before. Roughly 55% and 31%

of the respondents stated that they are somewhat or very familiar with the concept of AI-based drone systems, respectively, making them a perfect fit for the purpose of the survey.

Fig. 2. Statistics of the answers

Analyzing the responses from Fig. 2, along with the answers to the main question, which state that 69% are concerned about privacy, 24.1% are concerned about bias in algorithms, 55.4% are concerned about data security and misuse, and 44.8% are concerned about potential misuse in surveillance, it's apparent that privacy is the primary concern. This includes worries about drones capturing and storing images of people's faces and bodies, as well as images of their houses and properties. To address this concern, the previously developed AI model needs to be adjusted so that it doesn't save photos containing people for further training.

4.2 Adjustment of the AI model

The program code has been adjusted. In the revised code, a critical addition is a new function called detect_human_faces(), passed with an argument image_path, leveraging pre-trained Haar cascades from OpenCV library. Haar cascades are a type of machine learning-based approach used for object detection in images. They work by analyzing patterns of intensity or color gradients in an image to identify specific objects or features. In the case of human face and body detection, Haar cascades are trained on a large dataset of positive and negative images to learn characteristic patterns associated with human faces and bodies. This function inspects an image to identify the presence of human faces or bodies. Within the main () function, following the model training and saving processes, an example application of the human face detection function has been integrated. Based on the outcome, the script makes a decision whether to proceed with saving the image for subsequent training iterations. If human faces or bodies are detected, the script bypasses the saving process to uphold privacy standards, and will be saved in case the program has not identified any presence of human beings in the image. This approach ensures the privacy and dignity of individuals depicted in the images, safeguarding their integrity and respecting their rights.

4.3 Creation of a list of drones to be tested

Before computing the value of EIEM, it's essential to identify a comprehensive list of potential drone models and high-risk of wildfires and oil leaks areas where the drones are expected to fly and monitor. Following a thorough review of all candidates, the following list of drones has been compiled:

1. DJI Matrice 300 RTK (M300)
2. Parrot Anafi USA

3. Skydio X2D
4. Sensefly eBee X with RTK/PPK
5. Draganflyer X4-P
6. Autel Robotics EVO II Dual
7. Altavian Nova F7200
8. Yuneec H520

And the following list of high-risk areas:

1. Amazon rainforest, Brazil
2. California, United States
3. Alberta Tar Stands, Canada
4. Siberian Taiga, Russia
5. Peruvian Amazon, Peru
6. Niger Delta, Nigeria
7. Australian Outback, Australia
8. Indonesian Rainforest, Indonesia

In selecting these drones, several factors were considered. Firstly, each drone offers unique advantages directly related to disaster response applications, such as long flight time, advanced imaging capabilities. Secondly, the drones were chosen based on their compatibility with AI integration, including the ability to carry the hardware and sensors, as well as support for third-party SDKs for custom AI development. Also, factors such as reliability, durability, and ease of deployment were taken into account to ensure optimal performance in challenging disaster environments. Whereas the high-risk areas are characterized by their susceptibility to wildfires and oil leaks, posing environmental and ecological threats that require monitoring and response measures as well as past experiences.

4.4 Calculating EIEM for each model

In order to calculate the Environmental Impact Evaluation Metric (EIEM), it's essential to establish both weighting factors and a maximum allowed threshold for each factor (noise level, carbon emissions level and energy efficiency). The value of W_e (weighting of energy efficiency) has been designated as 0.2, because of its lower importance compared to factors like carbon emissions and noise pollution. This decision is based on the idea that the direct impact of energy efficiency of the drones on the environment is comparatively lesser than that of other factors. The weighting of carbon emissions (W_c) has been established at 0.5, showing its greater significance in environmental assessments. This value comes from the wide-ranging consequences associated with substantial carbon emissions, including climate change and ecosystem degradation. In contrast, noise pollution, while still relevant, is perceived to have a comparatively lesser impact on the environment.

Following the weightings, threshold values have to be determined. The maximum noise, not causing significant noise pollution in the areas listed before is 65 dB, as it does not disturb the wildlife and allows proper drone work, assigning the value of $N_{threshold}$ to 65 dB. The carbon emissions threshold ($C_{threshold}$) is set to be 200 kg per hour and is aligned under international agreements such as the Paris Agreement on climate change as well as global efforts to mitigate greenhouse gas emissions and combat climate change. Lastly, $E_{threshold}$ (the energy efficiency threshold) is set to be 4 watt-hours per kilometer traveled. This decision comes from a practical and inclusive standard. accommodating a wide range of both fixed-wing and multi-rotor drones, ensuring effective usage without excluding widely-used models.

DJI Matrice 300 RTK (M300)

The model DKI Matrice 300 RTK shows excellent payload capacity for carrying AI hardware and sensors. Long flight time allows for extended missions during disaster response as well as advanced flight safety features, including obstacle avoidance and redundant systems. All of the parameters of the drone have been measured several times and the mean has been recorded for low uncertainty in the results. $N_{measured}$ is 70 dB (in 2 meters radius). $C_{measured}$ has been calculated by multiplying the power of the drone in kW and the average global carbon intensity of electricity (0.5 kg CO_2 per kWh). The energy consumption of DJI Matrice is 500 joules per second, which is the equivalent of 500 watts or 0.5 kilowatts. So the value for $C_{measured}$ is 0.25 $kgCO_2/h$. However, that is the value per drone, but considering the dimensions of the high-risk areas, a minimum number of 500 drones will have to be deployed. So we multiply 0.25 by 500 and get 5. $E_{measured}$ (the energy efficiency) is calculated using the power of the drone, battery's voltage and distance possible to cover in 1 charge. For this specific model, the battery capacity is 5935 mAh at 44.4V (approx. 264 Wh per battery), flight time is up to 55 minutes (0.917 hours) and typical cruise speed is 15 m/s (54 km/h). Distance covered is 49.5 km (found by multiplying the flight time and speed). So energy efficiency is 264 Wh ÷ 49.5 km ≈ 5.33 Wh/km. By substituting all the values into the formula of EIEM, we get the value of 0.902.

Parrot Anafi USA

The Parrot Anafi USA offers several advantages, including its compact and lightweight design, making it highly portable and easy to deploy in various environments. With a maximum flight time of up to 32 minutes and a range of up to 4 kilometers, it provides endurance and range for mapping, surveillance, and inspection tasks. The drone's advanced imaging capabilities, including 32x zoom and thermal imaging, enable detailed and accurate data collection for various applications. The magnitude of EIEM for this model is 0.445.

Skydio X2D

The Skydio X2D boasts advanced autonomy and reliability features, making it adept at navigating complex environments with minimal human intervention. Its tough design ensures durability in adverse conditions, while flexibility allows customization for various mission requirements. However, its limited flight time and payload capacity, coupled with its pricing and regulatory considerations, may impact its suitability for certain applications.. The value of EIEM is calculated to be 0.673.

Sensefly eBee X with RTK/PPK

The Sensefly eBee X with RTK/PPK offers several advantages, including its fixed-wing design, which provides longer flight endurance and greater coverage area compared to multirotor drones. With a maximum flight time of up to 90 minutes and a range of up to 15 kilometers, it is well-suited for large-scale mapping, surveying, and agriculture applications. The value of EIEM is calculated to be 0.455.

Draganflyer X4-P

The Draganflyer X4-P offers several advantages, including a lightweight and portable design, which makes it easy to transport and deploy in various environments. However, its flight time is relatively short, limiting its use for extended missions. The value of EIEM is calculated to be 0.831.

Autel Robotics EVO II Dual

The Autel Robotics EVO II Dual combines several features, making it an excellent choice for various applications. It offers high-resolution imaging with an 8K camera and thermal imaging capabilities, providing valuable data for tasks such as search and rescue, inspection, and environmental monitoring. Additionally, while its thermal camera is useful, it may not match the resolution and sensitivity of specialized thermal drones. The value of EIEM is calculated to be 0.477.

Altavian Nova F7200

The Altavian Nova F7200 is a high-endurance drone designed for demanding applications, offering significant advantages in terms of range and payload capacity. Its long flight duration of up to 90 minutes and extensive range make it ideal for large-scale surveying, mapping, and monitoring missions. The drone's design allows it to carry high-resolution cameras and LiDAR sensors, providing versatile data collection capabilities. The value of EIEM is calculated to be 0.627.

Yuneec H520

The Yuneec H520 is a versatile drone known for its reliability and advanced features, making it suitable for a range of professional applications. One of its key advantages is the modular design, which allows users to easily swap out cameras and sensors. The H520 also offers impressive flight stability and precision thanks to its six-rotor design, even in challenging weather conditions. However, the Yuneec H520 has some limitations. Its flight time, while reasonable at around 28 minutes, is shorter compared to some other drones in its class, potentially requiring more frequent battery changes during long missions. The value of EIEM is calculated to be 0.570.

5. CONCLUSION AND FUTURE WORK

In conclusion, a comparison of the EIEM values for each drone is conducted to evaluate their environmental impact and efficiency.

Table 1. EIEM values of each drone

Drone name and model	EIEM value (3 s.f.)
DJI Matrice 300 RTK (M300)	0.902
Parrot Anafi USA	0.445

Skydio X2D	0.673
Sensefly eBee X with RTK/PPK	0.455
Draganflyer X4-P	0.831
Autel Robotics EVO II Dual	0.477
Altavian Nova F7200	0.627
Yuneec H520	0.570

From Table 1, it can be seen that the Parrot Anafi USA model is the most efficient and sustainable, having the lowest EIEM value. Closely following are the Sensefly eBee X and Autel Robotics EVO. Therefore, the following conclusion can be drawn: to mitigate environmental issues, drones with the smallest EIEM values should be utilized, making the Parrot Anafi USA an excellent choice. The EIEM factor considers both noise pollution and carbon emission levels, as well as energy efficiency. Then, to address ethical concerns, the AI model developed earlier in the study should be implemented, as it effectively addresses the most significant issues identified in the survey while maintaining high accuracy.

In future, it is planned to further develop the AI model so it can recognize other environmental hazards including but not limited to tsunamis, floods and hurricanes, as well as improve the algorithms for better accuracy.

REFERENCES

1. Sarkar, N. I., & Gul, S. (2023). Artificial intelligence-based autonomous UAV networks: A survey. Drones, 7(5), 322. https://doi.org/10.3390/drones7050322
2. MIT Center for International Studies. (n.d.). Attack of the drones: Ethical, legal and strategic implications of UAV use. https://cis.mit.edu/publications/attack-drones-ethical-legal-and-strategic-implications-uav-use
3. OriginStamp. (n.d.). The ethical concerns in drone technology. https://originstamp.com/blog/the-ethical-concerns-in-drone-technology
4. Morgan, F. E., Boudreaux, B., Lohn, A. J., Ashby, M., Curriden, C., Klima, K., & Grossman, D. (2020). Military applications of artificial intelligence: Ethical concerns in an uncertain world. RAND Corporation. https://www.rand.org/pubs/research_reports/RR3139.html
5. VisionPlatform. (2023). AI and drones: Advancements and applications in unmanned aerial vehicles. https://visionplatform.ai/ai-and-drones-advancements-and-applications-in-unmanned-aerial-vehicles/
6. Dyndal, G. L., Berntsen, J. T., & Redse-Johansen, S. (2017). Military autonomous drones (UAVs): No longer science fiction. Journal of Military Ethics, 16(3-4), 162-177. https://doi.org/10.1080/15027570.2017.1421281
7. Grose, T., & Gardner, S. (2023). Managing the drone revolution: A systematic literature review into the governance of drones. Journal of Technology and Governance, 12(2), 145-162.
   https://doi.org/10.1016/j.jtg.2023.02.001
8. Rachel G. MIT CSAIL (2023). Drones navigate unseen environments with liquid neural networks.
   https://news.mit.edu/2023/drones-navigate-unseen-environments-liquid-neural-networks-0419

JOURNAL OF BAKU ENGINEERING UNIVERSITY- MATHEMATICS AND COMPUTER SCIENCE
2024. Volume 8, Number 1 Pages 55-63

UOT:517.91./93 (517.95)
DOİ: https://doi.org/10.30546/09090.2024.110.206

GREEN'S FUNCTION OF AN IMPULSIVE STURM – LIOUVILLE OPERATOR

SUHEYLA BAHLULZADE[1]
[1]Baku Engineering University, Baku, Azerbaijan

ARTICLE INFO
Article history:
Received:2024-09-13
Received in revised form:2024-10-29
Accepted:2024-12-09
Available online
Keywords: Impulsive operators; Sturm – Liouville operators; Spectral singularities

ABSTRACT
This work is dedicated to the impulsive Sturm - Liouville operator on the whole axis with complex almost periodic potentials and the discontinuous coefficient on the right – hand side. We investigated the main characteristics of the fundamental solutions of the Sturm – Liouville equation. From the impulsive condition we found the transfer matrix. Using the impulsive condition and transfer matrix, we constructed Green's function and obtained the resolvent of the impulsive Sturm – Liouville operator. In future works, eigenvalues of the impulsive Sturm - Liouville operator will be investigated. The inverse problem will be formulated, a constructive procedure for the solution of the inverse problem will be provided.

1. Introduction

In the presented work, we consider the Sturm – Liouville equation on the whole axis

$$-y''+q(x)y=\lambda^2\rho(x)y, \quad x\in(-\infty,\infty)$$

where λ is a spectral parameter, and ρ is the density function.

In mathematical physics and quantum mechanics, boundary–value problems with discontinuities inside an interval are of great interest. To solve interior discontinuities, extra conditions, often called impulsive conditions, are imposed on the discontinuous point. The theory of impulsive differential equations was studied in detail in applied mathematics by Bainov and Simenov in 1995. Many authors have also studied the spectral theory of impulsive differential equations. Recently, the physical meaning and potential applications of spectral singularities of impulsive differential equations have been understood and studied by Mostafazadeh in 2011. Mostafazadeh, in his work, provided the physical meanings of eigenvalues and spectral singularities of the Schrödinger equation at a single point. In this work, we are concerned with the impulsive Sturm–Liouville operator on the whole axis, constructing Green's function and finding the resolvent.

2 Statement of the problem

Let's consider the Sturm – Liouville operator L in $L_2(-\infty,\infty)$ generated by the equation

$$-y''+q(x)y=\lambda^2\rho(x)y, \ x\in(-\infty,0)\cup(0,\infty) \tag{1}$$

with the impulsive condition

$$\begin{bmatrix} y(0^+) \\ y'(0^-) \end{bmatrix} = B \begin{bmatrix} y(0^-) \\ y'(0^-) \end{bmatrix}, \quad B = \begin{bmatrix} \alpha_1 & \alpha_2 \\ \alpha_3 & \alpha_4 \end{bmatrix} \tag{2}$$

where $\alpha_1, \alpha_2, \alpha_3, \alpha_4$ are complex numbers such that $\det B \neq 0$,

$$q(x) = \sum_{n=1}^{\infty} q_n e^{i\Lambda_n x} \tag{3}$$

and the condition

$$\sum_{n=1}^{\infty} |q_n| < \infty \tag{4}$$

is satisfied.

The set of exponents is a countable set of positive real numbers closed to the addition

$$M = \{\Lambda_1, \Lambda_2, \Lambda_3, \ldots \Lambda_n, \ldots\}, \ \Lambda_n > 0, \ n \in N. \tag{5}$$

The density function $\rho(x)$ has the form

$$\rho(x) = \begin{cases} 1, & x < 0 \\ \beta^2, & x > 0 \end{cases} \tag{6}$$

where $\beta > 0, \beta \neq 1$.

Furthermore, we denote the solutions of the equation (1) by y_- and y_+, respectively:

$$\begin{cases} y_-(x) := y(x), \ x < 0 \\ y_+(x) := y(x), \ x > 0 \end{cases} \tag{7}$$

Theorem 1. Equation (1) – (2) with potential $q(x)$ has the form of (3) and $\rho(x)$ defined as (6) has fundamental solutions of the form

$$f_1^{\pm}(x,\lambda) = e^{\pm i\lambda x}\left(1 + \sum_{n=1}^{\infty}\sum_{\alpha=n}^{\infty} \frac{V_{n\alpha}}{\Lambda_n \pm 2\lambda} e^{i\Lambda_\alpha x}\right) \tag{8}$$

on $(-\infty, 0)$ satisfying the asymptotic condition

$$\lim_{\operatorname{Im} x \to -\infty} f_1^{\pm}(x,\lambda) e^{\mp i\lambda x} = 1 \qquad \text{for } \pm \operatorname{Im}\lambda > 0$$

On the other hand, equation (1) – (2) has the other fundamental solutions in the form of

$$f_2^{\pm}(x,\lambda) = e^{\pm i\beta\lambda x}\left(1 + \sum_{n=1}^{\infty}\sum_{\alpha=n}^{\infty} \frac{V_{n\alpha}}{\Lambda_n \pm 2\beta\lambda} e^{i\Lambda_\alpha x}\right) \tag{9}$$

on the interval $(0,\infty)$ satisfying the asymptotic condition

$$\lim_{\operatorname{Im} x\to+\infty} f_2^{\pm}(x,\lambda)e^{\mp i\beta\lambda x}=1 \qquad \text{for } \pm\operatorname{Im}\lambda>0$$

here the numbers $V_{n\alpha}$ are determined from the following relations

$$\Lambda_\alpha(\Lambda_\alpha-\Lambda_n)V_{n\alpha}+\sum_{\beta\oplus\gamma=n}V_{n\beta}q_\gamma=0 \tag{10}$$

$$q_\alpha+\sum_{\beta\oplus\gamma=n}V_{n\beta}q_\gamma=0\,. \tag{11}$$

and series

$$\sum_{n=1}^{\infty}\Lambda_n^{-1}\sum_{\alpha=n}^{\infty}\Lambda_\alpha(\Lambda_\alpha-\Lambda_n)|V_{n\alpha}| \tag{12}$$

converges.

We easily see that at the points $\lambda=\mp\frac{\Lambda_n}{2}\left(\mp\frac{\Lambda_n}{2\beta}\right)$, $n\in N$ there can be simple poles to the function $f(x,\lambda)$.

Remark 1. If $\lambda\neq-\frac{\Lambda_n}{2}$ and $\operatorname{Im}\lambda<0$, then $f_1^+(x,\lambda)\in L_2(-\infty,0)$

Remark 2. If $\lambda\neq-\frac{\Lambda_n}{2\beta}$ and $\operatorname{Im}\lambda>0$, then $f_2^+(x,\lambda)\in L_2(0,\infty)$

Taking into account that the potential $q(x)$ can be extended to the upper semi – plane as an analytic function, we find

$$W\left[f_1^+(x,\lambda),\,f_1^-(x,\lambda)\right]=-2i\lambda \text{ for } \lambda\neq0,\pm\frac{\Lambda_n}{2} \tag{13}$$

$$W\left[f_2^+(x,\lambda),\,f_2^-(x,\lambda)\right]=-2i\beta\lambda \text{ for } \lambda\neq0,\pm\frac{\Lambda_n}{2\beta} \tag{14}$$

Therefore, the functions $f_1^+(x,\lambda),\,f_1^-(x,\lambda)\left(f_2^+(x,\lambda),\,f_2^-(x,\lambda)\right)$ are linearly independent solutions of the equation (1) for $\lambda\neq0,\pm\frac{\Lambda_n}{2},\pm\frac{\Lambda_n}{2\beta}$.

Using linearly independent solutions of (1) in the intervals $(-\infty,0)$ and $(0,\infty)$, we can express the general solution of (1) by

$$\begin{cases} y_-(x,\lambda)=A_-f_1^+(x,\lambda)+B_-f_1^-(x,\lambda), & x<0\\ y_+(x,\lambda)=A_+f_2^+(x,\lambda)+B_+f_2^-(x,\lambda), & x>0\end{cases} \tag{15}$$

where $A_{\pm}$ and $B_{\pm}$ are constant coefficients depending on λ.

Let's write the impulsive condition (2) and substitute in (15) instead of

$y_-\left(0^-,\lambda\right), y_+\left(0^+,\lambda\right), y_-'\left(0^-,\lambda\right)$ and $y_+'\left(0^+,\lambda\right)$.

We will get the following system of linear equations

$$\begin{cases} A_+ f_2^+(0,\lambda)+B_+ f_2^-(0,\lambda)=\alpha_1\left(A_- f_1^+(0,\lambda)+B_- f_1^-(0,\lambda)\right)+ \\ +\alpha_2\left(A_- f_1^{+\prime}(0,\lambda)+B_- f_1^{-\prime}(0,\lambda)\right) \\ A_+ f_2^{+\prime}(0,\lambda)+B_+ f_2^{-\prime}(0,\lambda)=\alpha_3\left(A_- f_1^+(0,\lambda)+B_- f_1^-(0,\lambda)\right)+ \\ +\alpha_4\left(A_- f_1^{+\prime}(0,\lambda)+B_- f_1^{-\prime}(0,\lambda)\right) \end{cases} \tag{16}$$

By solving (16) and after making some simplifications, we find:

$$A_+=\frac{\left[f_1^+(0,\lambda)\left(\alpha_1 f_2^{-\prime}(0,\lambda)-\alpha_3 f_2^-(0,\lambda)\right)+f_1^{+\prime}(0,\lambda)\left(\alpha_2 f_2^{-\prime}(0,\lambda)-\alpha_4 f_2^-(0,\lambda)\right)\right]A_-+}{f_2^+(0,\lambda)\,f_2^{-\prime}(0,\lambda)-f_2^{+\prime}(0,\lambda)\,f_2^-(0,\lambda)}$$
$$\frac{+\left[f_1^-(0,\lambda)\left(\alpha_1 f_2^{-\prime}(0,\lambda)-\alpha_3 f_2^-(0,\lambda)\right)+f_1^{-\prime}(0,\lambda)\left(\alpha_2 f_2^{-\prime}(0,\lambda)-\alpha_4 f_2^-(0,\lambda)\right)\right]B_-}{f_2^+(0,\lambda)\,f_2^{-\prime}(0,\lambda)-f_2^{+\prime}(0,\lambda)\,f_2^-(0,\lambda)} \tag{17}$$

$$B_+=\frac{\left[f_1^+(0,\lambda)\left(\alpha_1 f_2^{+\prime}(0,\lambda)-\alpha_3 f_2^+(0,\lambda)\right)+f_1^{+\prime}(0,\lambda)\left(\alpha_2 f_2^{+\prime}(0,\lambda)-\alpha_4 f_2^+(0,\lambda)\right)\right]A_-+}{f_2^-(0,\lambda)\,f_2^{+\prime}(0,\lambda)-f_2^{-\prime}(0,\lambda)\,f_2^+(0,\lambda)}$$
$$\frac{+\left[f_1^-(0,\lambda)\left(\alpha_1 f_2^{+\prime}(0,\lambda)-\alpha_3 f_2^+(0,\lambda)\right)+f_1^{-\prime}(0,\lambda)\left(\alpha_2 f_2^{+\prime}(0,\lambda)-\alpha_4 f_2^+(0,\lambda)\right)\right]B_-}{f_2^-(0,\lambda)\,f_2^{+\prime}(0,\lambda)-f_2^{-\prime}(0,\lambda)\,f_2^+(0,\lambda)} \tag{18}$$

If we write (17) – (18) in matrix form, we will get the following:

$$\begin{bmatrix} A_+ \\ B_+ \end{bmatrix}=\frac{1}{-2i\beta\lambda}\begin{bmatrix} f_2^{-\prime}(0,\lambda) & -f_2^-(0,\lambda) \\ -f_2^{+\prime}(0,\lambda) & f_2^+(0,\lambda) \end{bmatrix}\begin{bmatrix} \alpha_1 & \alpha_2 \\ \alpha_3 & \alpha_4 \end{bmatrix}\begin{bmatrix} f_1^+(0,\lambda) & f_1^-(0,\lambda) \\ f_1^{+\prime}(0,\lambda) & f_1^{-\prime}(0,\lambda) \end{bmatrix}\begin{bmatrix} A_- \\ B_- \end{bmatrix}$$

Then from the impulsive condition (3) we have transfer matrix M satisfying

$$\begin{bmatrix} A_+ \\ B_+ \end{bmatrix}=M\begin{bmatrix} A_- \\ B_- \end{bmatrix} \tag{19}$$

where

$$M:=\begin{bmatrix} M_{11} & M_{12} \\ M_{21} & M_{22} \end{bmatrix}=N^{-1}BD \tag{20}$$

with

$$D:=\begin{bmatrix} f_1^+(0,\lambda) & f_1^-(0,\lambda) \\ f_1^{+\prime}(0,\lambda) & f_1^{-\prime}(0,\lambda) \end{bmatrix} \tag{21}$$

and

$$N := \begin{bmatrix} N_{11} & N_{12} \\ N_{21} & N_{22} \end{bmatrix} \tag{22}$$

where

$$N_{11} = \left(1 + \sum_{n=1}^{\infty}\sum_{\alpha=n}^{\infty} \frac{V_{n\alpha}}{\Lambda_n + 2\lambda}\right)$$

$$N_{12} = \left(1 + \sum_{n=1}^{\infty}\sum_{\alpha=n}^{\infty} \frac{V_{n\alpha}}{\Lambda_n - 2\lambda}\right)$$

$$N_{21} = i\lambda\left(1 + \sum_{n=1}^{\infty}\sum_{\alpha=n}^{\infty} \frac{V_{n\alpha}}{\Lambda_n + 2\lambda}\right) + \left(\sum_{n=1}^{\infty}\sum_{\alpha=n}^{\infty} \frac{i\Lambda_\alpha V_{n\alpha}}{\Lambda_n + 2\lambda}\right)$$

$$N_{22} = -i\lambda\left(1 + \sum_{n=1}^{\infty}\sum_{\alpha=n}^{\infty} \frac{V_{n\alpha}}{\Lambda_n - 2\lambda}\right) + \left(\sum_{n=1}^{\infty}\sum_{\alpha=n}^{\infty} \frac{i\Lambda_\alpha V_{n\alpha}}{\Lambda_n - 2\lambda}\right)$$

It can be shown that $\det N = -2i\beta\lambda$, and $\det N^{-1} = \dfrac{1}{-2i\beta\lambda}$. Then we easily obtain the following:

$$M_{22}(\lambda) = \frac{i}{2\beta\lambda}\Big\{-f_2^{+\prime}(0,\lambda)\Big[\alpha_1 f_1^{-}(0,\lambda) + \alpha_2 f_1^{-\prime}(0,\lambda)\Big] +$$

$$+ f_2^{+}(0,\lambda)\Big[\alpha_3 f_1^{-}(0,\lambda) + \alpha_4 f_1^{-\prime}(0,\lambda)\Big]\Big\}, \tag{23}$$

$$M_{12}(\lambda) = \frac{i}{2\beta\lambda}\Big\{f_2^{-\prime}(0,\lambda)\Big[\alpha_1 f_1^{-}(0,\lambda) + \alpha_2 f_1^{-\prime}(0,\lambda)\Big] -$$

$$- f_2^{-}(0,\lambda)\Big[\alpha_3 f_1^{-}(0,\lambda) + \alpha_4 f_1^{-\prime}(0,\lambda)\Big]\Big\} \tag{24}$$

$$M_{21}(\lambda) = \frac{i}{2\beta\lambda}\Big\{-f_2^{+\prime}(0,\lambda)\Big[\alpha_1 f_1^{+}(0,\lambda) + \alpha_2 f_1^{+\prime}(0,\lambda)\Big] +$$

$$+ f_2^{+}(0,\lambda)\Big[\alpha_3 f_1^{+}(0,\lambda) + \alpha_4 f_1^{+\prime}(0,\lambda)\Big]\Big\} \tag{25}$$

$$M_{11}(\lambda) = \frac{i}{2\beta\lambda}\Big\{f_2^{-\prime}(0,\lambda)\Big[\alpha_1 f_1^{+}(0,\lambda) + \alpha_2 f_1^{+\prime}(0,\lambda)\Big] -$$

$$- f_2^{-}(0,\lambda)\Big[\alpha_3 f_1^{+}(0,\lambda) + \alpha_4 f_1^{+\prime}(0,\lambda)\Big]\Big\} \tag{26}$$

3. Construction of Green's function

Let us consider the non – homogeneous differential equation

$$-y''+q(x)y=\lambda^2\rho(x)y-f(x),\ \ x\in(-\infty,0)\cup(0,\infty) \tag{27}$$

together with the conditions (2) – (6).

We can represent the general solution of homogeneous differential equation corresponding to equation (27) in the form

$$U(x,\lambda)=\begin{cases} C_1 f_1^+(x,\lambda)+D_1 f_1^-(x,\lambda) & \textit{for}\ \ -\infty<x<0 \\ C_2 f_1^+(x,\lambda)+D_2 f_1^-(x,\lambda) & \textit{for}\ \ 0<x<\infty \end{cases}$$

where C_1, D_1, C_2 and D_2 are arbitrary constants.

By applying the standard method of variation of the parameters we will search the general solution of the non – homogeneous linear differential equation (27) in the form

$$U(x,\lambda)=\begin{cases} C_1(x,\lambda) f_1^+(x,\lambda)+D_1(x,\lambda) f_1^-(x,\lambda) & \textit{for}\ \ -\infty<x<0 \\ C_2(x,\lambda) f_1^+(x,\lambda)+D_2(x,\lambda) f_1^-(x,\lambda) & \textit{for}\ \ 0<x<\infty \end{cases} \tag{28}$$

where the functions $C_1(x,\lambda),\ D_1(x,\lambda)$ and $C_2(x,\lambda),\ D_2(x,\lambda)$ satisfies the linear system of equation

$$\begin{cases} C_1'(x,\lambda) f_1^+(x,\lambda)+D_1'(x,\lambda) f_1^-(x,\lambda)=0 \\ C_1'(x,\lambda) f_1^{+\prime}(x,\lambda)+D_1'(x,\lambda) f_1^{-\prime}(x,\lambda)=f(x) \end{cases} \tag{29}$$

for $x\in(-\infty,0)$ and

$$\begin{cases} C_2'(x,\lambda) f_2^+(x,\lambda)+D_2'(x,\lambda) f_2^-(x,\lambda)=0 \\ C_2'(x,\lambda) f_2^{+\prime}(x,\lambda)+D_2'(x,\lambda) f_2^{-\prime}(x,\lambda)=f(x) \end{cases} \tag{30}$$

for $x\in(0,\infty)$ respectively. Since

$$w_1(\lambda)=\left(f_1^+(x,\lambda),\ f_1^-(x,\lambda)\right)=-2i\lambda \quad \text{and} \quad w_2(\lambda)=\left(f_2^+(x,\lambda),\ f_2^-(x,\lambda)\right)=-2i\beta\lambda$$

each of the linear system of equations (29) and (30) has a unique solution. These solutions can be expressed as

$$C_1'(x,\lambda)=-\frac{1}{w_1(\lambda)} f_1^-(x,\lambda) f(x) \tag{31}$$

$$D_1'(x,\lambda)=\frac{1}{w_1(\lambda)} f_1^+(x,\lambda) f(x) \tag{32}$$

for $x\in(-\infty,0)$ and

$$C_2'(x,\lambda)=-\frac{1}{w_2(\lambda)} f_2^-(x,\lambda) f(x) \tag{33}$$

$$D_2'(x,\lambda) = \frac{1}{w_2(\lambda)} f_2^+(x,\lambda)\, f(x) \tag{34}$$

for $x \in (0,\infty)$, respectively. From equations (31) – (34), the following relations are obtained:

$$C_1(x,\lambda) = -\frac{1}{w_1(\lambda)} \int_{-\infty}^{x} f_1^-(t,\lambda) f(t)\,dt + C_1 \qquad x \in (-\infty,0)$$

$$D_1(x,\lambda) = -\frac{1}{w_1(\lambda)} \int_{x}^{0} f_1^+(t,\lambda) f(t)\,dt + D_1 \qquad x \in (-\infty,0)$$

$$C_2(x,\lambda) = -\frac{1}{w_2(\lambda)} \int_{0}^{x} f_2^-(t,\lambda) f(t)\,dt + C_2 \qquad x \in (0,\infty)$$

$$D_2(x,\lambda) = -\frac{1}{w_2(\lambda)} \int_{\infty}^{x} f_2^+(t,\lambda) f(t)\,dt + D_2 \qquad x \in (0,\infty)$$

where C_1, D_1, C_2 and D_2 are arbitrary constants. Substituting the above equations in (28), the general solution of non – homogeneous linear differential equation (27) are obtained as

$$U_-(x,\lambda) = -\frac{f_1^+(x,\lambda)}{w_1(\lambda)} \int_{-\infty}^{x} f_1^-(t,\lambda) f(t)\,dt + C_1 f_1^+(x,\lambda) - \frac{f_1^-(x,\lambda)}{w_1(\lambda)} \int_{x}^{0} f_1^+(t,\lambda) f(t)\,dt +$$
$$+ D_1 f_1^-(x,\lambda)$$

for $-\infty < x < 0$ (35)

$$U_+(x,\lambda) = -\frac{f_2^+(x,\lambda)}{w_2(\lambda)} \int_{0}^{x} f_2^-(t,\lambda) f(t)\,dt + C_2 f_2^+(x,\lambda) - \frac{f_2^-(x,\lambda)}{w_2(\lambda)} \int_{x}^{\infty} f_2^+(t,\lambda) f(t)\,dt +$$
$$+ D_2 f_2^-(x,\lambda)$$

for $0 < x < \infty$. (36)

Since $U_-(x,\lambda) \in L_2(-\infty,0)$ and $U_+(x,\lambda) \in L_2(0,\infty)$, $C_1 = 0$ and $D_2 = 0$.

Now by using the impulsive condition (2), let's find C_2 and D_1:

$$-\frac{f_2^-(0,\lambda)}{w_2(\lambda)} \int_{0}^{\infty} f_2^+(t,\lambda) f(t)\,dt + C_2 f_2^+(0,\lambda) = \alpha_1 \left[-\frac{f_1^+(0,\lambda)}{w_1(\lambda)} \int_{-\infty}^{0} f_1^-(t,\lambda)\, f(t)\,dt + D_1 f_1^-(0,\lambda) \right] +$$
$$+ \alpha_2 \left[-\frac{f_1^{+\prime}(0,\lambda)}{w_1(\lambda)} \int_{-\infty}^{0} f_1^-(t,\lambda)\, f(t)\,dt + D_1 f_1^{-\prime}(0,\lambda) \right]$$

$$-\frac{f_2^{-\prime}(0,\lambda)}{w_2(\lambda)} \int_{0}^{\infty} f_2^+(t,\lambda) f(t)\,dt + C_2 f_2^{+\prime}(0,\lambda) = \alpha_3 \left[-\frac{f_1^+(0,\lambda)}{w_1(\lambda)} \int_{-\infty}^{0} f_1^-(t,\lambda)\, f(t)\,dt + D_1 f_1^-(0,\lambda) \right] +$$
$$+ \alpha_4 \left[-\frac{f_1^{+\prime}(0,\lambda)}{w_1(\lambda)} \int_{-\infty}^{0} f_1^-(t,\lambda)\, f(t)\,dt + D_1 f_1^{-\prime}(0,\lambda) \right]$$

By solving the system of equations above, we obtain the following result:

$$D_1=\frac{M_{21}(\lambda)\int\limits_{-\infty}^{0} f_1^-(t,\lambda)\,f(t)\,dt-\frac{i}{2\beta\lambda}\int\limits_{0}^{\infty} f_2^+(t,\lambda)\,f(t)\,dt}{M_{22}(\lambda)}$$

$$C_2=\frac{-M_{12}(\lambda)\int\limits_{0}^{\infty} f_2^+(t,\lambda)\,f(t)\,dt-\frac{i}{2\beta\lambda}\int\limits_{-\infty}^{0} f_1^-(t,\lambda)\,f(t)\,dt}{M_{22}(\lambda)}$$

Finally, by substituting the coefficients C_i and D_i ($i=1,2$) in (35) and (36), the following formula is obtained for the resolvent $U(x,\lambda)$:

Furthermore, by using the representations

$$f^+(x,\lambda)=\begin{cases} f_1^+(x,\lambda) & for\ x\in(-\infty,0)\\ f_2^+(x,\lambda) & for\ x\in(0,\infty)\end{cases}$$

$$f^-(x,\lambda)=\begin{cases} f_1^-(x,\lambda) & for\ x\in(-\infty,0)\\ f_2^-(x,\lambda) & for\ x\in(0,\infty)\end{cases}$$

this formula can be rewritten in the form

$$U(x,\lambda)=-\frac{i\,f^+(x,\lambda)}{2\beta\lambda M_{22}(\lambda)}\int\limits_{-\infty}^{x} f^-(t,\lambda)f(t)\,dt-\frac{i\,f^-(x,\lambda)}{2\beta\lambda M_{22}(\lambda)}\int\limits_{x}^{\infty} f^+(t,\lambda)f(t)\,dt+$$

$$+\begin{cases}\dfrac{M_{21}(\lambda)}{M_{22}(\lambda)}f_1^-(x,\lambda)\int\limits_{-\infty}^{0} f_1^-(t,\lambda)\,f(t)\,dt & x\in(-\infty,0)\\ -\dfrac{M_{12}(\lambda)}{M_{22}(\lambda)}f_2^+(x,\lambda)\int\limits_{0}^{\infty} f_2^+(t,\lambda)\,f(t)\,dt & x\in(0,\infty)\end{cases} \tag{37}$$

$$U(x,\lambda)=\begin{cases}-\dfrac{f_1^+(x,\lambda)}{w_1(\lambda)}\int\limits_{-\infty}^{x} f_1^-(t,\lambda)f(t)\,dt-\dfrac{f_1^-(x,\lambda)}{w_1(\lambda)}\int\limits_{x}^{0} f_1^+(t,\lambda)f(t)\,dt+ & \\ +\dfrac{M_{21}(\lambda)}{M_{22}(\lambda)}f_1^-(x,\lambda)\int\limits_{-\infty}^{0} f_1^-(t,\lambda)\,f(t)\,dt-\dfrac{f_1^-(x,\lambda)}{M_{22}(\lambda)}\dfrac{i}{2\beta\lambda}\int\limits_{0}^{\infty} f_2^+(t,\lambda)f(t)\,dt & x\in(-\infty,0)\\ -\dfrac{f_2^+(x,\lambda)}{w_2(\lambda)}\int\limits_{0}^{x} f_2^-(t,\lambda)\,f(t)\,dt-\dfrac{f_2^-(x,\lambda)}{w_2(\lambda)}\int\limits_{x}^{\infty} f_2^+(t,\lambda)\,f(t)\,dt & \\ -\dfrac{M_{12}(\lambda)}{M_{22}(\lambda)}f_2^+(x,\lambda)\int\limits_{0}^{\infty} f_2^+(t,\lambda)\,f(t)\,dt-\dfrac{f_2^+(x,\lambda)}{M_{22}(\lambda)}\dfrac{i}{2\beta\lambda}\int\limits_{-\infty}^{0} f_1^-(t,\lambda)\,f(t)\,dt & x\in(0,\infty)\end{cases}$$

Thus, the resolvent of the boundary-value impulsive problem is obtained. We can find Green's function from the resolvent (37) easily. Namely, denoting

$$G(x,t,\lambda)=\begin{cases}-\dfrac{i}{2\beta\lambda M_{22}(\lambda)}f^+(x,\lambda)\,f^-(t,\lambda) & t<x,\quad x\neq 0,t\neq 0\\ -\dfrac{i}{2\beta\lambda M_{22}(\lambda)}f^-(x,\lambda)\,f^+(t,\lambda) & x<t,\quad x\neq 0,t\neq 0\end{cases}$$

We can rewrite the resolvent (37) in the next form:

$$U(x,\lambda)=\int_{-\infty}^{\infty} G(x,t,\lambda)f(t)\,dt+\begin{cases}\dfrac{M_{21}(\lambda)}{M_{22}(\lambda)} f_1^{-}(x,\lambda)\displaystyle\int_{-\infty}^{0} f_1^{-}(t,\lambda)\,f(t)\,dt & x\in(-\infty,0)\\ -\dfrac{M_{12}(\lambda)}{M_{22}(\lambda)} f_2^{+}(x,\lambda)\displaystyle\int_{0}^{\infty} f_2^{+}(t,\lambda)\,f(t)\,dt & x\in(0,\infty)\end{cases}$$

REFERENCE LIST:

1. Bainov, D.D., Simeonov, P.S. (1995). Impulsive Differential Equations: Asymptotic Properties of the Solutions. *Series on Advances in Mathematics for Applied Sciences*, (28) World Scientific, Singapore
2. Mostafazadeh, A. (2009). Spectral singularities of complex scattering potentials and infinite reflection and transmission coefficients at real energies. *Phys. Rev. Lett.* (102), 220402
3. Mostafazadeh, A. (2011). Optical spectral singularities as threshold resonances. *Phys. Rev. A* (83), 045801
4. Mostafazadeh, A. (2011). Spectral singularities of a general point interaction. J.Phys.*A,Math.Theor.*(44),375302(9 pp)
5. Bahlulzade, S.J. (2020). Construction of resolvent for Sturm-Liouville equation with almost periodic potentials and discontinuous right side Proceedings of the 7th international conference on control and optimization with industrial applications, 2, 116-118.
6. Bahlulzadeh, S.J. (2017). Spectral analysis of Sturm - Liouville equation with almost periodic potentials and discontinuous right hand Proceedings of the 6th international conference on control and optimization with industrial applications, 2, 95-97

2024. Volume 8, Number 1 Pages 64-72

UOT:002.6 (002.6:025.5/.6)

DOİ: https://doi.org/10.30546/09090.2024.110.212

PNEUMONIA DETECTION THROUGH CNN AND RESNET-50

FILZA JAVED

Baku Engineering University

filzaofficial4@gmail.com

ARTICLE INFO

Article history:
Received:2024-05-13
Received in revised form:2024-05-15
Accepted:2025-01-08
Available online

Keywords: Pneumonia, Convolutional Neural Network (CNN), ResNet-50, chest X-rays, deep learning.
JEL codes:
L86, O33, M15

ABSTRACT

Pneumonia is a prevalent illness that has a global impact, primarily affecting children and older individuals. Timely identification is essential for immediate intervention, particularly in regions with restricted healthcare availability. The purpose of this paper is to compare how well two methods work for finding pneumonia on chest X-rays creating a custom Convolutional Neural Network (CNN) and using a model that has been pre-trained, such as ResNet-50. The results indicated that although the customized CNN had difficulties achieving satisfactory performance, the ResNet-50 model demonstrated encouraging outcomes following the process of fine-tuning. This paper seeks to improve the detection of pneumonia, especially in disadvantaged places with limited medical resources, by utilizing modern technologies such as deep learning and pre-trained models. Considering the results gained to enhance patient outcomes and decrease mortality rates associated with pneumonia by enabling more precise and prompt detection, this has a beneficial effect on global public health

ОБНАРУЖЕНИЕ ПНЕВМОНИИ С ПОМОЩЬЮ CNN И RESNET-50

РЕЗЮМЕ

Пневмония — широко распространенное заболевание, имеющее глобальные последствия и поражающее в первую очередь детей и пожилых людей. Своевременное выявление имеет важное значение для немедленного вмешательства, особенно в регионах с ограниченной доступностью медицинской помощи. Цель этой статьи — сравнить, насколько хорошо работают два метода обнаружения пневмонии на рентгенограммах грудной клетки, создавая специальную сверточную нейронную сеть (CNN) и используя предварительно обученную модель, такую как ResNet-50. Результаты показали, что, хотя у настроенной CNN возникли трудности с достижением удовлетворительной производительности, модель ResNet-50 продемонстрировала обнадеживающие результаты после процесса тонкой настройки. Эта статья направлена на улучшение выявления пневмонии, особенно в неблагополучных местах с ограниченными медицинскими ресурсами, за счет использования современных технологий, таких как глубокое обучение и предварительно обученные модели. Учитывая полученные результаты по улучшению результатов лечения пациентов и снижению уровня смертности, связанной с пневмонией, за счет обеспечения более точного и быстрого выявления, это оказывает благотворное влияние на глобальное общественное здравоохранение.

Ключевые слова: Пневмония, сверточная нейронная сеть (CNN), ResNet-50, рентгенография грудной клетки, глубокое обучение.

1 Introductions

The advent of artificial intelligence has resulted in the utilization of a novel artificial intelligence model capable of rapidly evaluating the gravity of pneumonia. The automated deep learning system, as outlined in the Journal of Medical Imaging, facilitates the assessment of disease development and the monitoring of therapy responses using computed tomography, with a high degree of accuracy. And as rapid as precise hand measures conducted by medical professionals.[1] Manually outlining 3D lung lesions on hundreds of CT lung slices, each up to 1 millimeter thick, is an exceedingly challenging task for doctors. However, artificial intelligence can greatly expedite this procedure and accurately determine the volumetric size of the defect by calculating the proportion of lungs involved. Segmentation is crucial in medical imaging for analyzing X-ray pictures, as it allows for the extraction of important information through the process of image segmentation. Doctors employ a range of non-surgical methods, such as X-rays, CT scans, ultrasound, and other imaging techniques, to visualize and analyze the inside organs and structures of the human body. Using deep learning techniques like CNN has shown to have a big impact on finding this illness by allowing for accurate convergence [2]. The main objective of our research is to evaluate the performance superiority of the custom CNN in comparison to established models like RESNET-50 and Efficient-Net. Additionally, the goal is to train and evaluate several CNNs and track their effectiveness in detecting pneumonia. We can utilize advanced image processing algorithms developed in recent decades, construct our own CNN model, and then evaluate the outcomes using the identical dataset. We utilize the dataset. We conducted extensive research on several websites and reached out to other institutes to acquire a dataset suitable for our research. After extensive research, we successfully located the dataset from the renowned website "Kaggle." The dataset comprises a total of 5683 pictures.

2 Related work

2.1. Convolutional Neural Network

Deep learning is an artificial intelligence technique that enables computers to interpret data using algorithms that mimic the functioning of the human brain. Deep learning models utilize advanced algorithms to identify intricate patterns in many forms of data, such as photos, text, audio, and more, to generate precise insights and predictions [3]. Deep learning

techniques can be employed to automate tasks that traditionally necessitate human intellect, such as providing descriptions for photographs or converting an audio recording into written language. Deep learning algorithms are artificial neural networks that are designed to mimic the structure and functioning of the human brain. As an illustration, the human brain comprises several interconnected neurons that collaborate to acquire knowledge and handle data. Similarly, deep learning neural networks, also known as artificial neural networks, comprise multiple layers of artificial neurons collaborating within a computer [4]. Artificial neurons, known as nodes, are software units that employ mathematical computations to analyze inputs. Artificial neural networks are sophisticated deep learning algorithms that employ nodes to address intricate challenges.

2.2. Lung segmentation with deep learning

Deep learning has proven effective in medical picture segmentation, specifically lung segmentation. Lung segmentation is essential in multiple medical applications, including illness diagnosis, therapy planning, and monitoring.[1] Convolutional neural networks (CNNs), specifically deep learning models, have demonstrated impressive outcomes in precisely segmenting lung areas from chest X-ray and MRI images. These models utilize the capacity of CNNs to autonomously acquire and extract pertinent characteristics from the input images, allowing them to accurately capture the intricate anatomical structures and variances in lung imaging. [5] People widely use the U-Net architecture for lung segmentation. It incorporates skip connections and deep supervision to combine low-level and high-level information, allowing for multi-scale prediction and enhanced segmentation accuracy.[6] Another strategy entails employing residual blocks, which mitigate the issue of "vanishing gradient" and facilitate enhanced information dissemination in deep networks.[7] The deep learning models have undergone training and evaluation using benchmark datasets, which has shown their capacity to accurately separate lung areas with robustness and dependability. In summary, the application of deep learning in lung segmentation has significant potential to enhance the analysis of medical images and improve the quality of patient care [8].

2.3. Application of deep learning techniques for the classification of pneumonia

Deep learning has become a potent method for classifying pneumonia, especially when analyzing chest X-ray pictures. Pneumonia is a prevalent respiratory illness caused by different types of pathogens, such as bacteria, viruses, and fungi. Convolutional neural networks (CNNs), a type of deep learning model, have demonstrated significant promise in properly detecting and categorizing pneumonia cases using these images [5].

An effective method for classifying pneumonia using deep learning is to build convolutional neural network (CNN) models on extensive collections of chest X-ray images. These models are trained to identify important characteristics in images and categorize them into distinct groups, including normal, bacterial pneumonia, viral pneumonia, or COVID-19 pneumonia. Using deep learning, these models can identify intricate patterns and

irregularities in X-ray pictures that may not be readily detectable by human experts. [9] Transfer learning is a frequently employed technique in deep learning-based pneumonia categorization. Transfer learning involves using pre-trained convolutional neural network (CNN) models, such as AlexNet or CheXNet, as a starting point. These models have undergone training using extensive picture datasets, allowing them to acquire broad knowledge that may be utilized for various purposes, including the classification of pneumonia. Researchers can achieve excellent accuracy and efficiency in pneumonia classification tasks by refining these pre-trained models using pneumonia-specific datasets [1]. Utilizing deep learning for pneumonia categorization offers numerous benefits. Firstly, technology can aid in automating the diagnosis process, thus lessening the workload on medical practitioners, and perhaps enhancing the promptness and precision of diagnosis [2]. Furthermore, deep learning models can rapidly analyze extensive quantities of data, enabling the effective examination of chest X-ray pictures and the detection of possible pneumonia cases. Furthermore, deep learning models possess the capacity to acquire knowledge from a wide range of datasets, allowing them to exhibit strong generalization abilities and efficiently handle novel and unfamiliar scenarios. Ultimately, deep learning methods, including convolutional neural networks (CNNs) and transfer learning, have demonstrated encouraging outcomes in the categorization of pneumonia based on chest X-ray pictures.[10] These models possess the capacity to precisely detect and categorize instances of pneumonia, including distinguishing between bacterial, viral, and COVID-19 pneumonia. Utilizing deep learning in the classification of pneumonia can boost diagnostic precision, optimize productivity, and aid healthcare practitioners in delivering prompt and efficient treatment [11].

3 Research Methodology

Deep convolutional neural networks have demonstrated superior accuracy in handling massive datasets, making them widely adopted by academics as the default choice. This was achieved through the utilization of transfer learning, a technique that involves using pre-trained models learned on extensive datasets such as Efficient Net. It is a linear guide that outlines the steps to follow to make a comparison, starting from the first point. The dataset contains photos that are formatted as RGBA, which stands for Red, Green, Blue, and Alpha. The dataset initially consisted of three directories (train, validation, and test). [1] We developed our script to process the entire dataset instead of directly using code from Kaggle. We saved the processed dataset in a variable. After completing this step successfully, we divided the data into separate training and testing sets. During the model training process, we further divided the training data into a training set and a validation set. The CNNs were trained using Keras and TensorFlow, which are open-source Python frameworks, to distinguish characteristics for classifying pneumonia from chest X-ray pictures [5].

3.1. Dataset description

An alternative database that is more dependable than GitHub is the highly renowned chest X-ray database on "Kaggle." This collection comprises 5856 photos depicting normal, bacterial, and viral pneumonia cases. However, this investigation solely utilized chest X-ray pictures depicting normal and viral pneumonia, as illustrated in Fig 1. The dataset was divided into training, testing, and validation sets, with each set having annotated photos of both normal and pneumonia cases. A total of 3875 pictures were utilized for testing pneumonia cases. There are 234 cases of normal pneumonia and 390 cases of pneumonia for training. For validation, there are 1341 cases of normal pneumonia and 3875 cases of pneumonia. Additionally, there are 8 cases of normal pneumonia and 8 cases of pneumonia.

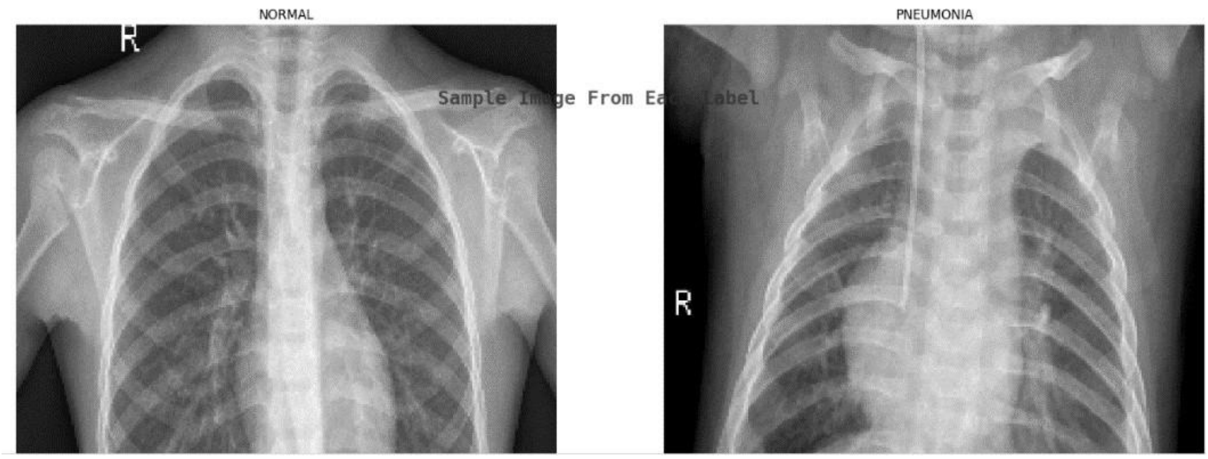

Fig. 1. Normal, and pneumonia

3.2. System requirements tools

Hardware for the studies included an 8th generation Core i7 laptop PC with 16GB of RAM, an NVIDIA GeForce 1060Ti GPU with 6GB of memory, and a 256GB SSD running the standard Windows operating system. When working on a deep learning project, the choice of operating system is generally not crucial, as we mostly rely on the Python environment. Miniconda and Anaconda are robust tools for managing the Python environment. Conda offers a versatile and user-friendly platform for the Python environment and essential libraries. Both Anaconda and Miniconda can be utilized, depending on the user's choices and requirements. Python is the primary programming language for our project. I specifically utilized version 3.10 for the development process. Methodology: We experimented with various approaches to determine the optimal answer. We encountered a significant amount of failure while striving for success, whether it was with our own customized CNN or the efficient network model. We will discuss several training experiments that have been conducted and present graphs illustrating the models' training progress.

3.3. ResNet-50

ResNet-50 is a popular convolutional neural network (CNN) structure comprising of 50 layers, which include 48 convolutional layers, one MaxPool layer, and one average pool

layer. The publication "Deep Residual Learning for Image Recognition" introduced it.[1], [12], [13] ResNet, also known as Residual Network, is an artificial neural network that employs residual blocks to construct deep networks. ResNet-50 utilizes skip connections, which are alternatively referred to as shortcut connections or identity mappings. These connections facilitate the network in circumventing specific layers, hence facilitating the smoother flow of the gradient during training. This aids in mitigating the issue of the vanishing gradient and enables the training of highly complex networks. ResNet-50 consists of residual blocks, which are fundamental units that comprise several convolutional layers. The residual blocks facilitate the network in acquiring residual mappings, which capture the disparity between the input and output of each block. This methodology enables the training of more complex networks with enhanced precision. ResNet-50 is commonly employed as a pretrained model, indicating that it has undergone training on a substantial dataset like ImageNet. It can be further adjusted or utilized as a feature extractor for diverse computer vision assignments. Pretrained models such as ResNet-50 offer a foundation for transfer learning, enabling researchers and practitioners to utilize the acquired features and customize them for specific tasks using smaller datasets. [12]ResNet-50 is a very influential and extensively utilized convolutional neural network (CNN) architecture that has made substantial contributions to the field of computer vision. The popularity of this method stems from its capacity to train deep networks and utilize skip connections, which are advantageous for various image-related applications.in Fig 2. Describe ResNet-50 A architecture.

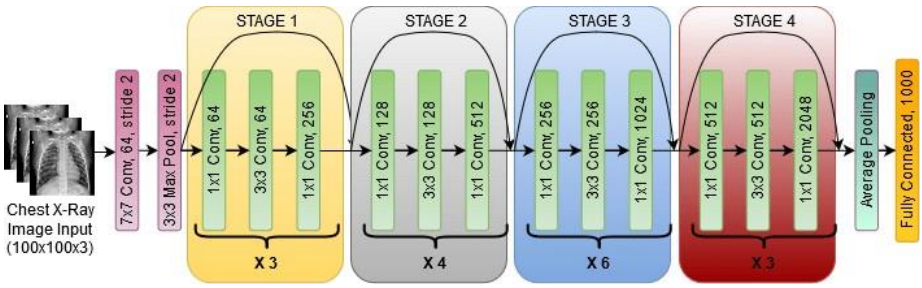

Fig.2. Describe ResNet-50 A architecture.

4 Experiential Results

Two distinct methodologies yielded the findings. We performed tests utilizing CNN and ResNet-50, pre-trained models, to differentiate between pneumonia images and normal chest X-ray images captured in high resolution from the anterior to posterior (AP/PA) direction. We chose ResNet-50 to address the constraints imposed by our limited resources. We used a conventional methodology to downsize the image into smaller dimensions, and then input them into the CNN for classification. The validation accuracy of our model surpassed that of other conventional approaches due to the efficacy of utilizing pre-trained models.

At the outset, while training the customized Convolutional Neural Network (CNN) model on the novel dataset, we encountered a difficulty: the validation score appeared unpromising. Despite conducting extensive experimentation with various dropout layers and

approaches, we were unable to achieve any significant improvements. As depicted in the training and validation loss graph above, the validation loss experienced a sudden increase, reaching a value of 0.70, while the validation accuracy remained at 50%. In Fig.3. training and validation loss in CNN and Fig.4.traning in validation accuracy in CNN.

Additionally, there was no notable enhancement in validation accuracy. We opted for an alternative strategy and implemented modifications to our code base. Instead of applying a freezer to the model's layers, we enabled them to be trainable during the training process. The modification had encouraging outcomes. By adjusting the dropout rate, specifically to achieve a training accuracy of 0.95% while maintaining a validation accuracy of 0.75%, we saw additional improvements in the model's performance.in Fig 5. Resnet50, and Fig.6. training and validation ResNet-50 accuracy.

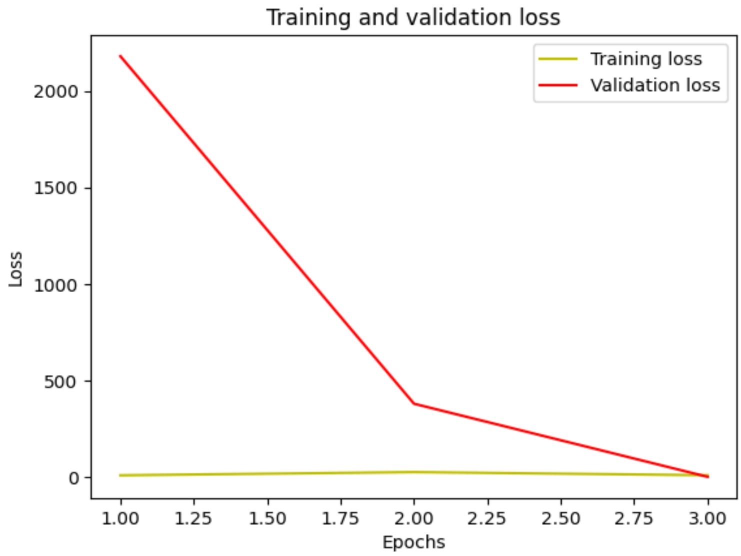

Fig.3. training and validation loss in CNN

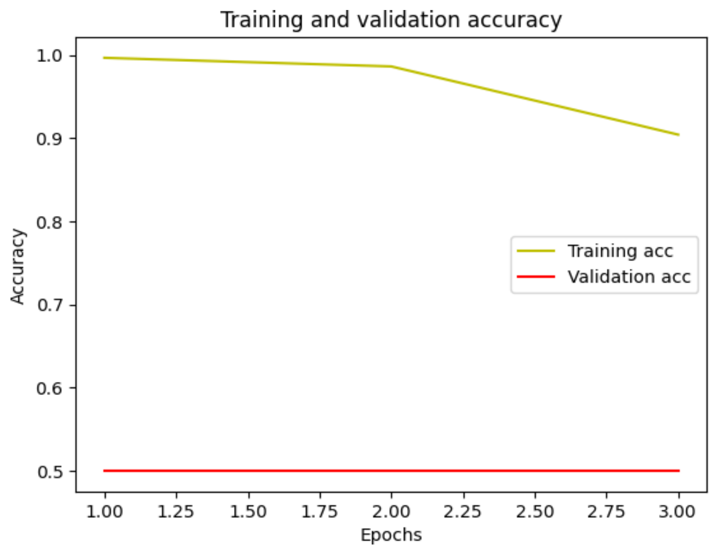

Fig.4. Traning in validation accuracy in CNN

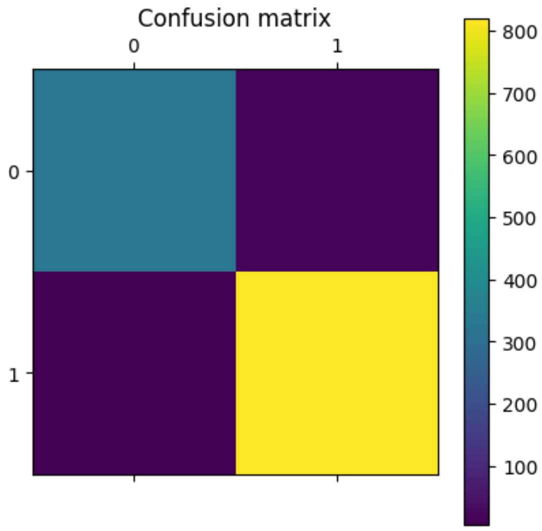

Fig 5. ResNet-50

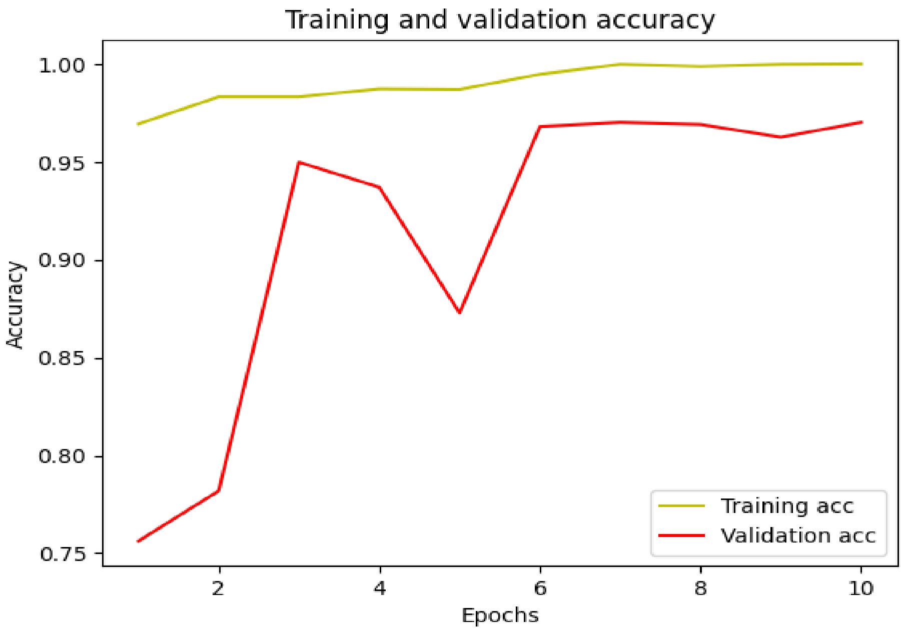

Fig.6. Training and validation ResNet-50 accuracy Experiment 1: Convolutional Neural Network (CNN):

The preliminary experiment demonstrated that the model encountered difficulties in comprehending the intricacy of the data, resulting in its ineffectiveness in acquiring any noticeable patterns. As a result, the model demonstrated inadequate performance on data that it had not before encountered or on data used for validation. Despite these disheartening outcomes, it prompts the inquiry of whether investing effort in building a CNN from the beginning is valuable. This experiment also yielded vital insights into the underlying process of Convolutional Neural Network (CNN) development. The statement emphasizes the significance of utilizing advanced models already designed for similar issue areas instead of starting from scratch.

Experiment 2: Utilizing the ResNet-50 model

We chose to omit the freezing step. In addition to this modification, we made some modifications to our code base. The model demonstrated substantial enhancements, namely following the adjustment of the dropout rate, resulting in the identification of an optimal-performing ResNet50 model. This experiment highlighted the importance of updating the weights of all layers, emphasizing that none should be kept unchanged. The dropout rate of 0.3, which is considered optimal, indicates that just a small number of layers need to be removed. This demonstrates the model's capacity to adapt to our specific use case and dataset with minimum modifications

5 Conclusion

Ultimately, the utilization of CNN and ResNet-50 in pneumonia identification has demonstrated encouraging outcomes in precisely discerning and categorizing instances of pneumonia from chest X-ray images. The improved ResNet-50 model had the best level of accuracy, reaching 95%, when compared to alternative techniques. Deep learning models, such as ResNet-50, can autonomously acquire and identify important characteristics from images. This allows them to accurately detect and analyze the intricate patterns and irregularities linked to pneumonia. These models have the capacity to enhance the precision and efficiency of diagnosing pneumonia, hence assisting in the early identification and prompt treatment of the condition. Utilizing deep learning techniques in pneumonia identification improves overall diagnostic accuracy and offers a quicker and more efficient method for diagnosing pneumonia cases, bringing fresh optimism for patients. Additional investigation and advancement in this field have the potential to enhance healthcare results and enhance patient care.

REFERENCES

[1] A. Victor Ikechukwu, S. Murali, R. Deepu, and R. C. Shivamurthy, "ResNet-50 vs VGG-19 vs training from scratch: A comparative analysis of the segmentation and classification of Pneumonia from chest X-ray images," *Glob. Transitions Proc.*, vol. 2, no. 2, pp. 375–381, 2021.

[2] T. A. Youssef, B. Aissam, D. Khalid, B. Imane, and J. El Miloud, "Classification of chest pneumonia from x-ray images using new architecture based on ResNet," in *2020 IEEE 2nd international conference on electronics, control, optimization and computer science (ICECOCS)*, 2020, pp. 1–5.

[3] A. Khan, A. Sohail, U. Zahoora, and A. S. Qureshi, "A survey of the recent architectures of deep convolutional neural networks," *Artif. Intell. Rev.*, vol. 53, no. 8, pp. 5455–5516, 2020.

[4] M. A. Alqudah, L. Muradkhanli, Z. Muradkhanli, and A. A. Salameh, "Using Artificial Intelligence Applications For E-Government Services As Iris Recognition," in *2023 IEEE 17th International Conference on Application of Information and Communication Technologies (AICT)*, 2023, pp. 1–7. doi: 10.1109/AICT59525.2023.10313183.

[5] A. V. Ikechukwu, S. Murali, R. Deepu, and R. C. Shivamurthy, "ResNet-50 vs VGG-19 vs training from scratch: A comparative analysis of the segmentation and classification of Pneumonia from chest X-ray images," *Glob. Transitions Proc.*, vol. 2, no. 2, pp. 375–381, 2021.

[6] M. Aledhari, S. Joji, M. Hefeida, and F. Saeed, "Optimized CNN-based diagnosis system to detect the pneumonia from chest radiographs," in *2019 IEEE International Conference on Bioinformatics and Biomedicine (BIBM)*, 2019, pp. 2405–2412.

[7] B. A. Skourt, A. El Hassani, and A. Majda, "Lung CT image segmentation using deep neural networks," *Procedia Comput. Sci.*, vol. 127, pp. 109–113, 2018.

[8] S. Gite, A. Mishra, and K. Kotecha, "Enhanced lung image segmentation using deep learning," *Neural Comput. Appl.*, vol. 35, no. 31, pp. 22839–22853, 2023.

[9] K. El Asnaoui, Y. Chawki, and A. Idri, "Automated methods for detection and classification pneumonia based on x-ray images using deep learning," in *Artificial intelligence and blockchain for future cybersecurity applications*, Springer, 2021, pp. 257–284.

[10] Y. Muhammad, M. D. Alshehri, W. M. Alenazy, T. Vinh Hoang, and R. Alturki, "Identification of pneumonia disease applying an intelligent computational framework based on deep learning and machine learning techniques," *Mob. Inf. Syst.*, vol. 2021, pp. 1–20, 2021.

[11] S. A. Rachman, D. C. Bagaskara, R. Magdalena, and S. Sa'idah, "Classification of Pneumonia Based on X-Ray Images with ResNet-50 Architecture," in *Proceeding of the 3rd International Conference on Electronics, Biomedical Engineering, and Health Informatics: ICEBEHI 2022, 5–6 October, Surabaya, Indonesia*, 2023, pp. 117–130.

[12] P. G. Sathvik, M. R. Kumar, G. H. Neeli, I. Y. Narasimha, T. Singh, and P. Duraisamy, "RESNET-50, CNN and HNN Medical Image Registration Techniques For Covid-19, Pneumonia and Other Chest Ailments Detection," in *2022 13th International*

[13] *Conference on Computing Communication and Networking Technologies (ICCCNT)*, 2022, pp. 1–7.

[14] A. M. Rifa'i, E. Utami, and D. Ariatmanto, "Analysis for diagnosis of pneumonia symptoms using chest X-Ray based on Resnet-50 models with different epoch," in *2022 6th International Conference on Information Technology, Information Systems and Electrical Engineering (ICITISEE)*, 2022, pp. 471–476.

INSTRUCTIONS FOR AUTHORS

1. "The Baku Engineering University Mathematics and Computer Science" accepts original unpublished articles and reviews in the research field of the author.
2. Articles are accepted in English.
3. File format should be compatible with **Microsoft Word** and must be sent to the electronic mail (**journal@beu.edu.az**) of the Journal. The submitted article should follow the following format:

- Article title, author's name and surname
- The name of workplace
- Mail address
- Abstract and key words

4. The title of the article should be in each of the three languages of the abstract and should be centred on the page and in bold capitals before each summary.
5. **The abstract** should be written in **9 point** type size, between **100** and **150** words. The abstract should be written in the language of the text and in two more languages given above. The abstracts of the article written in each of the three languages should correspond to one another. The keywords should be written in two more languages besides the language of the article and should be at least three words.
6. .**UDC** and **PACS** index should be used in the article.
7. The article must consist of the followings:

- Introduction
- Research method and research
- Discussion of research method and its results
- In case the reference is in Russian it must be given in the Latin alphabet with the original language shown in brackets.

8. **Figures, pictures, graphics and tables** must be of publishing quality and inside the text. Figures, pictures and graphics should be captioned underneath, tables should be captioned above.
9. **References** should be given in square brackets in the text and listed according to the order inside the text at the end of the article. In order to cite the same reference twice or more, the appropriate pages should be given while keeping the numerical order. For example: [7, p.15].

Information about each of the given references should be full, clear and accurate. The bibliographic description of the reference should be cited according to its type (monograph, textbook, scientific research paper and etc.) While citing to scientific research articles, materials of symposiums, conferences and other popular scientific events, the name of the article, lecture or paper should be given.

Samples:

a) ***Article:*** Demukhamedova S.D., Aliyeva İ.N., Godjayev N.M.. *Spatial and electronic structure af monomerrik and dimeric conapeetes of carnosine üith zinc,* Journal of structural Chemistry, Vol.51, No.5, p.824-832, 2010

b) ***Book:*** Christie ohn Geankoplis. *Transport Processes and Separation Process Principles*. Fourth Edition, Prentice Hall, p.386-398, 2002

c) ***Conference paper:*** Sadychov F.S., Aydın C., Ahmedov A.İ.. Appligation of Information – Commu-nication Technologies in Science and education. II International Conference."*Higher Twist Effects In Photon- Proton Collisions", Bakı, 01-03 Noyabr, 2007, ss 384-391*
References should be in 9-point type size.

10. The margins sizes of the page: - Top 2.8 cm. bottom 2.8 cm. left 2.5 cm, right 2.5 cm. The article main text should be written in Palatino Linotype 11 point type size single-spaced. Paragraph spacing should be 6 point.
11. The maximum number of pages for an article should not exceed 15 pages
12. The decision to publish a given article is made through the following procedures:

- The article is sent to at least to experts.
- The article is sent back to the author to make amendments upon the recommendations of referees.
- After author makes amendments upon the recommendations of referees the article can be sent for the publication by the Editorial Board of the journal.

YAZI VƏ NƏŞR QAYDALARI

1. “Journal of Baku Engineering University- Riyaziyyat və kompüter elmləri” - əvvəllər nəşr olunmamış orijinal əsərləri və müəllifin tədqiqat sahəsi üzrə yazılmış icmal məqalələri qəbul edir.
2. Məqalələr İngilis dilində qəbul edilir.
3. Yazılar **Microsoft Word** yazı proqramında, (**journal@beu.edu.az**) ünvanına göndərilməlidir. Göndərilən məqalələrdə aşağıdakılara nəzərə alınmalıdır:

- Məqalənin başlığı, müəllifin adı, soyadı,
- İş yeri,
- Elektron ünvanı,
- Xülasə və açar sözlər.

4. **Məqalədə başlıq hər xülasədən əvvəl** ortada, qara və böyük hərflə xülasələrin yazıldığı hər üç dildə olmalıdır.
5. **Xülasə** 100-150 söz aralığında olmaqla, 9 punto yazı tipi böyüklüyündə, məqalənin yazıldığı dildə və bundan əlavə yuxarıda göstərilən iki dildə olmalıdır. Məqalənin hər üç dildə yazılmış xülasəsi bir-birinin eyni olmalıdır. Açar sözlər uyğun xülasələrin sonunda onun yazıldığı dildə verilməklə ən azı üç sözdən ibarət olmalıdır.
6. Məqalədə UOT və PACS kodları göstərilməlidir.
7. Məqalə aşağıdakılardan ibarət olmalıdır:

- Giriş,
- Tədqiqat metodu
- Tədqiqat işinin müzakirəsi və onun nəticələri,
- İstinad ədəbiyyatı rus dilində olduğu halda orjinal dili mötərzə içərisində göstərməklə yalnız Latın əlifbası ilə verilməlidir.

8. **Şəkil**, **rəsm**, **grafik** və **cədvəllər** çapda düzgün, aydın çıxacaq vəziyyətdə və mətn içərisində olmalıdır. Şəkil, rəsm və qrafiklərin yazıları onların altında yazılmalıdır. Cədvəllərdə başlıq cədvəlin üstündə yazılmalıdır.
9. **Mənbələr** mətn içərisində kvadrat mötərizə daxilində göstərilməklə məqalənin sonunda mətn daxilindəki sıra ilə düzülməlidir. Eyni mənbəyə iki və daha cox istinad edildikdə əvvəlki sıra sayı saxlanmaqla müvafiq səhifələr göstərilməlidir. Məsələn: [7,səh.15].

Ədəbiyyat siyahısında verilən hər bir istinad haqqında məlumat tam və dəqiq olmalıdır. İstinad olunan mənbənin biblioqrafik təsviri onun növündən (monoqrafiya, dərslik, elmi məqalə və s.) asılı olaraq verilməlidir. Elmi məqalələrə, simpozium, konfrans, və digər nüfuzlu elmi tədbirlərin materiallarına və ya tezislərinə istinad edərkən məqalənin, məruzənin və ya tezisin adı göstərilməlidir.

Nümunələr:

a) ***Məqalə:*** Demukhamedova S.D., Aliyeva İ.N., Godjayev N.M.. *Spatial and electronic structure af monomeric and dimeric complexes of carnosine with zinc,* Journal of structural Chemistry, Vol.51, No.5, p.824-832, 2010

b) ***Kitab:*** Christie ohn Geankoplis. *Transport Processes and Separation Process Principles*. Fourth Edition, Prentice Hall, 2002

c) ***Konfrans:*** Sadychov F.S., Aydın C., Ahmedov A.İ.. Appligation of Information-Communication Technologies in Science and education. II International Conference. ”*Higher Twist Effects In Photon- Proton Collisions”, Bakı, 01-03 Noyabr, 2007, ss 384-391*

Mənbələr 9 punto yazı tipi böyüklüyündə olmalıdır.

10. **Səhifə ölçüləri:** üstdən 2.8 sm, altdan 2.8 sm, soldan 2.5 sm və sağdan 2.5 sm olmalıdır. Mətn 11 punto yazı tipi böyüklüyündə, **Palatino Linotype** yazı tipi ilə və tək simvol aralığında yazılmalıdır. Paraqraflar arasında 6 punto yazı tipi aralığında məsafə olmalıdır.
11. Orijinal tədqiqat əsərlərinin tam mətni bir qayda olaraq 15 səhifədən artıq olmamalıdır.
12. Məqalənin nəşrə təqdimi aşağıdakı qaydada aparılır:

- Hər məqallə ən azı iki ekspertə göndərilir.
- Ekspertlərin tövsiyələrini nəzərə almaq üçün məqalə müəllifə göndərilir.
- Məqalə, ekspertlərin tənqidi qeydləri müəllif tərəfindən nəzərə alındıqdan sonra Jurnalın Redaksiya Heyəti tərəfindən çapa təqdim oluna bilər.

YAZIM KURALLARI

1. "Journal of Baku Engineering University- Matematik ve Bilgisayar Bilimleri" önceler yayımlanmamış orijinal çalışmaları ve yazarın kendi araştırma alanın-da yazılmış derleme makaleleri kabul etmektedir.
2. Makaleler İngilizce kabul edilir.
3. Makaleler Microsoft Word yazı programında, (**journal@beu.edu.az**) adresine gönderilmelidir. Gönderilen makalelerde şunlar dikkate alınmalıdır:
- Makalenin başlığı, yazarın adı, soyadı,
- İş yeri,
- E-posta adresi,
- Özet ve anahtar kelimeler.
4. **Özet** 100-150 kelime arasında olup 9 font büyüklüğünde, makalenin yazıldığı dilde ve yukarıda belirtilen iki dilde olmalıdır. Makalenin her üç dilde yazılmış özeti birbirinin aynı olmalıdır. Anahtar kelimeler uygun özetin sonunda onun yazıldığı dilde verilmekle en az üç sözcükten oluşmalıdır.
5. Makalede UOT ve PACS tipli kodlar gösterilmelidir.
6. Makale şunlardan oluşmalıdır:
- Giriş,
- Araştırma yöntemi
- Araştırma
- Tartışma ve sonuçlar,
- İstinat Edebiyatı Rusça olduğu halde orjinal dili parantez içerisinde göstermekle yalnız Latin alfabesi ile verilmelidir.
7. **Şekil, Resim, Grafik** ve **Tablolar** baskıda düzgün çıkacak nitelikte ve metin içerisinde olmalıdır. Şekil, Resim ve grafiklerin yazıları onların alt kısımda yer almalıdır. Tablolarda ise başlık, tablonun üst kısmında bulunmalıdır.
8. **Kullanılan kaynaklar**, metin dâhilinde köşeli parantez içerisinde numaralandırılmalı, aynı sırayla metin sonunda gösterilmelidir. Aynı kaynaklara tekrar başvurulduğunda sıra muhafaza edilmelidir. Örneğin: [7,seh.15].

Referans verilen her bir kaynağın künyesi tam ve kesin olmalıdır. Referans gösterilen kaynağın türü de eserin türüne (monografi, derslik, ilmî makale vs.) uygun olarak verilmelidir. İlmi makalelere, sempozyum, ve konferanslara müracaat ederken makalenin, bildirinin veya bildiri özetlerinin adı da gösterilmelidir.

Örnekler:

a) ***Makale:*** Demukhamedova S.D., Aliyeva İ.N., Godjayev N.M.. *Spatial and Electronic Structure of Monomerik and Dimeric Conapeetes of Carnosine Üith Zinc*, Journal of Structural Chemistry, Vol.51, No.5, p.824-832, 2010

b) ***Kitap:*** Christie ohn Geankoplis. *Transport Processes and Separation Process Principles*. Fourth Edition, Prentice Hall, p.386-398, 2002

c) ***Kongre:*** Sadychov F.S., Aydın C., Ahmedov A.İ. Appligation of Information-Communication Technologies in Science and education. II International Conference. "*Higher Twist Effects In Photon- Proton Collisions", Bakı, 01-03 Noyabr, 2007, ss 384-391*

Kaynakların büyüklüğü 9 punto olmalıdır.

9. **Sayfa ölçüleri**; üst: 2.8 cm, alt: 2.8 cm, sol: 2.5 cm, sağ: 2.5 cm şeklinde olmalıdır. Metin 11 punto büyüklükte **Palatino Linotype** fontu ile ve tek aralıkta yazılmalıdır. Paragraflar arasında 6 puntoluk yazı mesafesinde olmalıdır.
10. Orijinal araştırma eserlerinin tam metni 15 sayfadan fazla olmamalıdır.
11. Makaleler dergi editör kurulunun kararı ile yayımlanır. Editörler makaleyi düzeltme için yazara geri gönderilebilir.
12. Makalenin yayına sunuşu aşağıdaki şekilde yapılır:
- Her makale en az iki uzmana gönderilir.
- Uzmanların tavsiyelerini dikkate almak için makale yazara gönderilir.
- Makale, uzmanların eleştirel notları yazar tarafından dikkate alındıktan sonra Derginin Yayın Kurulu tarafından yayına sunulabilir.
13. Azerbaycan dışından gönderilen ve yayımlanacak olan makaleler için,(derginin kendilerine gonderilmesi zamani posta karşılığı) 30 ABD Doları veya karşılığı TL, T.C. Ziraat Bankası/Üsküdar-İstanbul 0403 0050 5917 No'lu hesaba yatırılmalı ve makbuzu üniversitemize fakslanmalıdır.

ПРАВИЛА ДЛЯ АВТОРОВ

1. «Journal of Baku Engineering University» - Математики и информатики публикует оригинальные, научные статьи из области исследования автора и ранее не опубликованные.

2. Статьи принимаются на английском языке.

3. Рукописи должны быть набраны согласно программы **Microsoft Word** и отправлены на электронный адрес **(journal@beu.edu.az)**. Отправляемые статьи должны учитывать следующие правила:

- Название статьи, имя и фамилия авторов
- Место работы
- Электронный адрес
- Аннотация и ключевые слова

4. **Заглавие статьи** пишется для каждой аннотации заглавными буквами, жирными буквами и располагается по центру. Заглавие и аннотации должны быть представлены на трех языках.

5. **Аннотация**, написанная на языке представленной статьи, должна содержать 100-150 слов, набранных шрифтом 9 punto. Кроме того, представляются аннотации на двух других выше указанных языках, перевод которых соответствует содержанию оригинала. Ключевые слова должны быть представлены после каждой аннотации на его языке и содержать не менее 3-х слов.

6. В статье должны быть указаны коды UOT и PACS.

7. Представленные статьи должны содержать:

- Введение
- Метод исследования
- Обсуждение результатов исследования и выводов.
- Если ссылаются на работу на русском языке, тогда оригинальный язык указывается в скобках, а ссылка дается только на латинском алфавите.

8. **Рисунки, картинки, графики и таблицы** должны быть четко выполнены и размещены внутри статьи. Подписи к рисункам размещаются под рисунком, картинкой или графиком. Название таблицы пишется над таблицей.

9. **Ссылки** на источники даются в тексте цифрой в квадратных скобках и располагаются в конце статьи в порядке цитирования в тексте. Если на один и тот же источник ссылаются два и более раз, необходимо указать соответствующую страницу, сохраняя порядковый номер цитирования. Например: [7, стр.15]. Библиографическое описание ссылаемой литературы должно быть проведено с учетом типа источника (монография, учебник, научная статья и др.). При ссылке на научную статью, материалы симпозиума, конференции или других значимых научных мероприятий должны быть указаны название статьи, доклада или тезиса.

Например:

a) ***Статья:*** Demukhamedova S.D., Aliyeva I.N., Godjayev N.M. *Spatial and electronic structure of monomeric and dimeric complexes of carnosine with zinc,* Journal of Structural Chemistry, Vol.51, No.5, p.824-832, 2010

b) ***Книга:*** Christie on Geankoplis. *Transport Processes and Separation Process Principles.* Fourth Edition, Prentice Hall, 2002

c) ***Конференция:*** Sadychov F.S, Fydin C,Ahmedov A.I. Appligation of Information-Communication Nechnologies in Science and education. II International Conference. *"Higher Twist Effects In Photon-Proton Collision",* Bakı,01-03 Noyabr, 2007, ss.384-391

Список цитированной литературы набирается шрифтом 9 punto.

10. **Размеры страницы:** сверху 2.8 см, снизу 2.8 см, слева 2.5 и справа 2.5. Текст печатается шрифтом **Palatino Linotype**, размер шрифта 11 punto, интервал-одинарный. Параграфы должны быть разделены расстоянием, соответствующим интервалу 6 punto.
11. Полный объем оригинальной статьи, как правило, не должен превышать 15 страниц.

12. Представление статьи к печати производится в ниже указанном порядке:

- Каждая статья посылается не менее двум экспертам.
- Статья посылается автору для учета замечаний экспертов.
- Статья, после того, как автор учел замечания экспертов, редакционной коллегией журнала может быть рекомендована к печати.